INVESTIGATION OF TOOL WEAR IN GRINDING PROCESSES

By:

BATUHAN YASTIKCI

Submitted to the Graduate School of Engineering and Natural Sciences in partial fulfillment of the requirements for the degree of

Master of Science

Sabanci University

December 2016

INVESTIGATION OF TOOL WEAR IN GRINDING PROCESSES

APPROVED BY:

Prof. Erhan BUDAK .....

(Thesis Advisor)

Assoc. Prof. Bahattin KOÇ .....

Assoc. Prof. Mustafa BAKKAL .....

Date of Approval: 29.12.2016

INVESTIGATION OF TOOL WEAR IN GRINDING PROCESSES

Batuhan Yastıkcı

Industrial Engineering, MS Thesis, 2016

Thesis Supervisor: Prof. Dr. Erhan Budak

Keywords: Grinding, Wear Mechanisms, Tool Life, Hard to Machine Materials, Surface Quality

Abstract

Low cost, high quality and fast production are essentials of the competitive industry. Due to technological advances, grinding has come into the forefront for producing high quality parts in an economical way in recent decades. One of the most important critical issues in superabrasive machining processes is tool wear due to its impact on surface integrity, part quality and process cost.

The main aim of this thesis is to investigate the wear process of grinding wheels considering wear mechanisms, tool life and process outcomes. Wheel wear in grinding is a sophisticated phenomenon which can affect the entire grinding process profoundly. Different types of wear mechanisms such as attritious wear, grit fracture and pullout of the abrasive grits are studied. The effect of wear on the grinding forces and the quality of the part have been investigated. Grits were individually measured during the process and the wear mechanisms are discussed in detail. Some of the grits on the wheel surface are chosen randomly and all phases of worn grits are monitored during its lifetime under a microscope. Wear related surface roughness investigations are done for both the workpiece and the tool throughout the tool life.

The wear behavior of the grinding wheel is sensitive to the process parameters such as depth of cut, feed rate and cutting speed. An analysis on the effect of depth of cut on the wear and process results is done. Tool life criteria is provided for the selected wheel-workpiece pair. A new model is presented to predict the surface roughness of the electroplated CBN grinding wheel. The wear condition of the electroplated grinding wheel can be estimated by this model and the model can also be applied to the other type of single-layer wheels. The model can be used to predict the surface quality of the part, because surface roughness of the workpiece and grinding wheel are correlated to each other. The model is verified by experiments and good agreement is obtained.

TAŞLAMA İŞLEMLERİNDE TAKIM AŞINMA SÜRECİNİN İNCELENMESİ

Batuhan Yastıkcı

Endüstri Mühendisliği, Yüksek Lisans Tezi, 2016

Tez Danışmanı: Prof. Dr. Erhan Budak

Anahtar Kelimeler: Taşlama, Aşınma Mekanizmaları, Takım Ömrü, İşlenmesi Zor Malzemeler, Yüzey Kalitesi

Özet

Düşük maliyetli, kaliteli ve hızlı üretim, rekabetçi endüstrinin temel unsurlarıdır. Teknolojik gelişmelere bağlı olarak, taşlama, son yıllarda yüksek kalitede parçaları ekonomik bir şekilde üretmek için ön plana çıktı. Yüksek performanslı taşlama işlemlerinde en önemli kritik konulardan biri; yüzey bütünlüğü, parça kalitesi ve proses maliyeti üzerindeki etkisinden dolayı takım aşınmasıdır.

Bu tezin temel amacı aşınma mekanizmaları, takım ömrü ve proses sonuçları dikkate alınarak taşlama taşlarının aşınma süreçlerini incelemektir. Taşlama işlemlerinde taş aşınması, tüm taşlama işlemini derinden etkileyebilen komplike bir olaydır. Sürtünmeye bağlı aşınma, parçacık kırılması ve parçacık kopması gibi farklı türdeki aşınma mekanizmaları incelenir. Aşınmanın taşlama kuvvetleri ve parçanın kalitesi üzerindeki etkileri araştırılmıştır. Parçacıklar süreç boyunca ayrı ayrı ölçülmüş ve aşınma mekanizmaları ayrıntılı olarak tartışılmıştır. Taşlama taşı yüzeyindeki parçacıkların bazıları rasgele seçilir ve parçacıkların ömrü sürecinde aşınmış parçacıkların tüm safhaları mikroskop altında izlenir. Aşınma ile ilgili yüzey pürüzlülüğünün incelenmesi, takım ömrü boyunca hem iş parçası hem de taşlama taşı için yapılır.

Taşlama taşının aşınma davranışı, kesme derinliği, ilerleme hızı ve kesme hızı gibi proses parametrelerine duyarlıdır. Kesme derinliğinin aşınma ve proses sonuçları üzerindeki etkisi üzerine bir analiz yapılmıştır. Seçilen tekerlek-iş parçası çifti için takım ömrü kriterleri sağlanmaktadır. Elektrolizle kaplanmış CBN taşlama tekerleğinin yüzey pürüzlülüğünü öngörmek için yeni bir model sunulmuştur. Elektrolizle kaplanmış taşlama taşının aşınma durumu bu model tarafından tahmin edilebilir ve model tek katmanlı taşların diğer türlerine de uygulanabilir. Model parçanın yüzey kalitesini tahmin etmek için kullanılabilir, çünkü iş parçasının ve taşlama taşının yüzey pürüzlülüğü birbiriyle ilişkilidir. Model deneyler ile doğrulanmış ve iyi bir mutabakat sağlanmıştır.

ACKNOWLEDGEMENTS

First and foremost, I would like to express my genuine appreciation and thanks to my enthusiastic advisor Prof. Erhan Budak for all the support and encouragement he gave me. Not only his valuable academic guidance but also his wise point of view about life broaden my perspective. Without his guidance and constant feedback this work would not have been achievable.

I would also like to thank members of the committee; Assoc. Prof. Bahattin Koç and Assoc. Prof Mustafa Bakkal for their grateful assistance to my project.

I greatly appreciate the assistance of the Maxima R&D members; Dr. Emre Özlü, Esma Baytok, Veli Nakşiler, Anıl Sonugür, Ahmet Ergen, Tayfun Kalender, Dilara Albayrak. Also, special thanks to Ertuğrul Sadıkoğlu and Süleyman Tutkun for their guidance and friendly communication.

I would like to thank my fellow lab mates (MRL); especially to my ex roommate Mehmet Albayrak for making my life at Sabancı much enjoyable and Mert Gürtan for being a really good project and game mate, kind friends Mert K., Hayri, Samet, Gözde, Turgut, Cihan, Can, Faraz, Zahra, Amin, Milad, Hamid, Kaveh, Esra Hassan, Yaser for their continuous support, good friendship and all the fun we had.

Finally, I would like to thank TÜBİTAK (Scientific and Technological Research Council of Turkey) for supporting me financially throughout my project by granting a scholarship.

Last but not least, I am most thankful to my family; Muzaffer, Ülkü Cem, Arzu and Doğuhan Yastıkcı for supporting me spiritually throughout my life. They are the most important people in my world and I would like to dedicate this study to them.

TABLE OF CONTENTS

LIST OF FIGURES

LIST OF TABLES

1. INTRODUCTION

1.1. Introduction and Literature Survey

Abrasives has a significant role in the history of humanity due to its ability to shape materials such as weapons and tools. The area of utilization of abrasives are so wide. In early days, they were used to shape stones to build pyramids, to cut and polish gems etc. Nowadays abrasives are being used in many industrial applications and grinding is one of them being used as a finishing process.

Hard to machine materials are becoming more and more common in aerospace and automotive industries to increase efficiency, reduce weight and decrease pollution. They are difficult to machine due to high heat resistance, high strength at even elevated temperatures, low thermal conductivity and high hardness resulting in very low machinability. Very low speeds must be used in milling and cutting even then tool life is very short. Some of these hard to machine materials such as nickel alloys can be better produced using abrasive processes [1, 2]. Abrasive processes are widely used in the machining industry such as; lapping, polishing, honing and superfinishing because of their high dimensional accuracy [3]. In this study, grinding and superabrasive machining have been investigated in terms of wear.

Principles of grinding processes are similar to the other known machining processes [4]. Grinding processes can be divided into two separate topics which are conventional and superabrasive processes. One of the important properties to distinguish the process type is the abrasive material. Grinding wheels mainly consist of abrasive particles (grits) and bonding material. While the abrasive particles make the cutting action, bonding material sticks the abrasives to the base (hub). Due to the bonding material, pores occur at the structure. Abrasive materials are randomly distributed over the bonding material except the special structures. Due to the randomness, the cutting tool exhibits irregular distribution of cutting edges which makes the modeling of grinding processes harder. On the contrary to the other operations such as milling and turning, in grinding

operations cutting processes occurs via negative cutting angles which cause unfavorable chipping condition. The determination of the grinding tool and parameters such as feed, depth of cut and cutting speed should be arranged considering the desired grinding process's needs. Correct selection of process details enables less expensive and more efficient machining in terms of grinding [5].

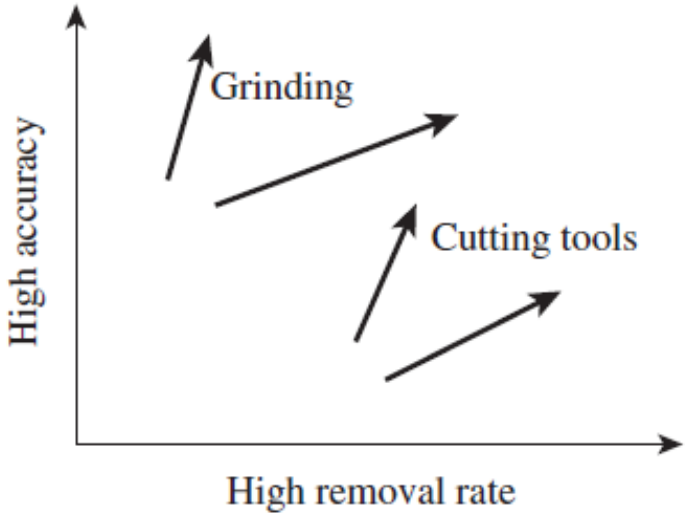

Figure 1- Comparison of Grinding and Cutting Tools [3]

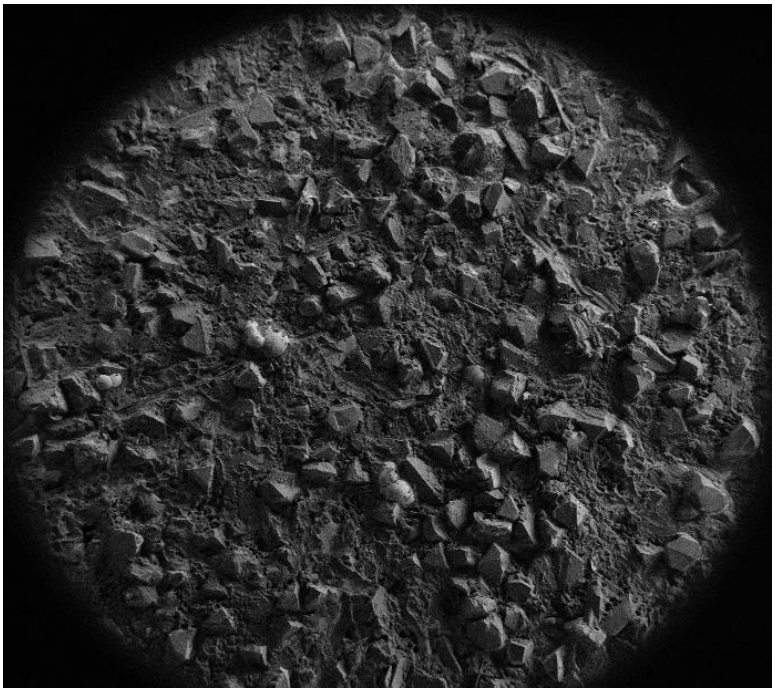

Figure 2-Random Distribution of Grits on Electroplated CBN Wheel, SEM

The grinding tool is made up of abrasives, bonding and pores. Chip removal process is performed by abrasive particles which can be seen in Figure 3. The type of the abrasive is determined by the material to be machined. In grinding tools aluminum oxide (Al_2O_3), silicon carbide (SiC), cubic boron nitride(CBN) and diamond are used as an abrasive particle. Aluminum oxide and silicon carbide are referred as conventional abrasives. On the other hand, CBN and diamond are referred to super abrasives due their excessive hardness. Diamond knows as the hardest material. Ductile materials are machined using CBN or aluminum oxide, whereas diamond and silicon carbide are recommended for brittle materials.

Selection of abrasive size is important for process' needs. Fine grits are used materials harder to chip and they are used for better surface finish due to their low penetration through the material. Also, they produce small chips. On contrary, coarse grits are used for roughing operations due to their high material removal capabilities and mostly they are preferred for easier to chip materials.

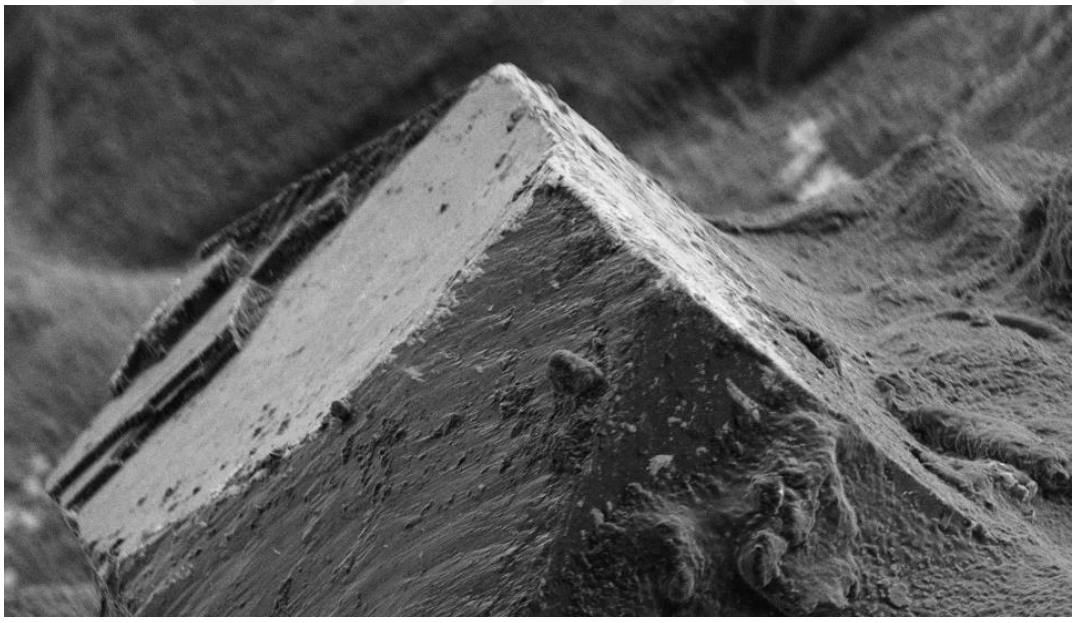

Figure 3-Sharp Cutting Edges of a CBN Grit, SEM

Superabrasive machining(SAM) is a special abrasive process where CBN plated tools are used. Due to tool size, sometimes very high spindle speeds must be used (e.g. 80000 rpm) to increase the cutting efficiency. This process needs very high volume of coolant due to extreme material removal rates, also needs advance filtering systems to remove powder from the coolant and eliminate them to get into the process again.

Inconel 718 is a nickel based super alloy that exhibits excellent tensile and impact strength. Also, it has good oxidation and corrosion resistance at temperatures encountered in jet engines and gas turbines operations [6]. Grinding of Inconel 718 with electroplated cubic boron nitride (CBN) wheels will be more general in today's aerospace industry because of its significant advantages compared to conventional wheels [1, 7, 8]. The cutting action by these wheels is achieved by randomly distributed grains over electroplated nickel bond which can be seen in Figure 2. Because of the single layer formation dressing cannot be carried out on these wheels. Thus, the wheel life and grinding performance are considerably restricted by wear since the changes in the wheel topography directly affect the process consequences. Accordingly studying the wear behavior of this kind of wheel is highly important to improve grinding performance.

Wear behavior of the grain cutting edges have been studied in recent years. Wear in conventional grinding wheels can occur due to four mechanisms, namely attritious wear, fracture of the grits (micro & macro) and bond fracture [9, 10]. Different grinding wheel-workpiece pairs show different dominant wear trends. For example, E.J. Duwell [11] showed that the dominant wear mechanism for silicon carbide grits for cutting mild steel is attritious while both attritious and fracture wear occurred for aluminum oxide grits for the same work material. The wear mechanisms for bonded wheels are shown in Figure 4.

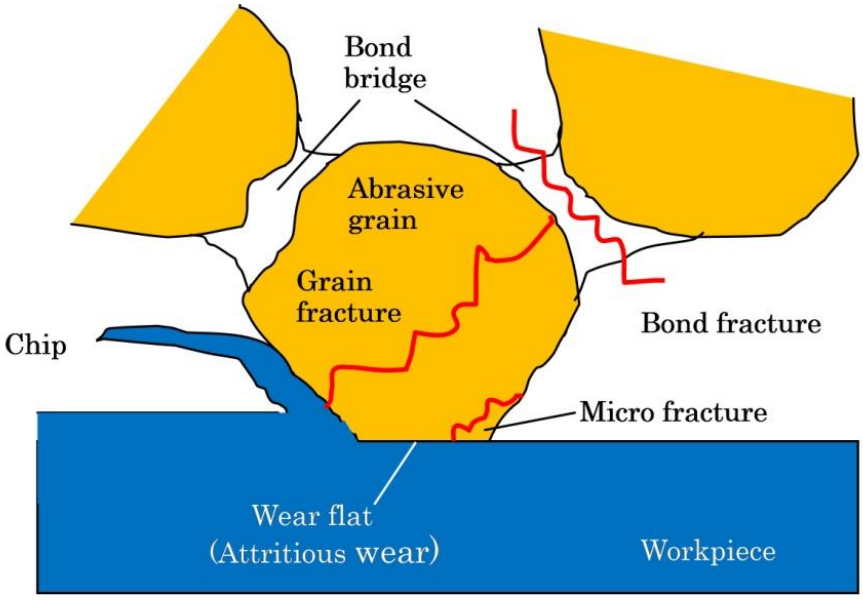

Figure 4-Wear Types Observed on Bonded Wheels

Grinding wheel's ability to remove material is called G-ratio [3]. During the cutting action both workpiece and the grinding wheel lose material. G-ratio can be defined as volume of material removed divided by volume of wheel wear. Besides the wear mechanisms, grinding performance is also affected by workpiece materials which fill in the pores of the wheel and decrease the effectiveness of the cutting edges. An example is given in Figure 5. Filled material at the wheel surface causes an increase in the grinding power. Due to inability to cut material with the filled surface, surface burns may occur which is not the desired result.

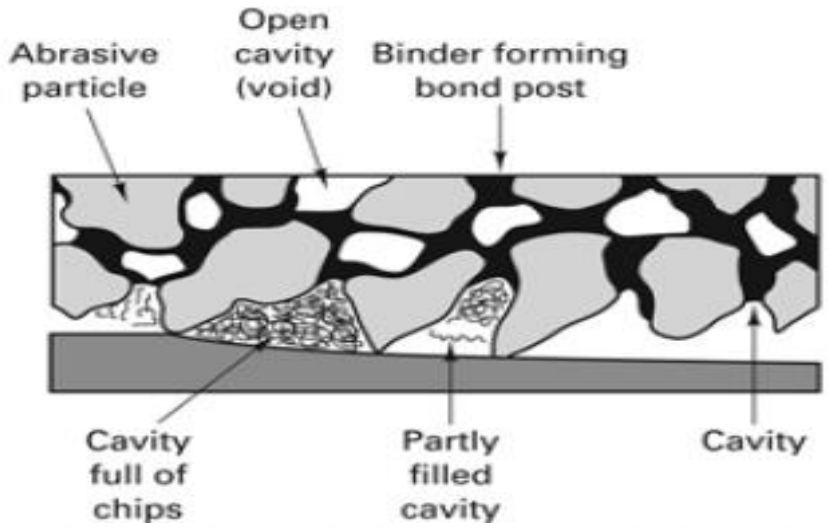

Figure 5-Filled Cavity of a Bonded Grinding Wheel

CBN and diamond abrasives have been investigated in terms of wear behavior [12, 13, 14, 15]. Some studies in the literature show the changes in the wear mechanisms *during the tool life* which provides more specific and detailed analysis of wear mechanisms. Shi and Malkin clarified that most of the wear caused by pullout during the initial stages of the wheel life and fracture is dominant wear mechanism in steady-state regime [16]. Attritious wear causes dulling of the grits which results in enhancing grinding power. So that temperature escalates and most of the heat flows towards the wheel instead of workpiece [17]. Moreover, bond strength of brazed CBN wheels has been researched at high and low specific load conditions on the grits by Chattopadhyay et al. [18]. At high load condition abrasives were seemed to be broken at bond level by leaving flat surface behind. Contrary to the bonded wheels, bond fracture does not occur in plated wheels because of the single-layer structure. Instead, pullout is observed. The four main wear types are shown in Figure 6. This study focused on these four wear types.

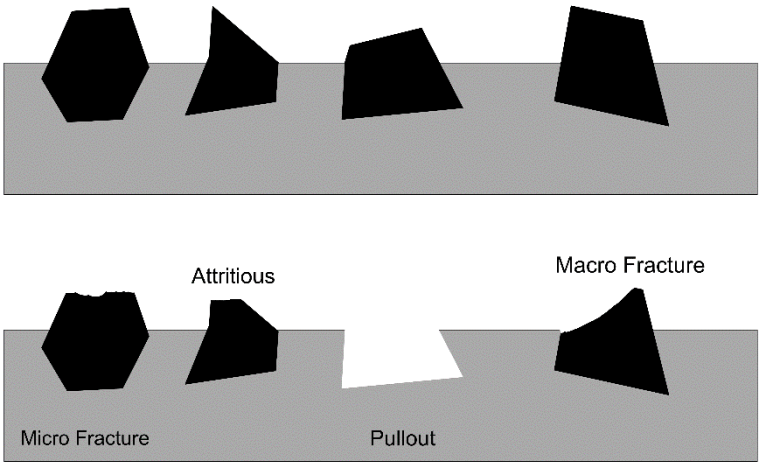

Figure 6- Wear Types Observed on Electroplated Wheels

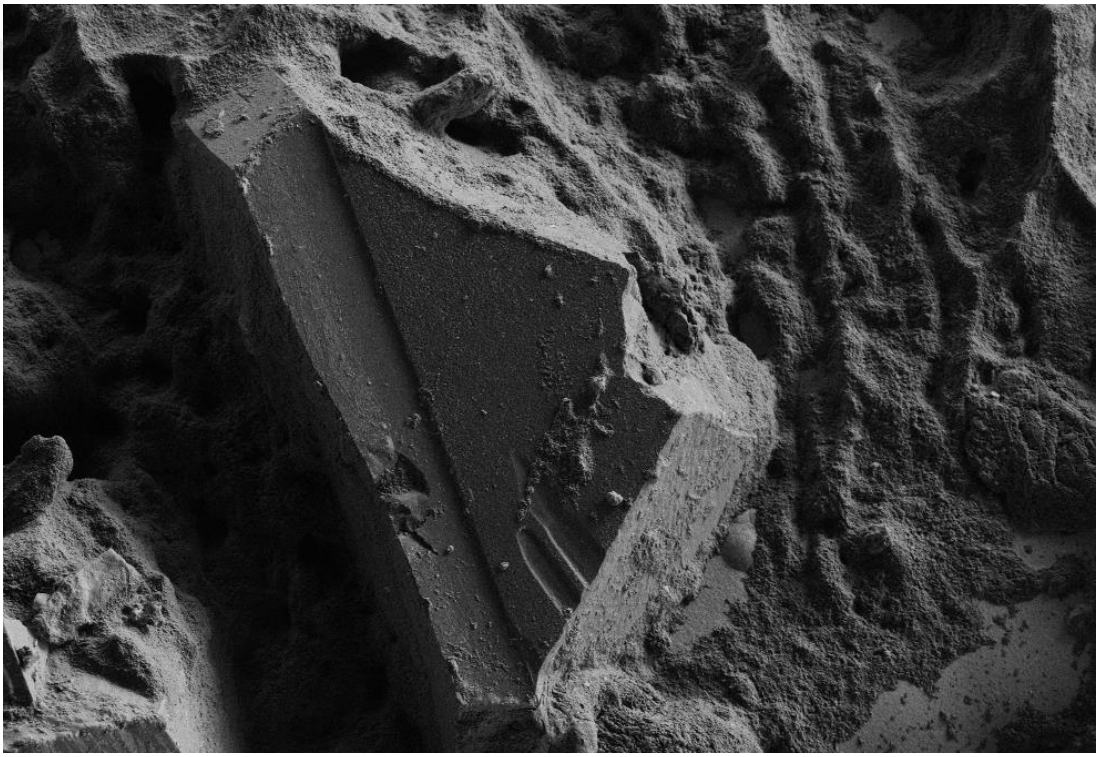

Figure 7-Fracture at the Tip of the Grit, SEM

In the previous studies, attritious wear was measured via microscope by using the reflection of light [7, 8]. Fracture mechanism was measured under the name of bond and grain fracture via weight calculation [10]. Pullout mechanism was measured by counting the pockets in the surface via microscope [19]. Whereas, in this study individual grit investigation has been applied gradually to observe the wear mechanisms. This approach provides more accurate outcomes because it enables to distinguish wear types in each step.

Volume of material removed was used to determine the *tool life* for the grinding processes [7]. Grain and bond fracture or filled material amount at the surface of the conventional wheels decrease the grinding wheel performance, the ability to cut and consequently decreases tool life. Dressing and truing operations can be applied to reshape the surface of the grinding wheel. However, since single-layer plated tools only have a limited amount of abrasive grits on the surface, it is not possible to do dressing. On the other hand, truing process is not desired in the scope of this study because it causes loss of abrasive materials. Wheel topography alters during the tool life due to wear and the grinding performance of electroplated wheels change remarkably.

Quality can be defined as performing all aspects of a part accurately. Dimensional accuracy, surface texture and form are noticeable aspects of quality. Grinding can provide better quality in dimensions compare to the other cutting processes, also even in surface quality. In many cases, integrity of the material at the cutting zone is remarkably significant. For instance, after a hardening operation, the part should not be cracked or softened. It is also critical to avoid tensile residual stresses that decrease strength and shorten service life. Thereby, grinding processes needs precise design and control to achieve high quality and to avoid surface burns. Wear of grinding wheel has significant consequences on output parameters [20, 21].

1.2. Objective

Considering today's technological and economic conditions, manufacturing companies tend to do the optimum in their fields due to strong competition. Thereby, in order to increase efficiency, reliable and accurate manufacturing conditions should be applied by computer-aided manufacturing, flexible manufacturing systems and well-educated engineers in order. However, most of them confront some cost related problems. One of the most influential things to overcome this issue is decreasing the tool consumption. At this point, increasing the utilization time of the tools becomes crucial. Superabrasive machining enhances every day and due to its high cost wheels, importance of tool consumption is highly essential.

The main objective of this thesis is to investigate the wear effect in the grinding processes. Considering the equipment that is possessed, small electroplated CBN wheels were determined to be examined. Because small wheels are worn easier and observing them under microscope is more suitable due to placing.

Even though some researches have been done on grinding wear concept, in this study more detailed analysis of wheel wear mechanisms in the electroplated CBN wheels were experimentally investigated with regards to attritious wear, fracture and pullout. The aim is to understand the effect of the wheel-workpiece interaction on the grits by investigating the wear behavior *individually*. Since cutting force is an important indicator of wear mechanism [7], force measurements were used to monitor in-process wear effect.

Since grinding is used as a final process, surface quality of the final workpiece is substantial. Nevertheless, research has been conducted not only for surface quality, but also considering the other aspects of the grinding process such as force and tool life. Moreover, a model has been developed to predict the surface roughness of the grinding wheel. Model has been advanced based on electroplated wear mechanics but it can be also used for other single-layer tool types.

1.3. Layout

The organization of the thesis is as follows:

In Chapter 2, grinding CNC machine and measurement devices are presented. Also, an experimental study is shown which focuses on geometrical measurements of grits, process forces and wear.

In Chapter 3, wear mechanisms of an electroplated CBN grinding wheel are presented in detail. The measurement techniques that have been used to observe the wear mechanisms are explained. Fracture, attritious wear and pullout are expressed. Also, percentage of the observed wear mechanisms are given. The effect of wear on the outcomes of the grinding process is discussed such as force, surface roughness of the workpiece and grinding wheel.

In Chapter 4, wear mechanisms of an electroplated CBN grinding has been investigated eight times throughout its tool life. All the changes on the selected grits are provided with 3D pictures at each step. Active grit increment is proved by experimental measurements. The wear effect on all process parameters are discussed. The effect of depth of cut on wear, surface quality and force are presented. Tool life criteria is provided for the selected cutting conditions and workpiece-wheel pair.

In Chapter 5, a model to predict surface roughness of an electroplated CBN wheel is presented. The advantages of the model are discussed. Verification of the model is presented with two different test sets.

In Chapter 6 and 7, suggestions for further research and conclusion are presented.

2. EXPERIMENTAL INVESTIGATION OF GRINDING PROCESS MECHANICS

2.1. Introduction

The purpose of starting the thesis with this chapter is to give an insight about grinding processes and the equipment that have been used during this study. Moreover, this chapter includes some experimental work to express what has been investigated except wear. It is important to understand grinding process characteristics before starting the wear investigation.

2.2.Grinding Process

2.2.1. General View

Grinding is used as a finishing process in the machining industry. The material removal rate is low compared to the other cutting processes. The elements of grinding process are shown in Figure 8. It consists of workpiece, grinding wheel, coolant and sometimes dressing tool depending on the wheel type. Cutting speed, feed rate and depth of cut are the parameters that are adjusted before the process. The change in these parameters affect the cutting forces, wear behavior and surface integrity [3, 22].

In the experimental stage of the thesis, face grinding operations have been studied. In the operations, it is difficult to reach desired depth of cut in one pass. Even the grinding wheel is set to a point, during the pass it deflects upwards due to the reaction of the workpiece as shown in Figure 9. a_p is the desired depth of cut, a_e is the real depth of cut and x is the deflection given in the figure. This concept has been investigated under the name of *spark-out* in the following parts in this chapter with regards to force.

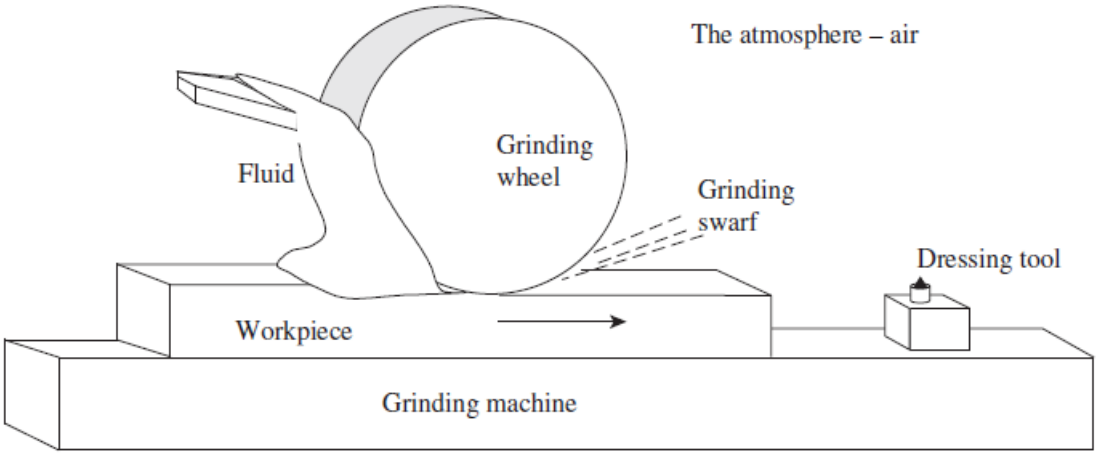

Figure 8- Elements of Grinding Process [5]

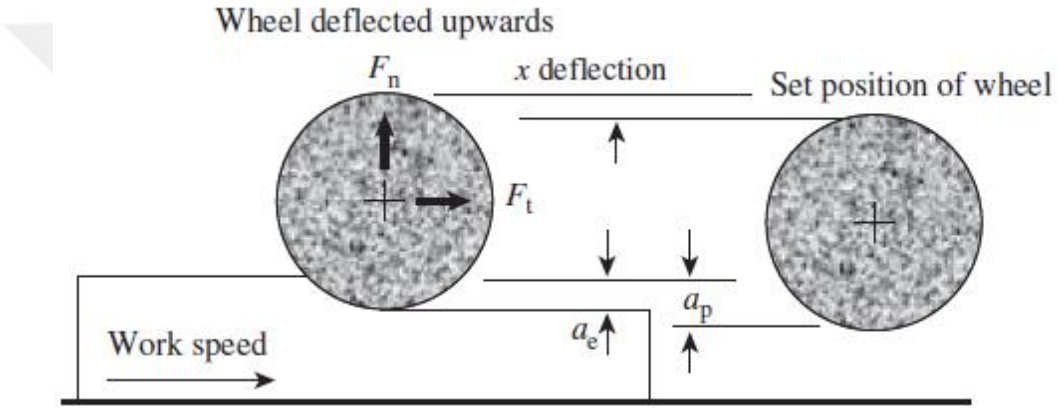

Figure 9- Deflections in Grinding Processes [5]

2.2.2. Process Mechanics

All the process mechanics are related to each other. So before go into details of the wear investigation, brief information about process mechanics has been given in this part. Chip formation in the grinding process occurs at micro levels in three stages. At the initial contact elastic deformation occurs. Then, elastic and plastic deformations occur simultaneously. After some point, chip removal is included to the other two. Grinding operation can be considered as a milling operation with many cutting teeth. Thus, grinding process can be modeled by using milling analogy [34]. However, in this study wear approach to the grinding processes has been done instead of process modeling.

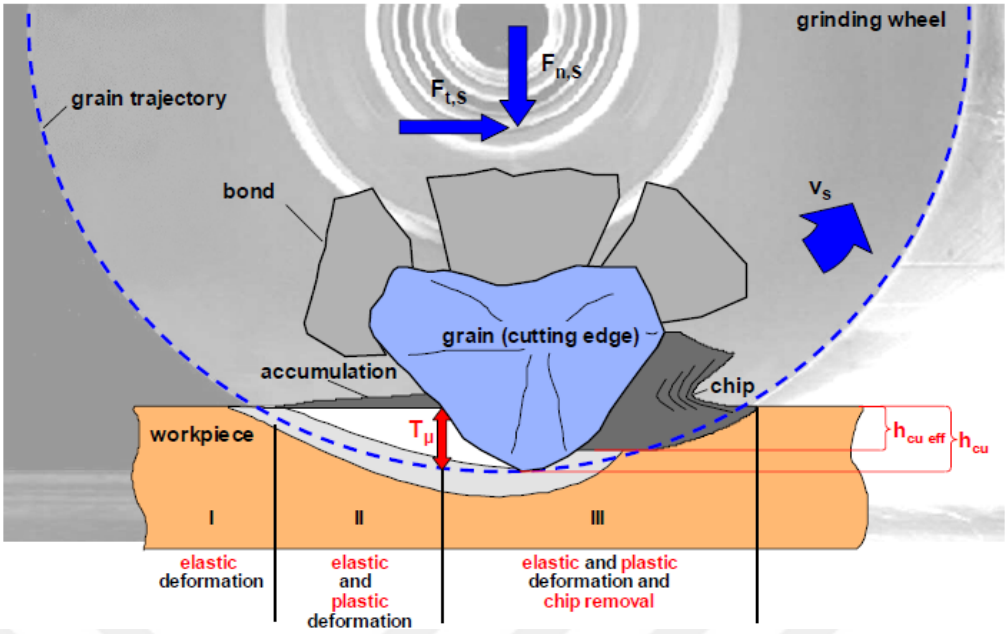

Figure 10-Chip Formation in Grinding

2.3. Equipment

In this part, the equipment that have been used in this study was explained. They can be divided into two sections such as CNC machine and measurement devices. All of them were explained briefly and their importance to the study has been clarified.

2.3.1. CNC Machine Properties

Chevalier Smart B818 CNC Profile & Forming Grinding CNC machine was used in surface grinding experiments. Two different spindles can be used in this CNC machine. Spindles provide different spindle speed intervals and torques which makes the tool selection significant in terms of size and type. Maximum rpm (revolution per minute) limits are 7k and 40k for these spindles. Because of the torque capacity of the 40k rpm spindle, its usage is not suitable for large diameter grinding wheels. Thereby, grinding wheels with small diameters have been chosen for the experiments.

Process parameters should be determined carefully due to safely precautions. Grinding parameters mainly depend on the workpiece-tool type. Also, capability of the CNC machine and coolant are also significant in the selection of cutting parameters.

Figure 11- Chevalier B818 CNC Machine

For conventional wheels, such as aluminum oxide and silicium carbide, cutting speed should be selected between 25-35 m/s to be stay in the safe region. At 40k rpm spindle speed, minimum of 10 mm and maximum of 20 mm diameter of grinding wheels are safe to use. For example, cutting speed should be adjusted around 30-45 m/s for CBN wheels and steel workpiece interactions.

Briefly, even super abrasive wheels are in progress, wheel diameter should not exceed 30 mm at the 40k rpm. Grinding wheels up to 40 mm in diameter can be used if the spindle speed is decreased. However, the performance of the process would not be satisfying after decreasing the built-in spindle speed more than 20-25%. In the structure of the high-speed spindles, there are small and low strength bearings. Thus, using large diameter tools should be avoided. Using parameters at limits and the cases with large contact area between tool and the workpiece should also be avoided.

CNC machine is capable of moving in three axis x-y-z and this is sufficient for surface grinding. Workpiece is stabilized to the CNC machine via electromagnetic table. Most of the time workpiece has been positioned on the dynamometer.

2.3.2. Measurement Devices

2.3.2.1.Nanofocus

Nanofocus is a microscope which is used for inspections on the grinding wheels. It can provide areal or individual view of the grits which is highly important for wear

observations. The measurements in Nanofocus microscope are performed via light reflections, and 3D view of the grits can be obtained accurately by scanning them. The picture of the Nanofocus can be seen in Figure 12.

Figure 12- Nanofocus

Two lenses were used in wear investigations, which provide 20x and 50x zooming. 20x lens was used for areal investigation and was able to show 0.64 mm^2 area which can be seen in Figure 13. In this area, grits are seen as black regions and approximately 30 grits were observed for the given example. However, geometrical details of the grits such as rake angle, nose radius etc. cannot be seen by using this lens. Thereby, it is better to use it for counting grits on the wheel surface. In order to observe the micro properties of the grits, more precise lens should be used.

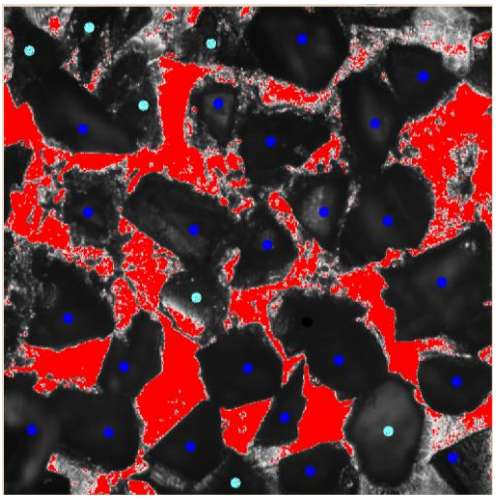

Figure 13- 20x Measurement via Nanofocus

On the other hand, 50x lens was used for the individual investigations of grits. It can provide 0.1024 mm^2 view on the wheel surface which can be seen in Figure 14. In this area, approximately 2-3 grits can be seen clearly. However, some of the grits are buried under the plate, that's why sometimes huge amount of them cannot be seen. Those grits were considered as inactive and they were not investigated at the initial stages. Grit properties such as height and shape can be seen via 50x lens.

In grinding operations, the cutting process is performed by abrasives located on the wheel surface. Thus, their condition determines the tool life. Individual investigation of grits is highly important. In the literature, most of the studies have focused on general behavior of the tool wear [24, 4, 5, 7]. However, in this study tool wear has been investigated from various of aspects.

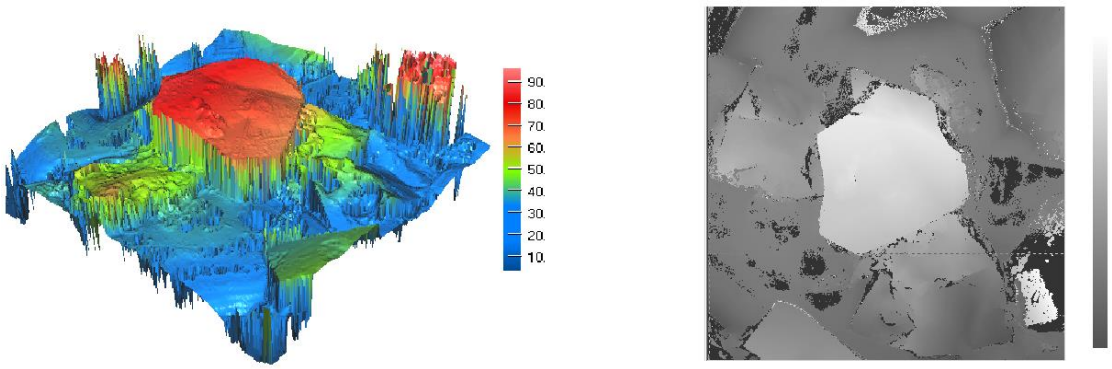

Figure 14- 50x Measurement of a Single Grit

2.3.2.2.Internal Grinding Wheel Stabilizer

Investigation of abrasive particles are very difficult, because they are randomly distributed on the grinding wheel surface. Focusing an area repetitively is really troublesome in stepwise investigation of grinding wheel due to the random distribution of the grits and micro dimensions of the grits.

In the previous studies of this project, large size grinding wheels were used. Grinding wheel does not fit under the microscope because of its size, so it was really difficult to observe the particles. They had to break the wheel to fit it under the microscope, but after that wheel became useless. However, to be able to observe the wear effect on the grinding wheel, after each test wheel should be investigated under microscope. Because of these reasons smaller size grinding wheels were used in wear investigations.

After the wheel size problem had been solved, the next problem was fixing the grinding wheel under the microscope. By this way same area or same abrasive can be investigated even after the wheel is dislocated. The location of the desired area or abrasive can be easily recorded. That is why grinding wheel stabilizer was developed. The grinding wheel's other tip was modified by threading the mile, in order to make it fixed every time it is attached. It can be seen in Figure 15.

Figure 15- Threading the Grinding Wheel Mile

The first version of the stabilizer was so big and it was standing apart from the microscope. It can be seen in Figure 16. On the left, there is Nanofocus microscope and on the right stabilizer was located and fixed. Grinding wheel is fixed and extended through the microscope. Not moving both was so critical since they were separated. If one moves a little bit, all the locations are lost. So, it was not useful in long-term investigations. More importantly, stabilizer can only rotate around itself. It does not move along the x and y axis, so that the observable area was restricted. Due to these reasons, grinding wheel version 2 was developed.

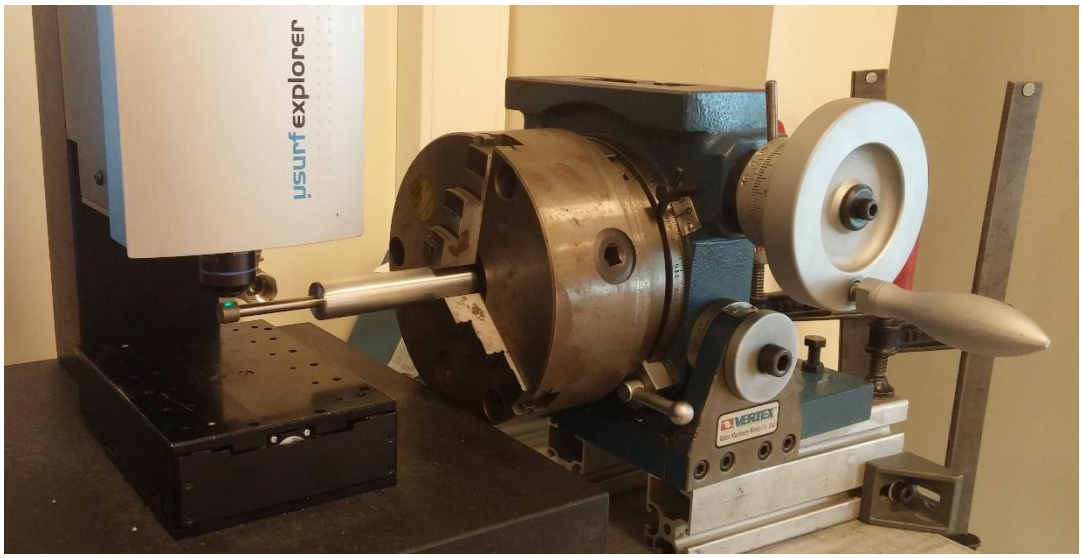

Figure 16- Stabilizer Version 1

The development of grinding wheel stabilizer version 2 was highly critical for wear investigations. It provided two very important features which were moving along the x-y axis and it was fixed to the microscope so the locations were stable. The grinding wheel stabilizer version 2 can be seen in Figure 17.

The benefits of stabilizer:

1-) 360-degree rotational observation around the wheel.

2-) Motion in x-y axis via Nanofocus (10 nanometer accuracy).

3-) Due to threading, every time the tool is located it fits the same position.

4-) Located grits can be observed after fixing the tool on or off.

Thus, it provides a total control over the wheel surface.

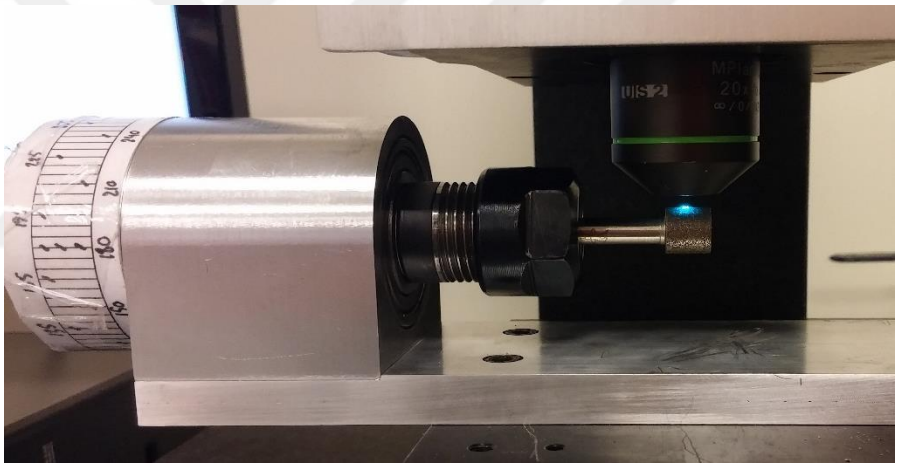

Figure 17- Stabilizer Version 2

2.3.2.3.Talysurf Surface Profilometer

In grinding operations one of the most significant thing is the quality of the surface of the final workpiece. Some parameters can affect the quality however, it is mostly determined by the surface condition of the grinding wheel. To understand the grinding wheel surface condition, its surface has been measured gradually during experiments via Talysurf. Talysurf has a 2µ diamond probe at the tip which provides accurate results.

Talysurf was used to obtain Ra and Rz values of the grinding wheel surface and the workpiece. Also, it provides 2D view of the section by tracing the tip of the probe.

Examples for surface profiles of workpiece and grinding tool measurements can be seen in Figure 18 and Figure 19.

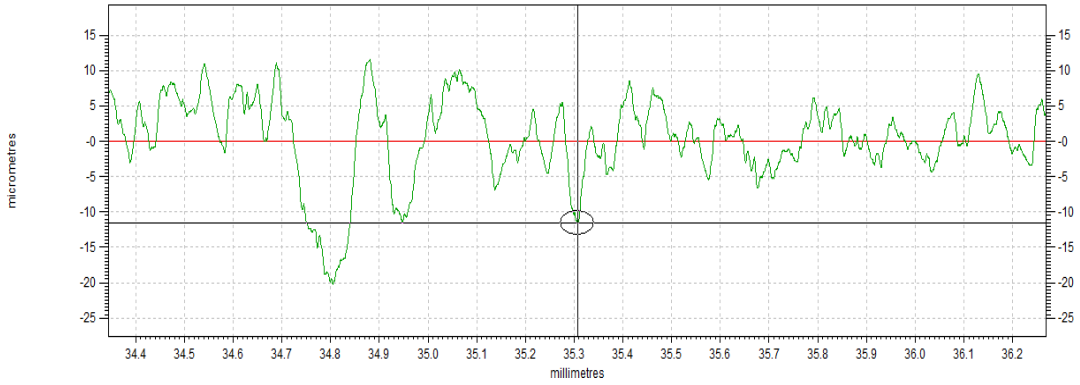

Figure 18-Surface Profile and Ra & Rz Results for Workpiece

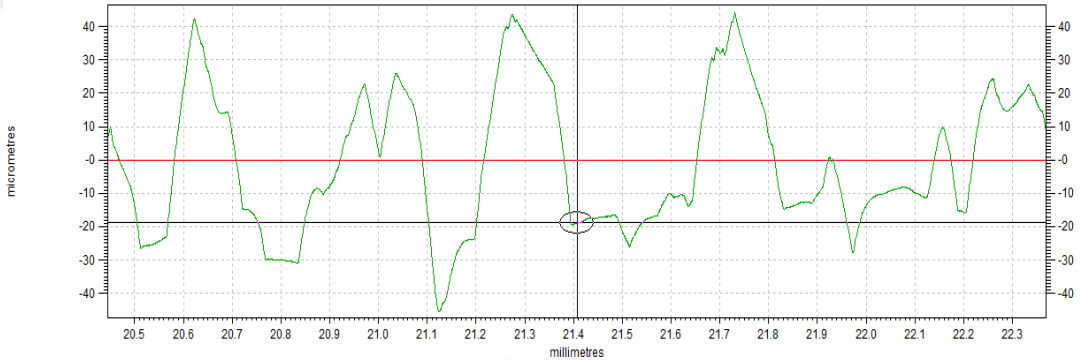

Figure 19-Surface Profile and Ra & Rz Results for Grinding Wheel

2.3.2.4.Kistler Dynamometer

Kistler dynamometer was used in the grinding experiments for force measurements. The purpose of measuring the force was to relate the wear to force increaments. After every wear test, forces was measured along the X axis (feed direction) and Z axis (surface normal direction). The abrasives are randomly distributed over the grinding wheel surface so that the wheel has not a characteristic property in Y direction (perpendicular to the feed direction). Because of the grinding wheel nature, the forces in the Y axis have not been investigated.

2.4. Experimental Investigation of Electroplated CBN Tool

In this section details of an experimental work are presented, it consists;

- Geometrical Measurements of Abrasive Grits
- Experimental Test Setup
- Spark-out Investigation
- Stepwise Force Investigation
- Observations on Change of Grit Shapes

2.4.1. Investigation of Geometric Properties of the Electroplated CBN Tool

Most of the time the grinding tool properties given by the suppliers would not be sufficient to understand the behavior of the grinding tool. Stochastic nature of the grinding wheel allows a generalization method for geometric calculations. Therefore, geometric properties of the tools are measured by μsurf Explorer Nanofocus measurement device before the experiments. These geometric properties are significant in the modeling of grinding processes. After sufficient measurements have been completed on geometric properties of the abrasives, it is possible to model the abrasive particles according to the normal distribution of geometric properties [23].

Abrasive particles have been chosen randomly on the grinding wheel surface via 50x lens. Software of Nanofocus can obtain a 3D and 2D visuals of a grit as seen in Figure 20. Moreover, software provides the geometric properties of a grit.

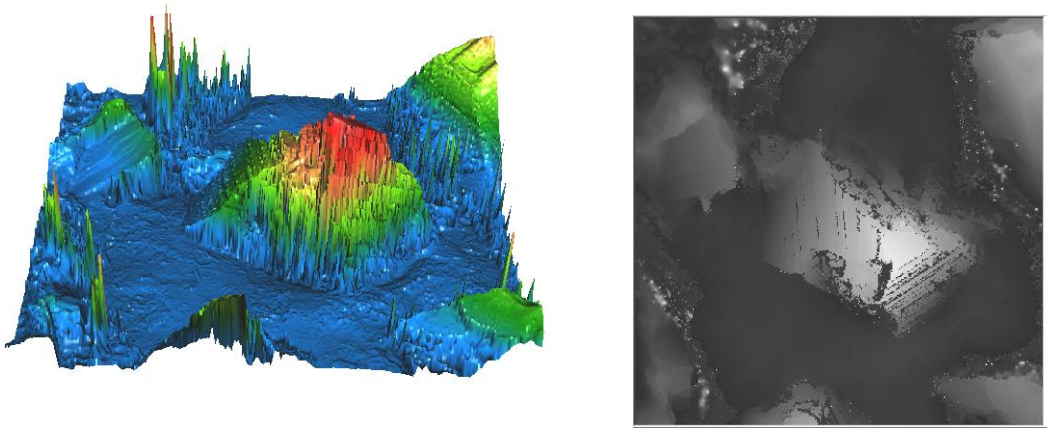

Figure 20-Individual Grit via 50x Lens

In total of 25 grits have been measured separately in terms of height, width, rake angle, oblique angle and edge radius. Nanofocus software can provide the profile of a grit that

enables to obtain its width, rake angle and height. The example measurements are given in Figure 21, Figure 22 and Figure 23. In Figure 21, a_e represents the rake angle, h1 represents the height of the grit and w0 represents the width of the grit. In Figure 22, edge radius is shown with red circle. In Figure 23, oblique angel is shown with red line. The geometric parameters were calculated considering the flow direction.

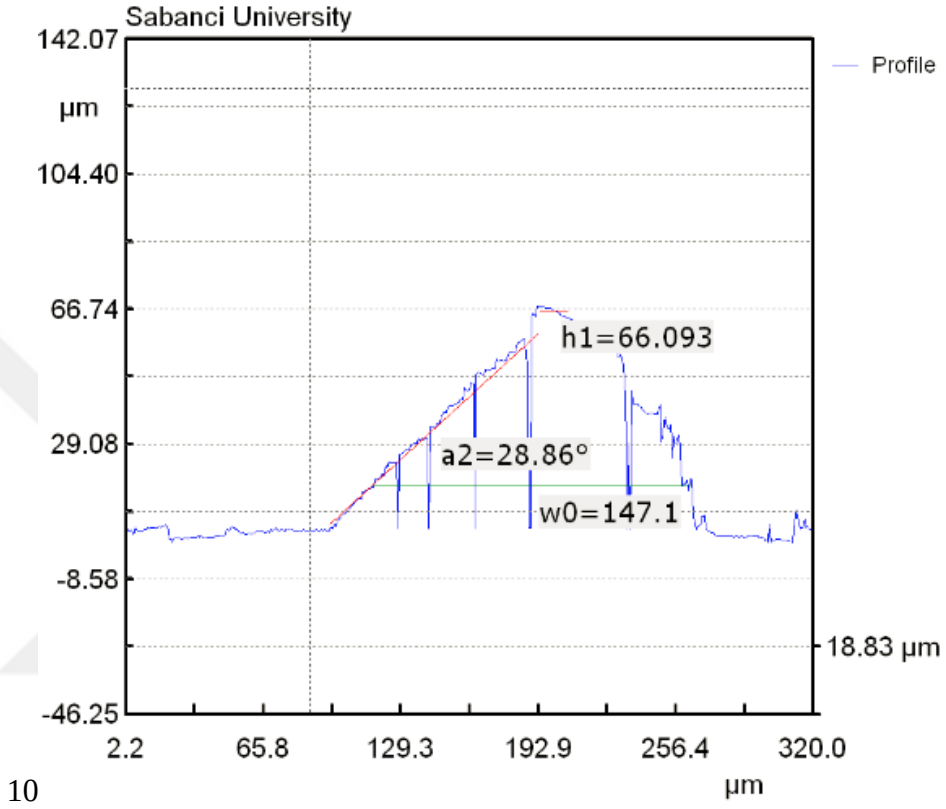

Figure 21-Geometric Properties (Height, Width and Rake Angle) of a Grit

The measurement of 25 girts have been completed individually and all their geometric properties have been obtained to be used in process models. The statistics of the results are shown in Table 1.

Statistics	Width (µm)	Height (µm)	Rake Angle (°)	Oblique Angle (°)	Edge Radius (µm)
Average	142.12	63.32	-44.92	31.82	20.98
Standard Deviation	39.23	14.86	27.53	17.62	19.99

Table 1-Statistical Information of the Electroplated CBN Grinding Wheel

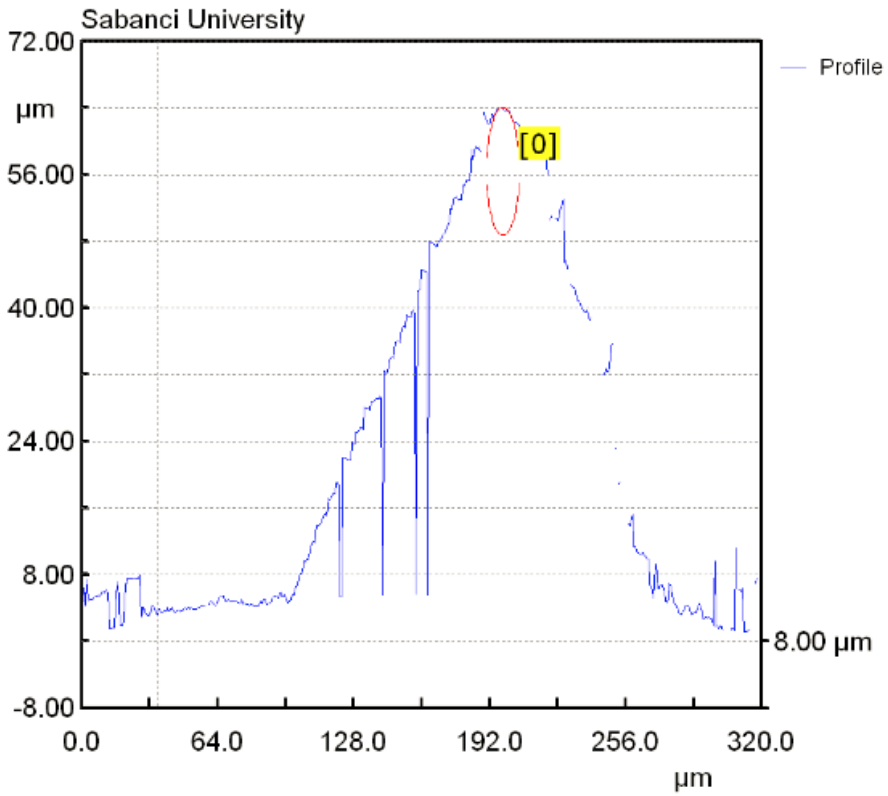

Figure 22-Edge Radius Measurement of a Grit

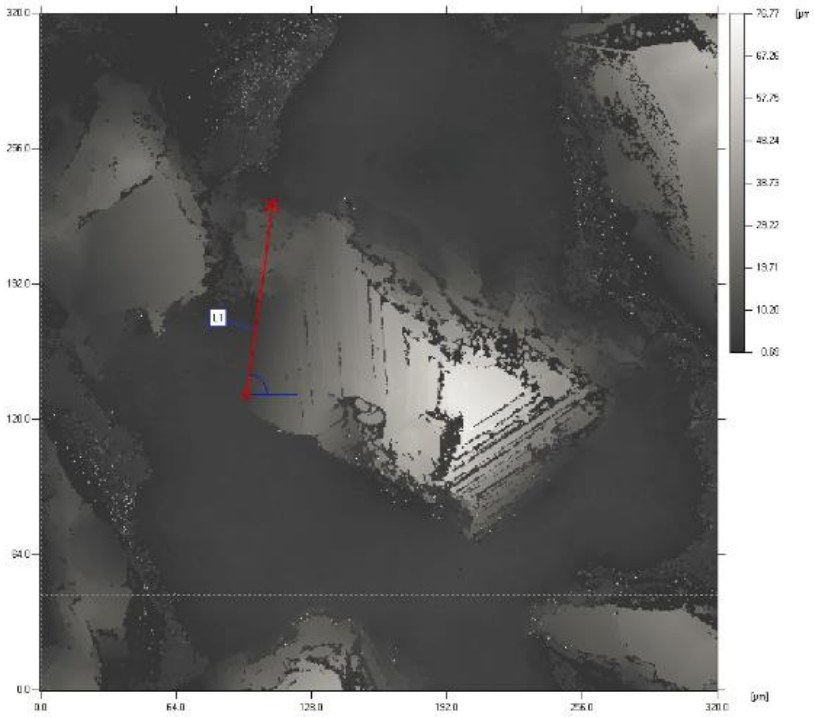

Figure 23-Oblique Angle Measurement of a Grit

2.4.2. Test Setup

Geometric characteristics of the electroplated CBN wheel has been obtained via microscope. Then a proper test setup was adjusted to perform cutting tests. The main goal of this experiment was to understand the force behavior of the electroplated CBN wheel while cutting Inconel 718 material and observing the changes on grits during the experiment. Moreover, various feed rates were used and their effect on force was investigated. The test setup was installed in grinding CNC machine and it consisted electroplated CBN grinding wheel, Inconel 718 material as a workpiece, dynamometer and coolant supplier as seen in Figure 24. By using this setup, two different test set have been conducted.

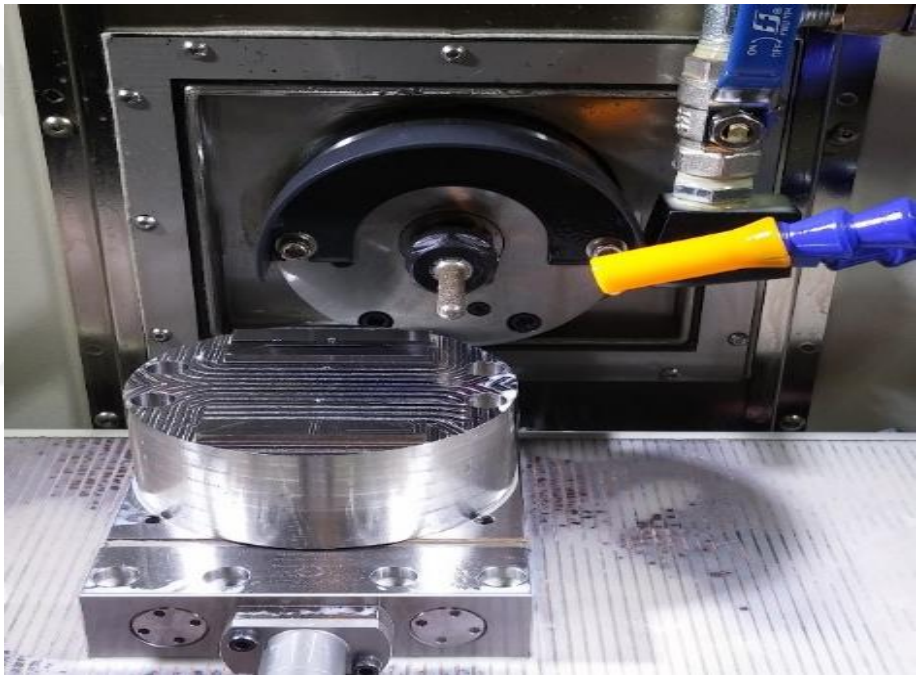

Figure 24- Test Setup for ALP Tool

Test conditions was chosen close to the real manufacturing conditions. Operation type was selected as surface grinding because the tool-workpiece interaction was easier achieve. Spindle speed and depth of cut have been kept constant at 36,000 rpm and 0.1 mm during the cutting action. Four different feed rates have been used, 150, 200, 250 and 300 mm/min. At each feed rate, cutting forces have been measured via dynamometer. Thus, ploughing forces of this tool was also obtained.

Operation Type	Surface Grinding
Cutting Type	Down Cutting
Workpiece Material	Inconel 718 (31 HRC)
Grinding Wheel Type	Electroplated CBN 120
Coolant	5% boron oil-water mixture
Spindle Speed [rpm]	36000
Feed [mm/min]	150-200-250-300
Cutting Speed [m/s]	14,25
Radial Cutting Depth [mm]	0,1
Axial Cutting Depth [mm]	10
Wheel Diameter [mm]	7,56

Table 2-Cutting Conditions and Experiment Details for ALP Tool

The tool and the workpiece have been arranged in a way that the tool tip would not participate in the cutting action because it had a spherical shape at the tip. Straight part of the tool cut the material during passes. Top view of the tool and the cutting area of the workpiece are shown in Figure 25.

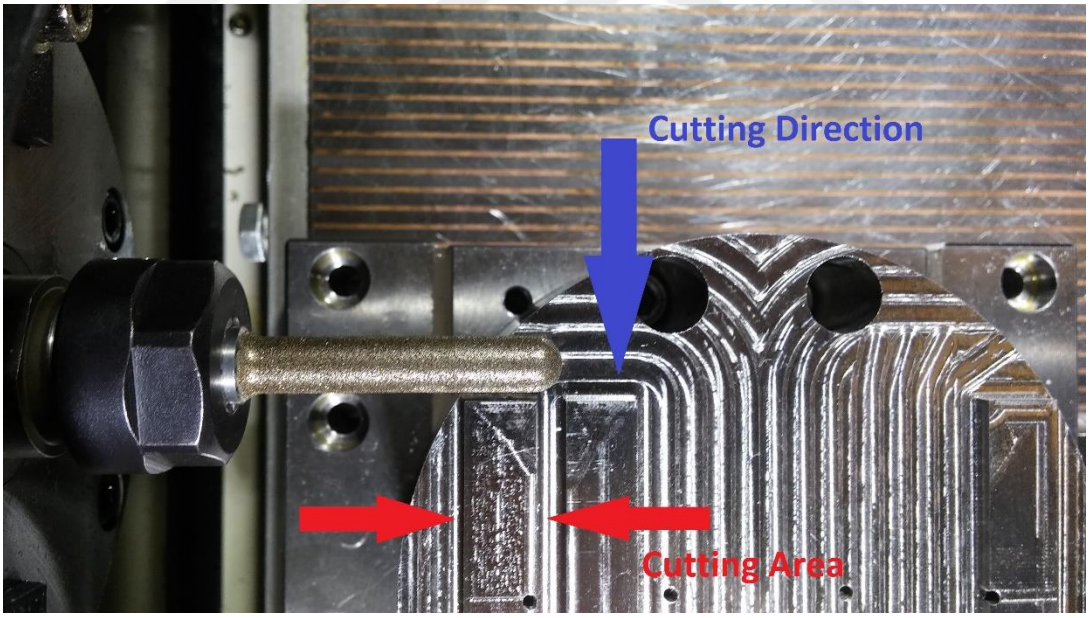

Figure 25-Feed Direction and Cutting Area

2.4.3. Test Results

Two different force test sets have been conducted. First one is the spark-out investigation and the second one is stepwise force investigation. In the first test set, spark-out investigation has been done with four different feed rate. On the other hand, second test focused on the stepwise force measurements and tool wear. Moreover, ploughing force results are also presented for brand-new tool and worn tool. Finally, change in shape for four different grits are shown.

2.4.3.1. Investigation of Spark-out

Most of the time grinding wheel can not remove the desired depth of cut in one pass. Even the desired depth of cut has been set before the pass, it is not always the case due to deflection of the wheel. So, in order to remove the desired material from the workpiece more passes are needed. These extra passes are called spark-outs. In this section, spark-out research has also been conducted. Rowe [3] has mentioned the effect of spark-out in Figure 26.

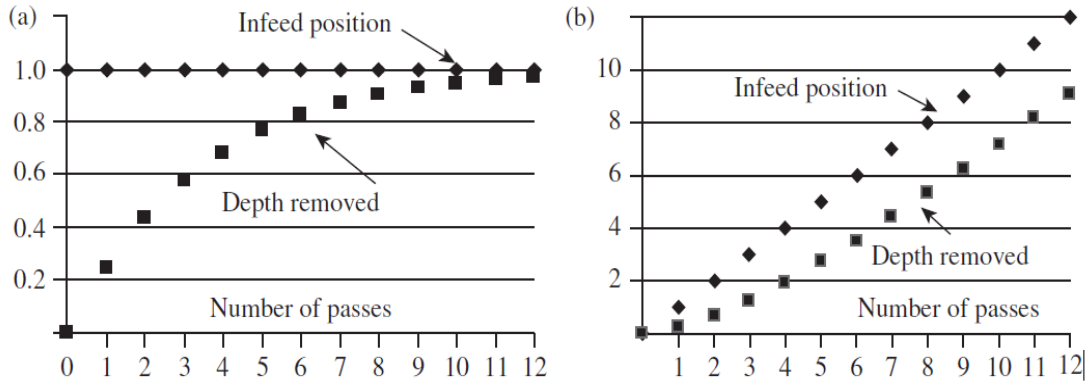

Figure 26-Effect of Spark-out [3]

Figure 26-a shows material removal amount related to the number of passes at the same depth of cut level. Even the depth of cut has been adjusted to 1.0 unit, it could only remove approximately 0.22 unit in the first pass. The remaining 0.88 unit can be removed in 11 passes. Moreover, this graph shows that first pass removes the most material compared to the other passes. On the other hand in Figure 26-b, infeed position is also changing with number of passes and result shows that the uncut material is increasing at each step. That means, if spark-out passes are not applied, the grinding wheel tries to cut more material in each further infeed position.

Spark-out experiments have been conducted with 4 different feed rates, 150, 200, 250 and 300 mm/min. The experiment started with 150 mm/min feed rate and forces have been measured in each step. First, cutting process without spark-out has been done and it was observed that at every new step the cutting forces was increasing because the tool tries to cut more material at each step. After that z-position adjusted at the same level and spark-out passes have been done. The criteria for spark-out was determined as when the measured force becomes less than 3N. 3N limit is determined because the coolant generates 3N error without the cutting action. It was observed that at 150mm/min feed rate, 2 spark-out passes were required to remove the desired material at the same cutting depth. The force results can be seen in Table 3. The blue lines are the infeed cutting actions (Z-axis is increasing). On the other hand, green lines show spark-out passes (Z-axis is stable). The decrease in the forces in spark-out passes can be seen more clearly in Figure 27.

Spark-out		Average Forces		
Test	Feed (mm/min)	Fx(N)	Fz(N)	Z-axis Position
1	150	3,2	18,6	-189,36
2	150	3,8	25	-189,46
3	150	4,3	28,7	-186,56
4	150	1,1	6,8	-186,56
5	150	0,3	2,3	-186,56
6	150	4,1	25,1	-189,66
7	150	4,6	34	-189,76
8	150	5,3	38,8	-189,86
9	150	1,7	7,9	-189,86
10	150	0,5	0,5	-189,86
11	150	4	28,3	-189,96
12	150	5	34,4	-190,06
13	150	5,2	38	-190,16
14	150	1,5	10,1	-190,16
15	150	0,2	2	-190,16

Table 3- Force Results for Spark-out with 150 mm/min

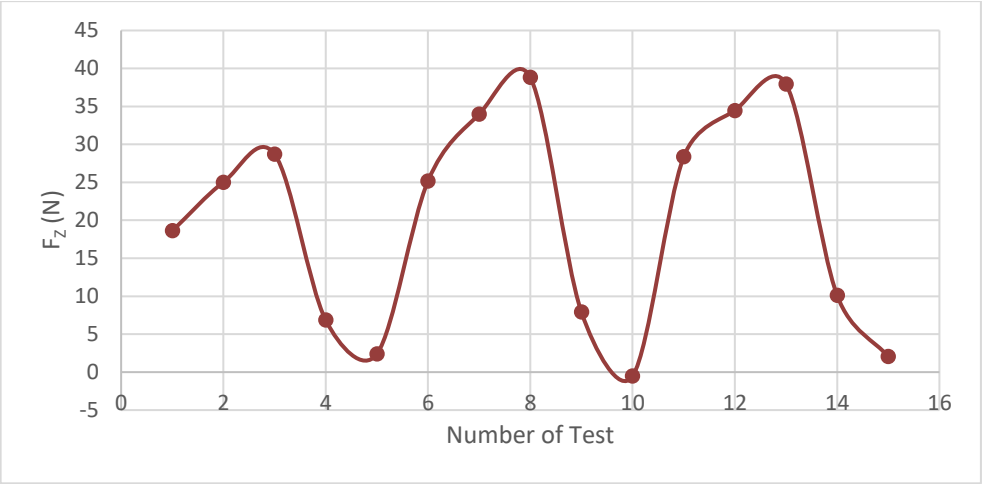

Figure 27-Spark-out Investigation for 150 mm/min Feed Rate

The same process has been conducted for 200, 250 and 300 mm/min feed rates. The test results are shown in below figures and tables.

Spark-out		Average Forces		
Test	Feed (mm/min)	Fx (N)	Fz (N)	Z-axis Position
1	200	11,6	37	-191,25
2	200	4	11,2	-191,25
3	200	0,5	0,9	-191,25
4	200	10,2	30	-191,35
5	200	3,4	11,3	-191,35
6	200	0,5	0,8	-191,35

Table 4- Force Results for Spark-out with 200 mm/min

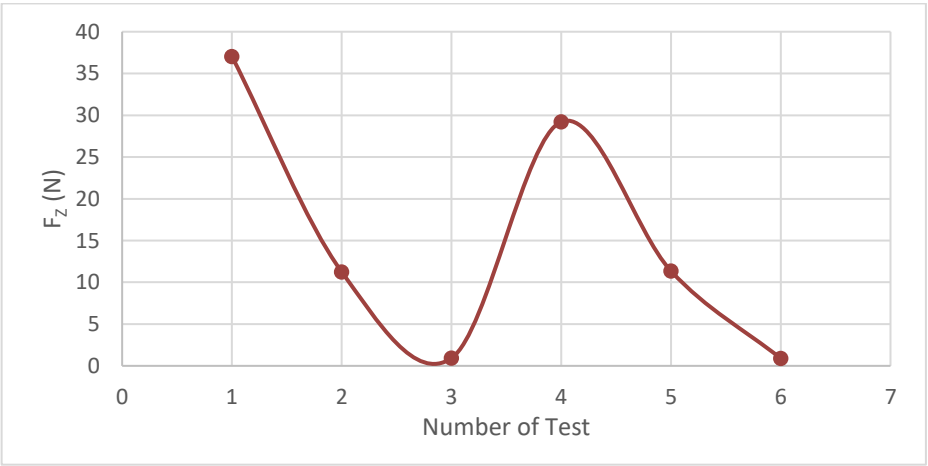

Figure 28- Spark-out Investigation for 200 mm/min Feed Rate

Spark-out		Average Forces		
Test	Feed (mm/min)	Fx (N)	Fz (N)	Z-axis Position
1	250	13,3	39,5	-191,45
2	250	5,1	13,4	-191,45
3	250	3,2	7,2	-191,45
4	250	1,4	1,8	-191,45
5	250	14,4	44,2	-191,55
6	250	5,6	13,8	-191,55
7	250	3,4	7,6	-191,55
8	250	1,8	1,9	-191,55

Table 5- Force Results for Spark-out with 250 mm/min

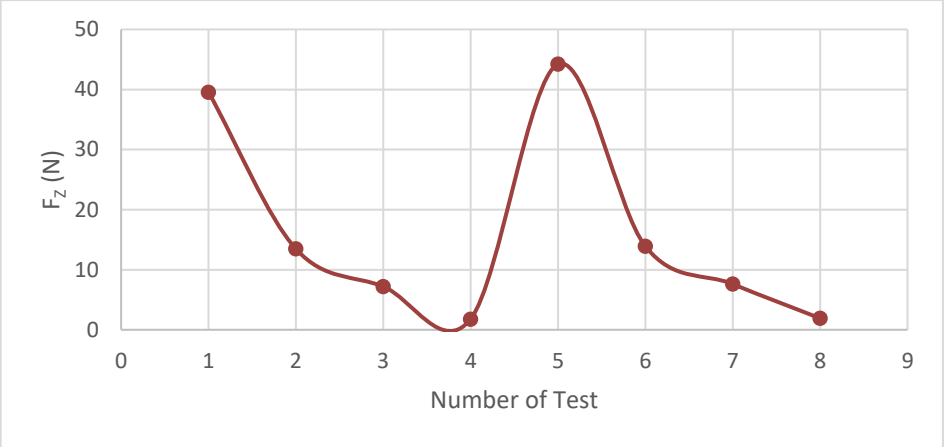

Figure 29- Spark-out Investigation for 250 mm/min Feed Rate

Spark-out		Average Forces		
Test	Feed (mm/min)	Fx (N)	Fz(N)	Z-axis Position
1	300	15,3	45,9	-191,65
2	300	6,3	18,6	-191,65
3	300	3,9	6,9	-191,65
4	300	0,9	4,7	-191,65
5	300	1,2	2,3	-191,65
6	300	15,1	44,5	-191,75
7	300	5,8	14,3	-191,75
8	300	2,2	4,6	-191,75
9	300	1,8	5,8	-191,75
10	300	0,1	0,6	-191,75

Table 6- Force Results for Spark-out with 300 mm/min

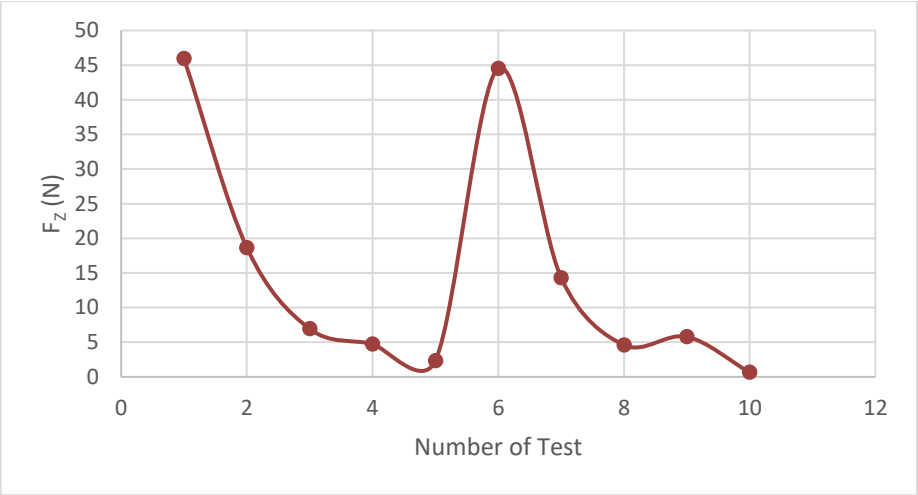

Figure 30- Spark-out Investigation for 300 mm/min Feed Rate

The test results show that, 200 mm/min feed rate also requires 2 spark-out passes. When the spark-out force results are compared for 150 mm/min and 200 mm/min feed rates, forces in 200 mm/min was higher. On the other hand, spark-out force results for 250 mm/min feed rate was higher than the 150 mm/min and 200 mm/min, also it required 3 spark-out passes to reset the surface level. In addition, 300 mm/min feed rate needs 4 spark-out passes and its spark-out force results were the highest among the others. There are two main reasons for high spark-out forces. First one is that high feed rate results in high force and the second one is due to the remaining uncut material from the previous pass.

The spark-out-feed rate relation is shown in Table 7. When feed was increased, spark-out number was also increasing, because increasing feed decreased the material removal amount in one pass and more material remains on the surface of workpiece. To conclude, in the cutting processes with high feed rates, if spark-out passes was not taken into consideration, the remaining uncut material amount will increase in each step and that may break the tool.

Feed (mm/min)	150	200	250	300
Number of Spark-Out Passes	2	2	3	4

Table 7-Spark-out and Feed Relation

2.4.3.2. Stepwise Force Investigation:

Methodology:

The main purpose of these experiments was to observe the effect of wear on cutting forces. Moreover, wear types were also investigated. Inconel 718 with 31 HRC material has been used as a workpiece. The cutting type was down cutting and 5% bore-oil mixture has been used as a coolant. The tool had 7.56 mm diameter and with the 36k rpm, it reached 14.25 m/s cutting speed. Feed was set to *250 mm/min*.

Test was divided into 7 steps. It mainly contains measurement of the tool, ploughing and cutting tests.

First step: Measurement of the Tool1

Second Step: Ploughing Force Test1

Third Step: Stepwise Force Measurement Test1

Fourth Step: Measurement of the Tool2

Fifth Step: Stepwise Force Measurement Test2

Sixth Step: Ploughing Force Test2

Seventh Step: Measurement of the Tool3

Force Results:

The first test set has been conducted 26 times by moving 0.1 mm deeper in each step. During the cutting experiments, force has been measured at every new cutting depth. Spark-out passes have not been performed.

Figure 32 shows the force results in normal direction. It is obvious that it has an increasing behavior. However, it is not possible to totally distinguish the reasons for the force increment. There are two main reasons for that. The first one is tool has worn during the cutting action and it caused a rise in the force. The second one is the uncut material has been increasing at each step because spark-out passes have not been performed. So that tool tried to cut more material at each step.

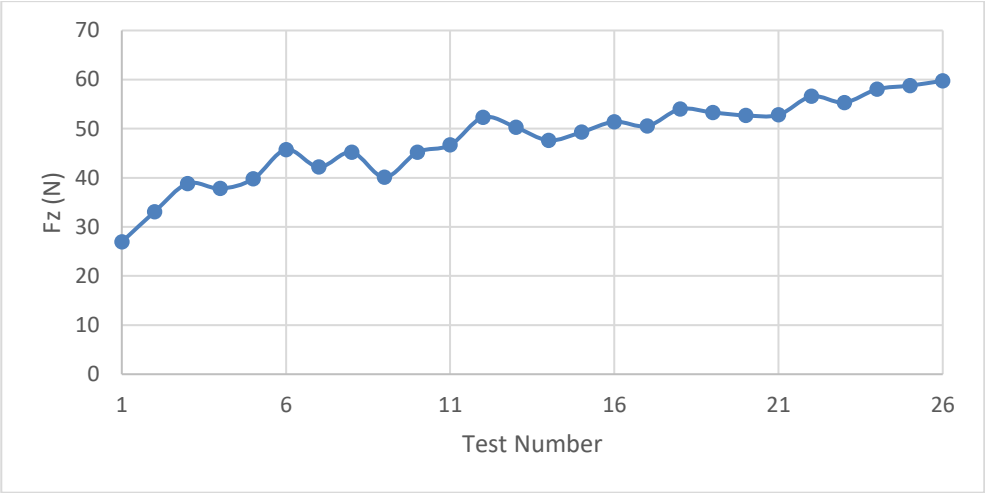

Figure 32-First Test Results

The ploughing forces have been found by using linear regression method. The ploughing forces have been investigated as before and after the tool wears. 4 different feed rates were used; 150, 200, 250, 300 mm/min. The ploughing forces in Z-axis found higher. The results are shown in Figure 33 and Figure 35.

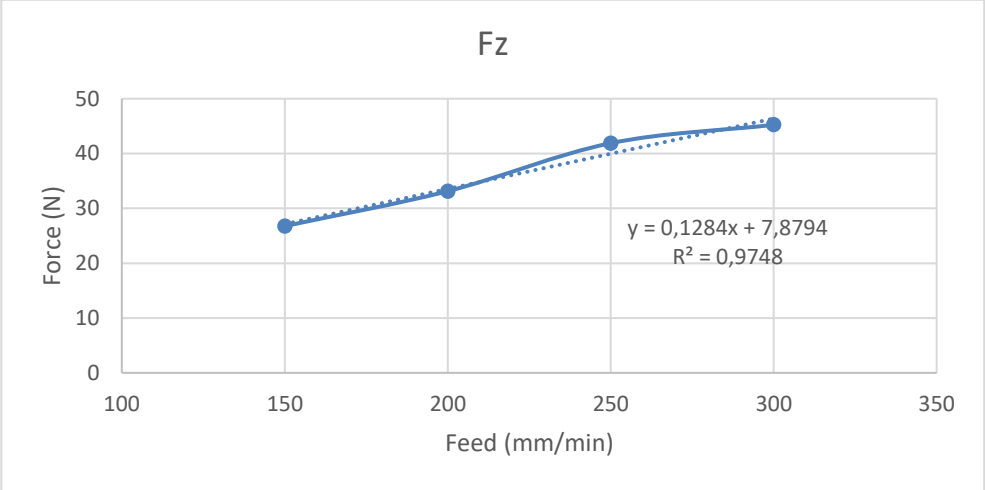

Figure 33- Ploughing Forces Before Tool Worn

Second test set includes 18 step. Same process for first set has been applied. Similar to the first test, force results show an increasing behavior as seen in Figure 34. Since all the parameters have kept constant, the reason for increase in force is mainly wear.

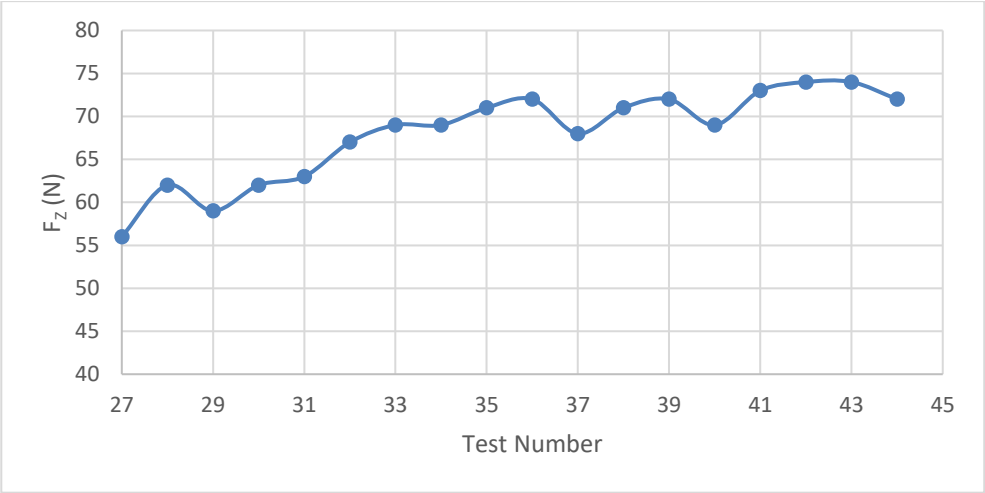

Figure 34-Ploughing Forces After Tool Worn

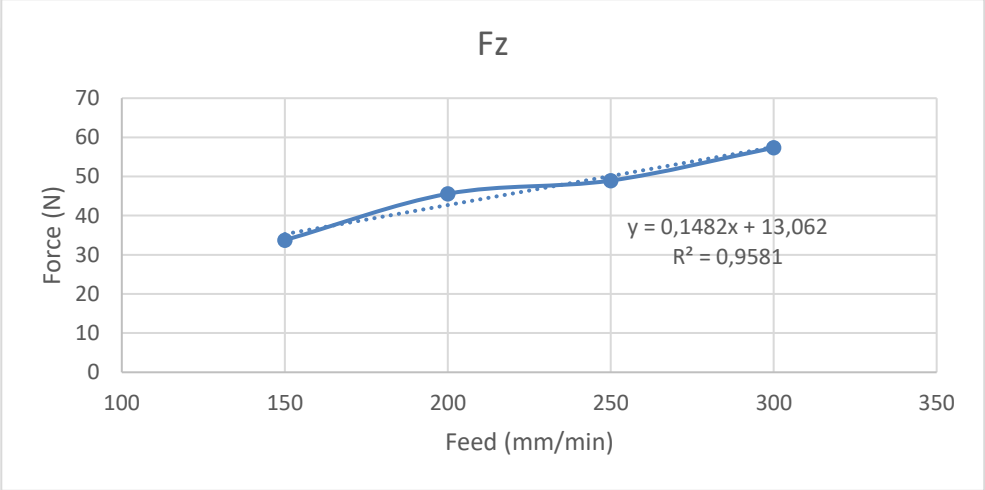

Figure 35-Second Ploughing Test Results

Comparison of Ploughing Forces for Brand-new Tool and Worn Tool:

As it is seen in Figure 33, increase in feed rate causes an increase in average force results in x-direction (feed direction). There are both ploughing and cutting forces in the measured force results. In order to distinguish these forces linear regression method was used and it was also shown in the Figure 33. Theoretically ploughing force is not related to feed rate. Its effect on measured forces would be the same as it is shown in Figure 33. Thereby, ploughing force was calculated and then extracted from the measured forces to obtain cutting forces.

The forces in axial direction has been occurred due to the oblique angle of the particles. However, oblique angles are distributed totally random over the surface so that, it has not a logical behavior. They may be in the +y or -y direction. Thus, they cancel each other. The forces in axial direction (y direction) are low compared to the other directions so that they are not taken into consideration.

On the other hand, the forces on the z-direction (normal to the workpiece surface) seemed to be the highest force among the all axis. F_z was totally related with the feed rate and it showed an inclination when feed was increased.

In the first test, ploughing forces have been found as 0, 0.25, 7.87 N in x, y and z axis respectively. First test represents the initial state of the tool which can be considered as brand-new tool. Then, some more cutting tests have been conducted and tool has become worn.

Second test represents the worn tool state and an increase in ploughing force results have been seen. Ploughing forces have become 4, 2.2, and 13 N in the worn state. Thus, when the tool is used, it loses some active grits on the surface and becomes dull. Ploughing forces have been increased.

	Ploughing Forces (N)		
	x	y	z
Test 1	0	0,25	7,87
Test 2	4,09	2,21	13,06

Table 8- Ploughing Force Investigation

Observations of the Grit Shapes:

The wear mechanics over the grits have been measured by 50x lens via Nanofocus. Before the tests there have been 4 grits determined to be investigated and their locations were recorded. After wear tests, their conditions have been measured. These 4 grits are given in Figure 36, Figure 37, Figure 38 and Figure 39 corresponds to 0, 90,180 and 270 degrees around the wheel. Even the grits were chosen randomly, grits were selected homogeneously-distributed around the wheel to obtain accurate results. In the given below figures, the picture on the left shows the initial state of the grit, and second and third states are shown nearby. Colors show the height distribution on that region.

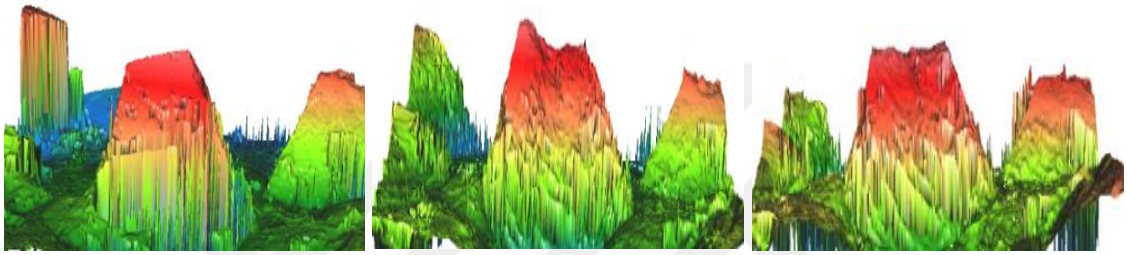

Figure 36- Grit @0°

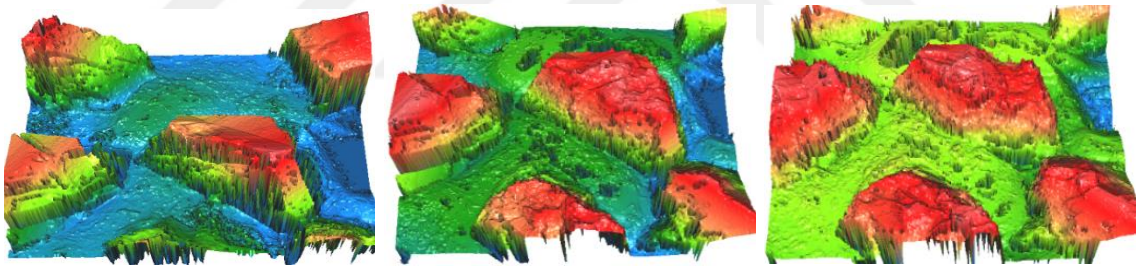

Figure 37- Grit @90°

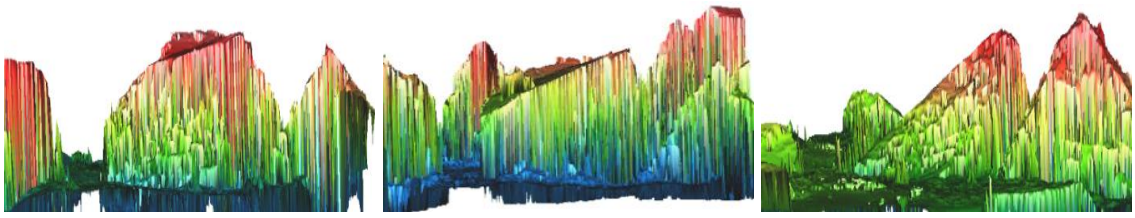

Figure 38- Grit @180°

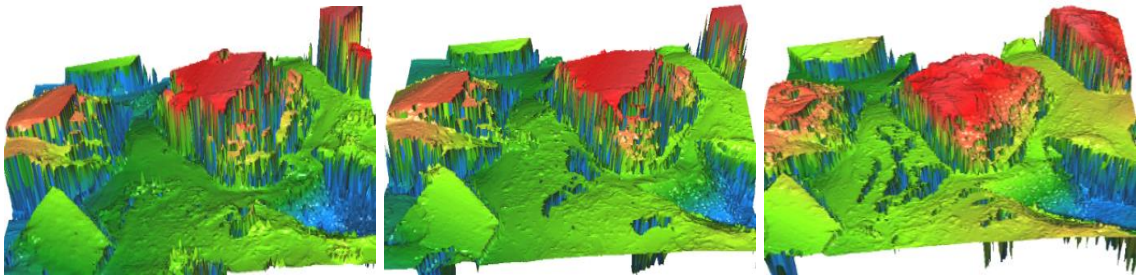

Figure 39- Grit @270°

It is obvious from the above figures that the located grits have been affected by wear. In Figure 36, at the first sight it had a micro fracture and then attritious wear was observed. In Figure 37 and Figure 39, attritious wear is more dominant because they have a flat shape. However in Figure 38, macro fracture was observed and huge amount of the grit has been lost. More detailed analysis of the wear effect on the grits is presented in the following sections.

2.5. Summary

In this chapter, experimental investigations on grinding processes was explained in detail. The objective of this chapter is to give an opinion about the grinding processes before go into the details of wear analysis. Chapter starts with the brief information section about the cutting action of the grinding processes. Then, CNC machine and the other measurements devices that have been used in this research have been explained with their benefits and usages to the whole study.

Details of an experimental work has been expressed with steps. First, geometrical measurements of abrasive grits have been mentioned. The geometrical properties such as rake angle, oblique angle, nose radius, height and width were expressed by showing their measuring techniques. After that, several tests were conducted to analyze force behavior. A detailed spark-out investigation was presented. It was found that *increase in feed rate advanced the required number of spark-out passes*, because one grinding pass with a high feed rate has low capability of removing material compared to the low feed rate. Then, stepwise force investigation was introduced and increasing force behavior of the tool was observed due to wear. Ploughing force were analyzed as before and after the tool wears. It was seen that after the tool has worn, *ploughing forces were increased* in all axis. Finally, some grit shapes have been recorded before the tool was used. Their

geometrical shapes were briefly investigated considering wear behaviors. Attritious wear and fracture were presented shortly.

3. WEAR MECHANISMS

3.1. Introduction

In this chapter, wear mechanisms of electroplated CBN grinding wheels have been investigated. Chapter starts with a brief information about the differences between multi-layer (bonded) and single-layer (plated) wheels in terms of wear mechanisms. Then, the details of the experiments that have been conducted with electroplated CBN wheel were presented. Effect of wear on *grit shapes*, *cutting forces* and *surface parameters* were shown. One of the important things about this study is that the changes on grits have been observed *individually*, which is not common in the literature.

Wear mechanisms on grinding wheels depend on many factors. For example, wheel type, bond type, abrasive type, size of the wheel etc. can be considered as the wear mechanisms due to the nature of the wheel. On the other hand, dressing and truing conditions, cutting speed, feed rate, depth of cut, selection of coolant etc. can be regarded as external factors that affect the wear mechanisms of the grinding wheel.

For conventional bonded wheels, wear mainly occurs due to grit breakage, bond breakage and abrasive wear. These mechanisms and more can be seen in Figure 40. In addition to these, during grinding action some of the workpiece material fills the pores at the wheel surface and make it blunt which cause an increase in the grinding force. In that case, dressing should be applied and new fresh surface should be obtained. Otherwise, surface burns may occur at the workpiece surface due to high friction. Dressing lines can be seen at the wheel surface due to filled material in Figure 41. Wear behavior of the conventional grinding wheel is fully dependent on the dressing conditions [24].

Single-layer electroplated CBN grinding wheels have been used in our experiments and dressing of them in not possible due to their single layer formation. However, they can be trued for some specific applications to decrease eccentricity. Whereas, truing process is not desired in our research since abrasives are the only particles that make the cutting action. Thus, losing some part of them decreases the cutting-edge capacity. Because motivation of this research is not only focusing the finishing process but also the roughing process is important.

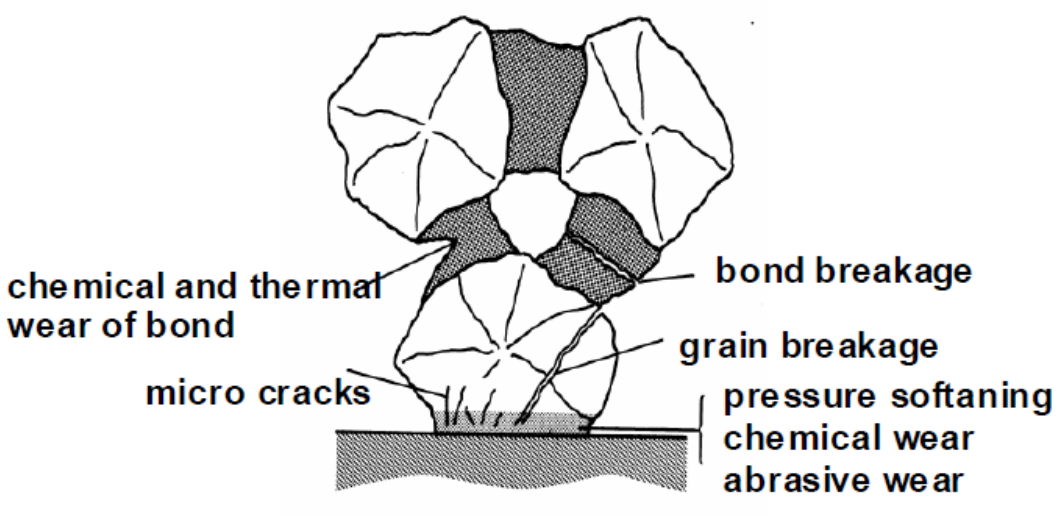

Figure 40-Wear Types for Bonded Wheels

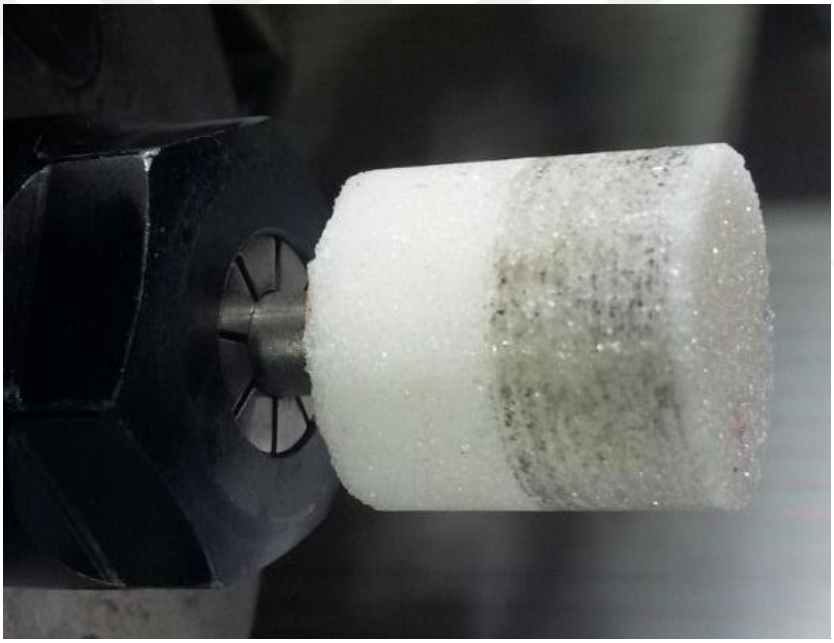

Figure 41-Filled Wear Example for Conventional Wheels

Wheel wear in grinding is a sophisticated phenomenon which can affect the whole grinding process profoundly. In this chapter, wear mechanisms of an electroplated grinding tool have been investigated in detail. The objective is to understand the effect of the wheel-workpiece interaction on the grits by investigating wear behavior *individually*. The effect of wear mechanisms on the grinding forces and the workpiece surface have been taken into account. Surface grinding experiments were conducted on Inconel 718 workpiece and the change in the wheel topography and the grinding

behavior were investigated. Since cutting force is an important indicator of wear mechanism [7], force measurements are used to monitor the wear. Material properties of Inconel 718 with a density of 8190 kg/m^3 is provided in Table 9 [6].

Property	Value
Tensile Strength	1365 MPa
Yield Strength	1034 MPa
Elasticity Modulus	206 GPa
Shear Modulus	100 GPa
Poisson Ratio	0.26
Elongation	12%
Reduction in Area	15%
Specific Heat Capacity	435 J/kg*K
Thermal Conductivity	11.4 W/m*K
Melting Temperature	1265 °C

Table 9-Mechanical and Thermal Properties of Inconel 718

3.2. Experimental Set-Up

In order to investigate the wear mechanisms of electroplated CBN wheels, surface grinding tests have been carried out on a Chevalier Smart B818III grinding machine while applying a 5% water-oil mixture. The tests were conducted on Inconel718 specimen with the dimensions of 55mm in length and 7mm in width which is shown in Figure 42-a. Table 10 shows the cutting conditions and detailed properties of the workpiece and the wheel. Cutting conditions have been specified according to literature and previous experiences [7, 8, 19, 17].

Workpiece	Inconel 718 (31 HRC)
Wheel	Electroplated single layer 120 grit CBN wheel with diameter of 10 mm, width of 8 mm
Cutting speed [m/s]	18.85
Feed rate [mm/min]	250
Depth of cut [mm]	0.1
MRR [mm^3/s]	2.92
Specific MRR [mm^2/s]	0.42

Table 10- Cutting Conditions and Wheel & Workpiece Properties

The grinding tests were conducted for 150 passes. The number of passes has been determined according to the force and wear results during the tests. When an increase of 15% was observed in the force, the test was stopped and the wheel surface was measured. Grinding forces in feed and radial directions were measured by a Kistler dynamometer during every pass and average of the force data was used in order to see the effect of the wear on the force.

After 10, 25, 40 and 75 passes the grits of the wheel were observed via Nanofocus microscope and compared with the initial condition of the wheel. For this purpose, 30 individual grits were chosen randomly, and at every 10, 25, 40 and 75 passes (henceforth referred to as step) the same grits were investigated on the microscope with magnification of 50 (0.1024 mm^2). The purpose of this measurement is to observe the specific changes on the grits individually. These changes are classified as fracture, attritious wear of the grit and no change. If the height of the grit is reduced and it has a flat rough surface, it is classified as attritious wear which can be seen in Figure 48. If some part of the grit has been destroyed, it is classified as fracture which can be seen in Figure 47. Also height changes of the grits were calculated by measuring surface and the tip of the flat face of the grits in order to observe radial wear. Observation of the same grits individually after each step is a direct method to see the more precise effect of workpiece-wheel interaction on the grits which was applied in this experimental work. Figure 42-b shows the setup in order to see the same grits after each step where the green light shows the focused area on the wheel. This setup provides a 360^o peripheral view of the wheel so that the whole peripheral surface can be seen step by step.

Furthermore, in order to observe the effect of the workpiece-wheel interaction on a larger area, lower magnification was also employed using a 20 x lens (0.64 mm^2 field of view). 10 areas were chosen and similar to the observations made in case of 30 individual grits, the same area was investigated after each step. This magnification was carried out in order to investigate pullout mechanism of the wheel. Pullout mechanism has been measured by analyzing the changes in reflection of the light on the grits. The black and grey colors indicate grits and ground, respectively. Here, ground refers to the measurement surface. If reflections were observed lower than the near ground reflections, that grit was called a pullout. Because of the circular shape of the wheel, it is not possible to focus whole area in one frame. Thus, all black dots have been investigated individually. During this method, when every point was selected on the surface, all other points as high as the selected point will be displayed with red color. Mentioned measurement can be applied to compare the level of grits. As is shown in Figure 43, due to black color of displayed grits between red area, concludes that this grit is not at the same level as red area. In addition, when the mentioned grit is selected as the level of measurement, it was found to be at same level as the point previously perceived as being at lower level.

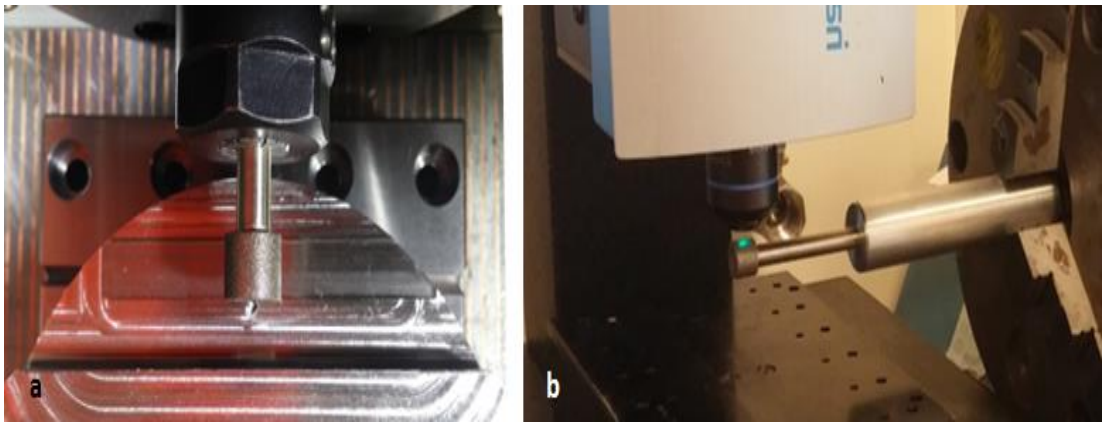

Figure 42- a) Test Setup, b) Nanofocus Measurement Setup

Surface roughness (Ra and Rz) of the wheel and the workpiece have also been measured after every step via Talysurf surface profile measurement device. By measuring the wheel surface profile, radial wear can be identified. Measuring height change of the grits individually can also be used to determine the radial wear. Both methods provide close results for radial wear.

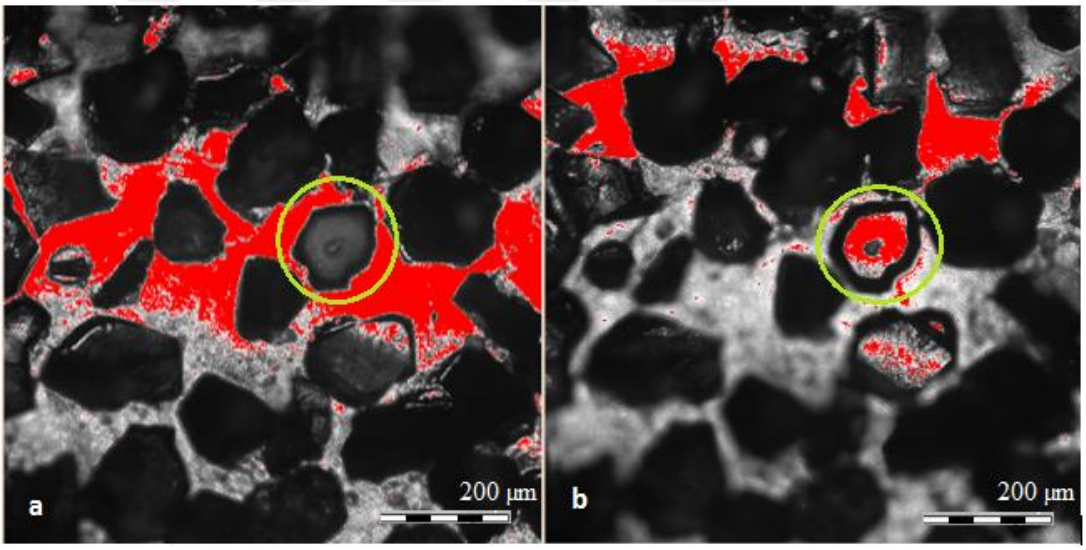

Figure 43-Pullout Measurement; a) Focused on Higher height, b) Focused on Lower Height

3.3.Pullout Mechanism

In Figure 44, surface topography is given after each step where a step consists of a specific number of passes as defined earlier in experimental setup. During individual investigation of the black areas, some black points were found to be lower than the surface, so their condition needed to be further evaluated. In order to examine the same, a comparison of the wheel surface after every cutting test was made by marking the black dots with two different colors. If a black point was found as being lower than the

surface, it was represented through a turquoise dot. If the point was found to be higher than the near ground it was marked with a blue dot. The increase in the turquois dots can be seen clearly in Figure 44.

AMR (mm^3)	0		385		1347.5		3272.5		7892.5	
Position	Grit	Pullout	Grit	Pullout	Grit	Pullout	Grit	Pullout	Grit	Pullout
0	29	0	28	1	28	1	28	1	28	1
36	31	0	27	4	26	5	25	6	25	6
72	27	0	26	1	26	1	25	2	25	2
108	25	0	22	3	21	4	21	4	21	4
144	27	0	26	1	26	1	24	3	24	3
180	25	0	25	0	25	0	25	0	24	1
216	32	0	30	2	29	3	29	3	29	3
252	29	0	28	1	24	5	24	5	24	5
288	31	0	24	7	24	7	23	8	23	8
324	23	0	20	3	20	3	20	3	20	3
TOTAL	279	0	256	23	249	30	244	35	243	36

Table 11- Grit and Pullout Numbers in 0.64 mm^2 Area After Each Step

Grit and pullout numbers are given in Table 11 for 10 different selected areas. Although all pullout numbers at the beginning seem zero, initial condition of the tool has some pullouts. While counting the grits, initial pullouts have considered as none and counting of pullouts started after first cutting test. It can be observed that in some regions there is almost no pullout.

Figure 45 shows the number of grits pulled out during the tests. It can be seen from the figure that in the initial stages corresponding to low accumulated MR, there are considerably large number of pulled out grits in a short time. After some time, number of pulled out grits saturates as there are almost no grits pulled out during the remaining passes. This can be explained by this fact that there is a low bonding force between some grits and the wheel due to the manufacturing process of the wheel and they are pulled out due to the grinding forces acting on them.

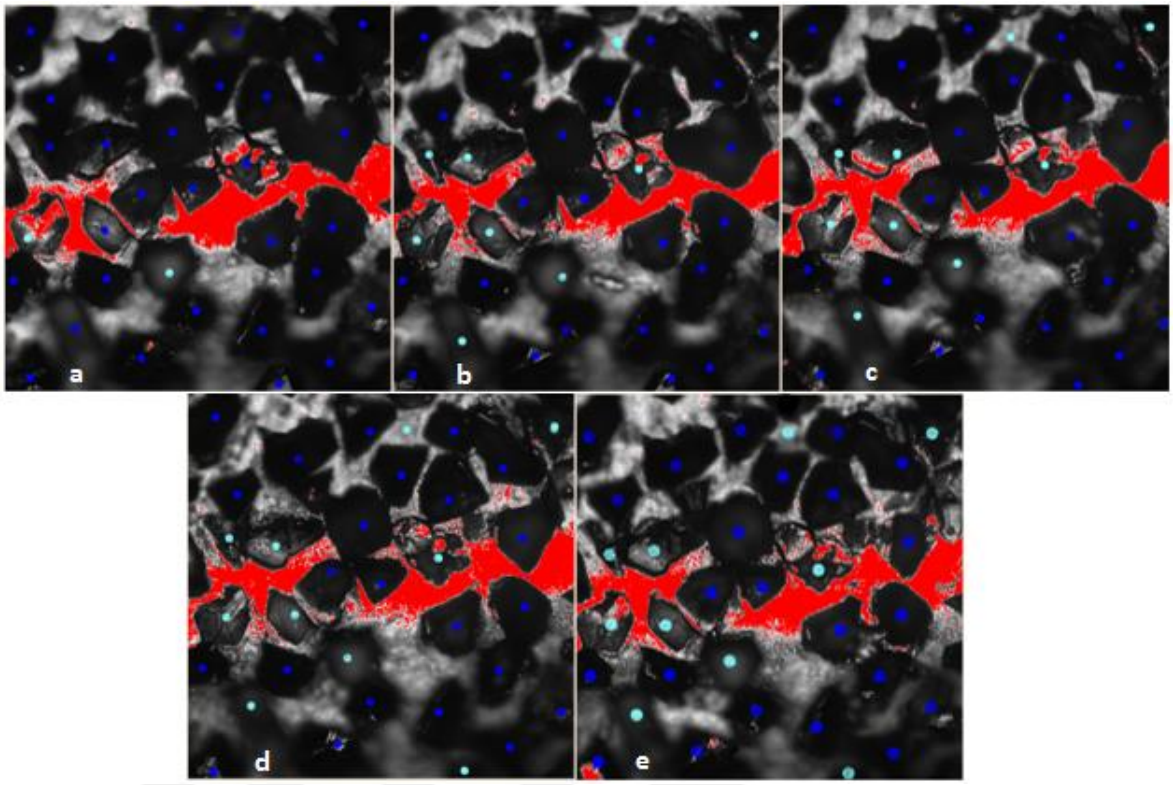

Figure 44- Pullout Mechanism in Steps; a)Before Test, b)After 10 passes, c)After 35 passes, d)After 75 passes, e)After 150 passes

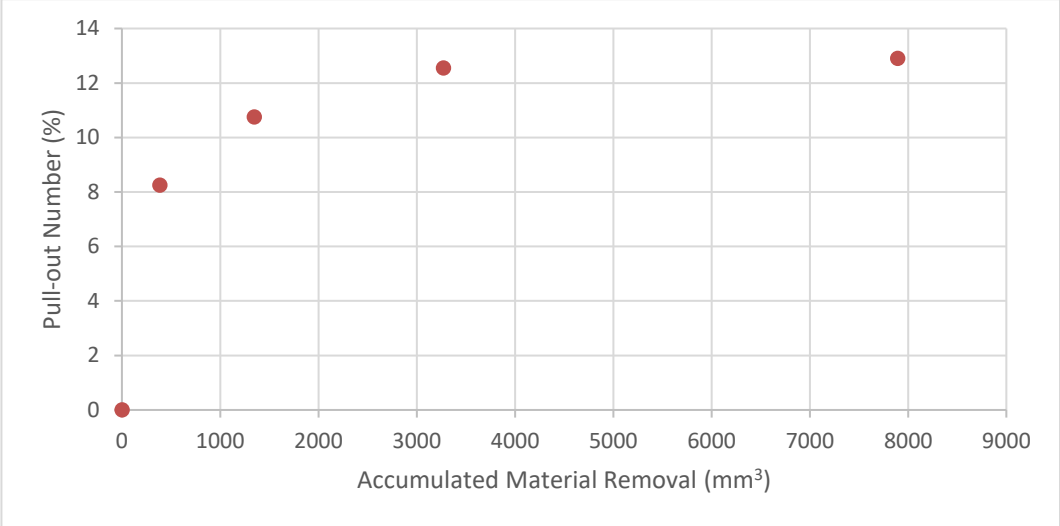

Figure 45- Change in the Pullout Number

3.4.Individual Grit Investigation

An individual investigation has been conducted on selected grits. An example for a randomly selected grit can be seen in Figure 46. Figure consists front views and top views of the grit for each step. First step represents the initial state of the grit and it had 64µ height. After some cutting process, attritious wear has been observed and its height decreased to 58µ. In the third phase a macro fracture can be seen with a very short

height change. In fourth step, grit preserved its shape however, it lost some of its height and reduced to 46μ. In the fifth step, its height decreased to 44μ without a huge change. By looking this phase change, we can say that some grits may have both attritious wear and fracture during its lifetime.

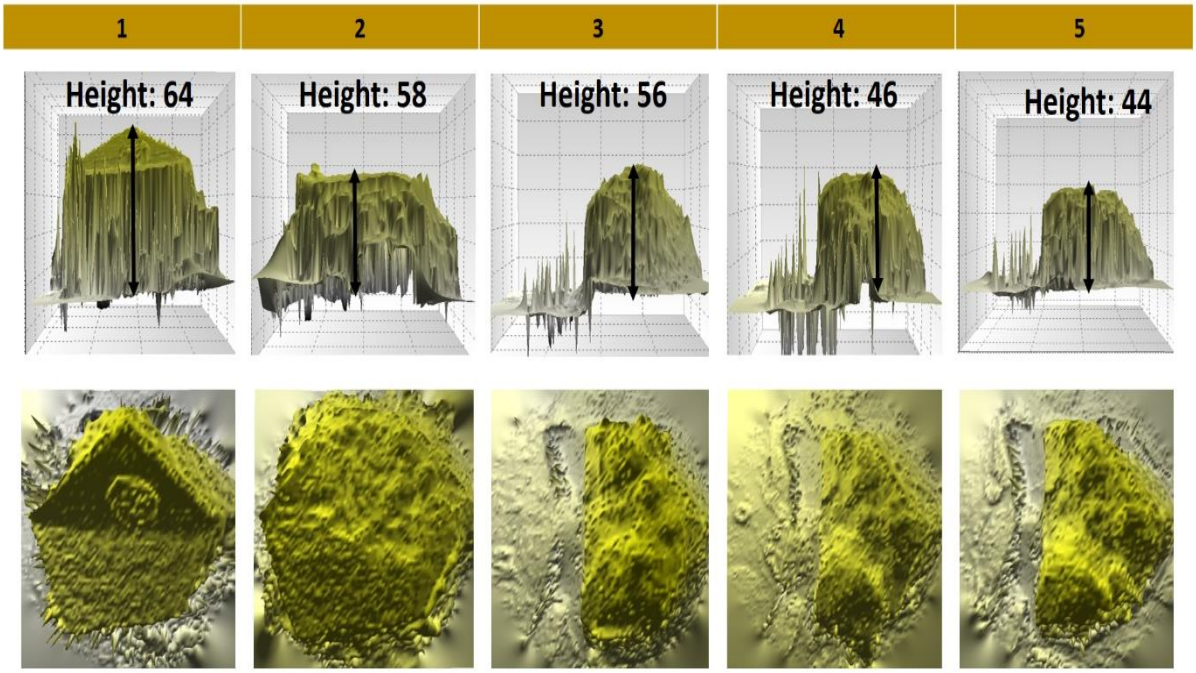

Figure 46- Phases of a Grit

3.5. Fracture Mechanism & Attritious Wear

Fracture mechanism is defined as losing some part of the grit. After investigation of 30 grits, it was observed that while some of them had attritious wear, some others had fracture and some did not change at all. Among the investigated grits, 14.7% of them seemed to have fracture after 150 passes. Fracture mechanism can be seen in Figure 47. On the other hand, it was observed that 61.8% of the grits had attritious wear. Their heights were shortened 27% after 150 passes and had rough flat top section. The reduction of the height can be seen in Figure 48. The initial and the last state of one grit is given and the destroyed part of the grit is shown. The percentage distribution of attritious and fracture wear mechanisms are shown in Figure 49.

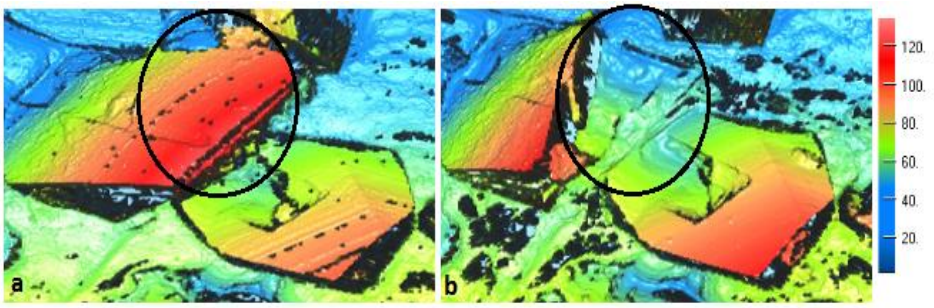

Figure 47- Fracture On a Single Grit; a) Initial State, b) After 150 Passes

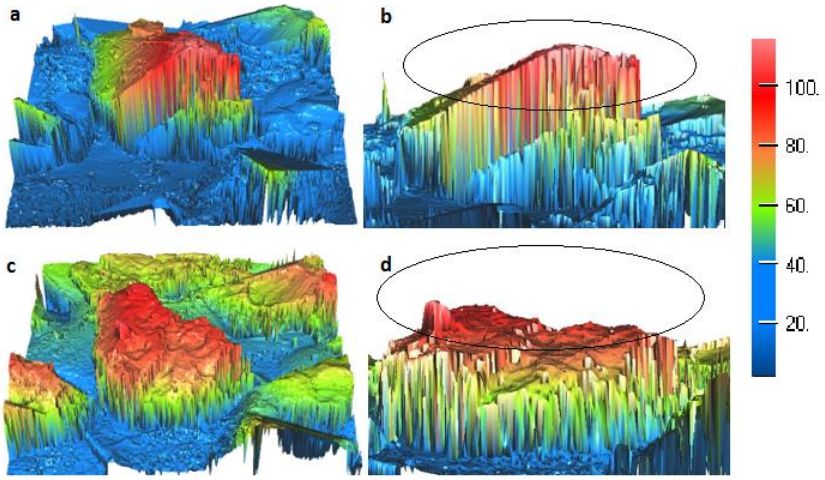

Figure 48- Attritious Wear on a Single Grit; a) Initial State, b) Front View of Initial State, c) After 150 passes, d) Front View of After 150 Passes

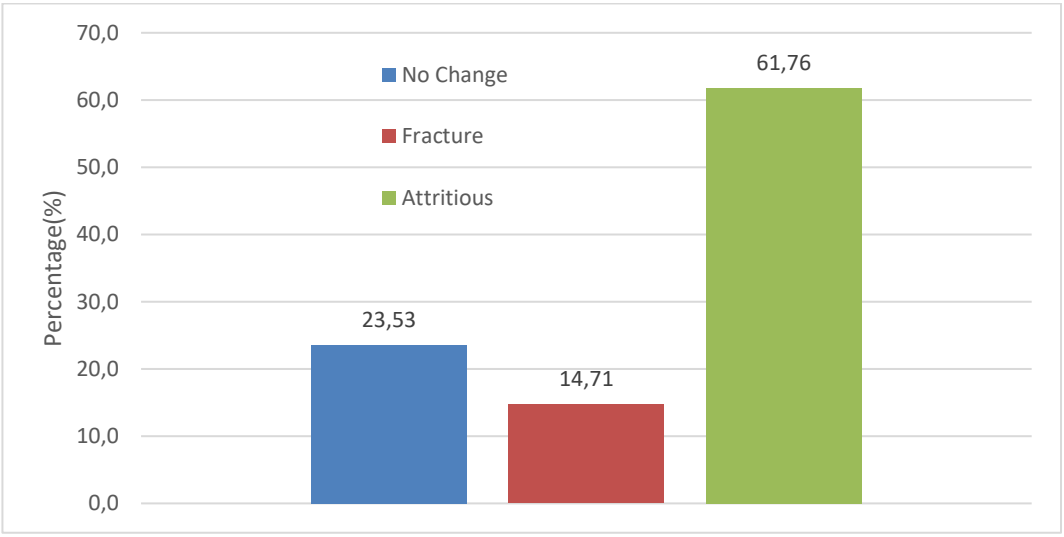

Figure 49- Percentages of Grit Wear Mechanisms

3.6. Radial Wear of the Wheel and Surface Roughness of the Wheel and Workpiece

Height changes of the 30 grits were measured individually after each step via Nanofocus with 50x lens and the results are shown in Figure 50. Before the test, it was

observed that the average height of 30 grits was approximately 60.7 µm. At the end the average height measured as 44.3 µm. The change in the height is 27%.

On the other hand, wheel surface topography was also measured in terms of Ra and Rz after every cutting test which can be seen in Figure 51 and Figure 52. Ra and Rz changes before starting the cutting and after 150 passes were observed as 26.8 % and 25.2%, respectively. The height changes of grits have been measured by two techniques. First one is by looking grits individually. The second one is by looking Ra and Rz values of the wheel. It was found that both of them provided very close results. It means that considering 30 grits to study wear mechanism was sufficient to represent the behavior of grits for the whole wheel in this work. Height changes of the grits after each step are presented in Figure 50.

Surface roughness Ra measurements of the wheel and workpiece can be seen in Figure 51. Both of them decrease with increased accumulated material removal as expected [8].

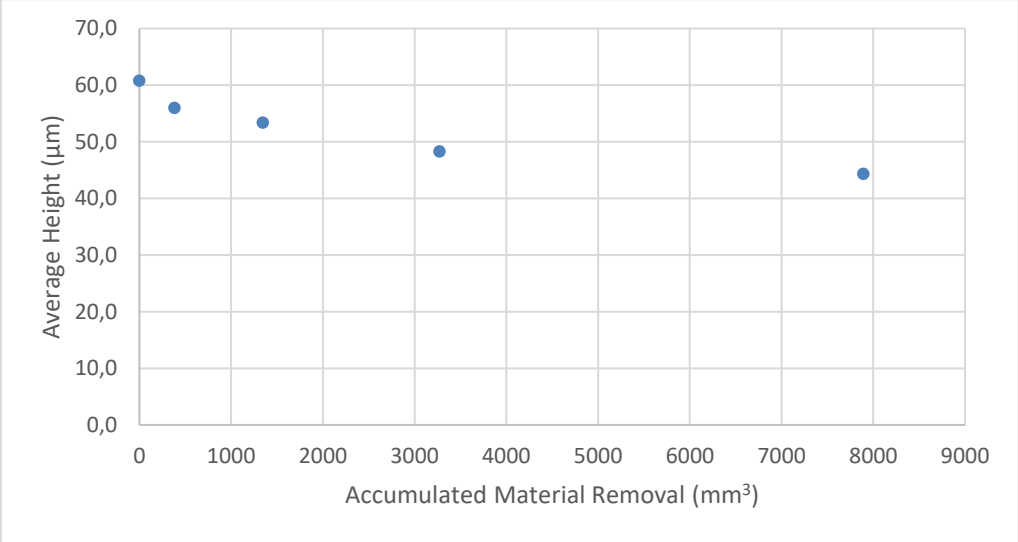

Figure 50- Average Height Changes of the Grits After Each Step

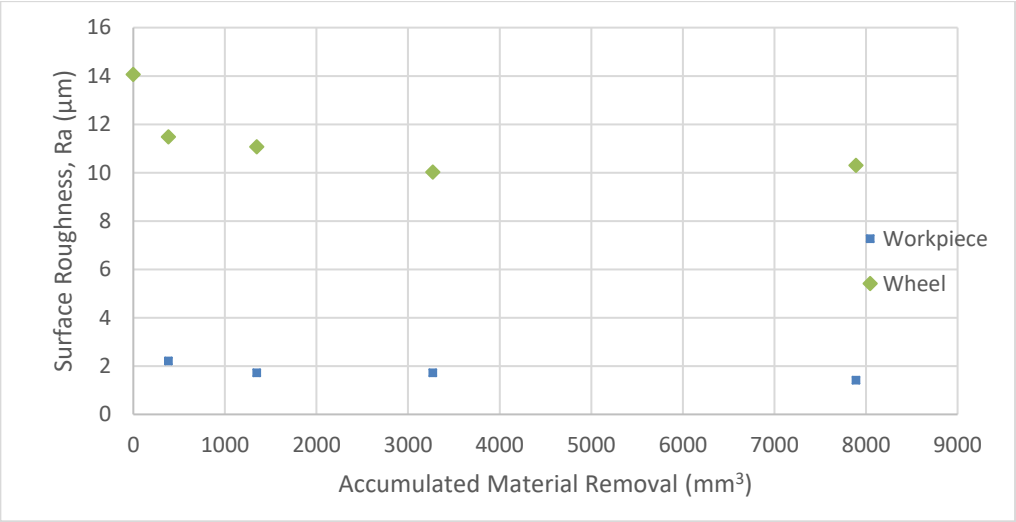

Figure 51- Surface Roughness (Ra) of the Wheel & Workpiece

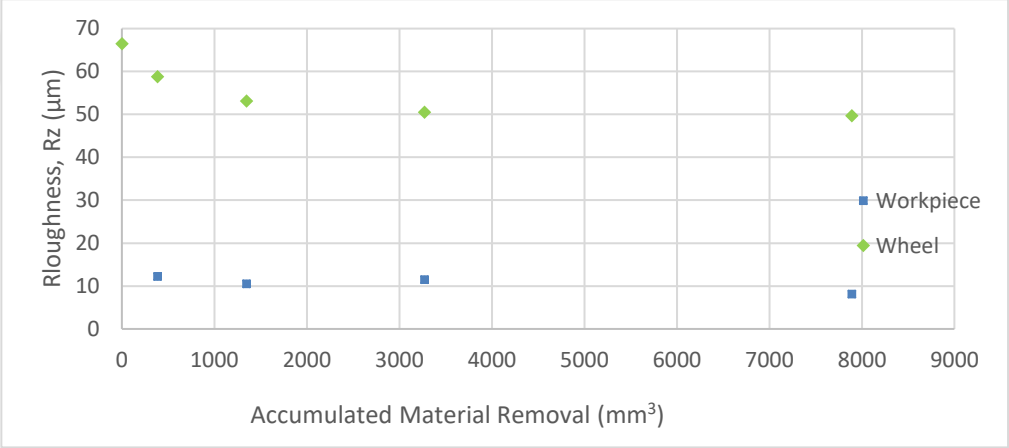

Figure 52- Surface Roughness (Rz) of the Wheel & Workpiece

3.7. Effect of Wear on Grinding Force

Grinding forces in the tests are directly affected by wear of the wheel. During cutting tests, average forces were measured and effect of the wear on forces is shown in Figure 53. Forces have increasing trend as most of the cutting edges of the grits were dulled because of attritious wear. So, grits can not penetrate workpiece easily. Force is increased 55.6% at the end of the tests compared to the first step. It should be mentioned that there was a noise due to coolant and vibration of the spindle. Magnitude of the noise was around 3 N.

During the measurements of individual grits; although coolant was used, it was observed that some chips were stuck between the grits. This situation has been considered in measurements.

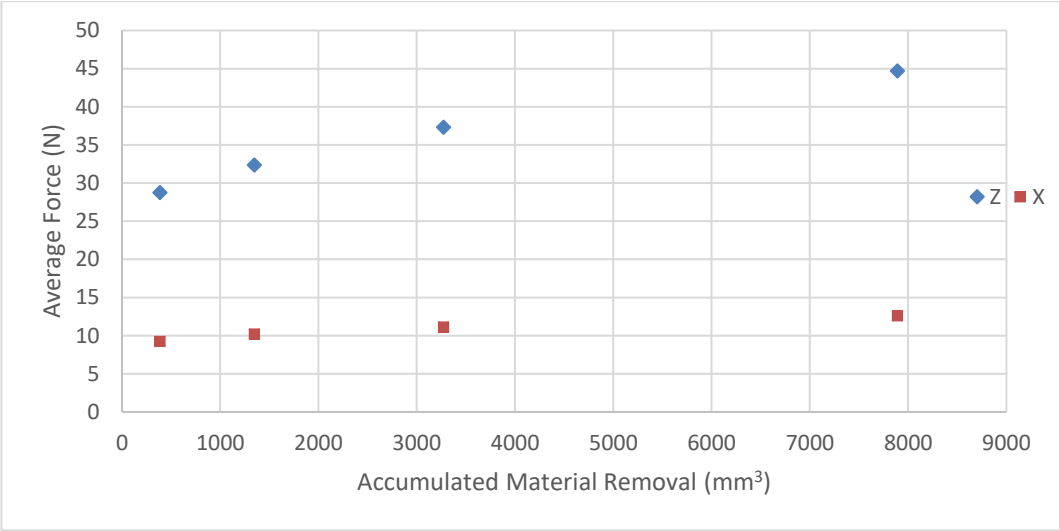

Figure 53- Average Forces During Tests

3.8. Summary

This chapter presents an individual investigation method for grits in electroplated CBN tools. By this method, attritious and fracture wear can easily be seen. Two separate methods were used for radial wear. First one was observing the changes in average heights of 30 grits. The second one is measuring the surface roughness of the wheel by a profile measurement device. Both of those measurements were compared and it was observed that they yielded very close results. It was found out that attritious wear was more dominant wear mechanism than fracture wear throughout the process, which can be seen in Figure 49 in detail. On the other hand, pullout mechanism was effective in the early stages of the grinding as some grits have low bonding force. Surface roughness of the workpiece showed a declining trend because of the decreasing grits heights' due to attritious wear. Force results showed an increasing behavior because of dulling of the grits.

Contrary to literature [8], attritious wear was considered as micro fractures and particle losses due to friction on the grit. In the scope of this work, attritious wear can be thought as height decrement without being exposed to instant high loss of a part of a grit, on the other hand, the other wear mechanism "fracture" is defined as loss of a huge part of a grit suddenly. In conclusion, attritious wear has been found more dominant wear mechanism under specified cutting conditions.

4. TOOL LIFE

4.1. Introduction

Due to CBN abrasives' high potential to the machining processes, they are being widely used in the industry [25, 26]. Their featured properties can be listed as follows:

- Wear resistance
- Extreme hardness
- High temperature resistance
- Thermal conductivity
- High toughness

The most important disadvantage for these tools, on the other hand, is that they are very expensive since only a few manufacturers supply them. Therefore, tool life is highly critical for electroplated grinding processes in order to justify their high cost. Tool life is directly related to the wear of the tool, which is why both of them are investigated in detail in this chapter. Tool wear is a result of the mechanics whereas tool life is determined based on the wear amount on the tool. In the literature [7], observed burns occurred at the workpiece surface to determine tool life. Also Malkin [8] states that, grinding wheel life is determined as when the radial wear reaches 70-80% of the grain dimension. Another approach for tool life criteria is provided in this chapter for the selected grinding conditions and wheel-workpiece pair.

As mentioned in the literature [20], wear does not only affect the size and the geometry of workpiece, but also surface quality and process forces. Thereby, in addition to tool life; surface roughness, force and wear type variation have also been investigated during the experiments.

Malkin [8] identified the active grits by considering the wear flat areas or the grits with same tip protrusion height. In this chapter, also activeness of grits was investigated by similar method.

In the previous chapter, the mechanisms of tool wear "based on grits" has been investigated. Similar and more detailed versions have been found and they are expressed in detail with pictures. For this chapter, the wear mechanisms have been

investigated throughout *the tool life*. Tool life research mainly based on experimental investigation. However, at the last chapter a model was presented to predict the surface roughness of the electroplated CBN wheel and the validation of the results has been made.

Depth of cut is one of the most important factors that affect the grinding process, the tool wear and tool life. A discussion about the effect of depth of cut on surface quality, grinding force, pullout percentage and tool life was presented.

4.2. Methodology

The methodology that has been used for tool life experiments is shown below:

Step 1: Identification and Determination of Electroplated CBN Grinding Wheel Properties

Some grits have been chosen randomly to investigate wear behaviors on them and their locations have been noted.

Step 2: Cutting Process

Wheel has been mounted to the CNC machine and cutting process had been performed.

Step 3: Measurements

After the cutting process, the cutting forces of the worn wheel have been measured via dynamometer. Also, after every cutting experiment, wheel has been measured under the Nanofocus microscope. The wear effect has been investigated on previously determined grits. Moreover, surface roughness of the wheel and the workpiece have been measured by using Talysurf surface profilometer.

These 3 steps were carried out 8 times during the tool life experiments. The reason for doing these 8 times is controlling the wear behaviors firmly and observing the wear mechanisms in more detail. Small diameter grinding wheel has been used in the experiments because it is easier to observe the changes over its whole surface and it is easier to make it wear due to less abrasive amount.

4.3. Test Setup

Test setup is shown in Figure 54. Tool life experiments have been conducted on Chevalier B818III CNC machine. Workpiece has been located over the dynamometer. The coolant positioned carefully towards the cutting zone. Also, tool eccentricity was measured and it was found that it was not more than 4-5µ. The eccentricity is so important because spreading the cutting action uniformly to overall wheel surface was desired to obtain correct results. In addition to that, depth of cut becomes stable for all grits when the eccentricity is low.

Cutting conditions were held similar to the production conditions. The details about the experiment can be seen in Table 12. Only the parameter that would be investigated has been changed which is depth of cut. The cutting depth of cut has been changed to 20µ, which was 100µ in the previous tests (Chapter 3), and the results were compared later.

Workpiece	Inconel 718 (31 HRC)
Grinding Wheel	Electroplated CBN Grinding Wheel with 120 grit size; 10mm diameter, 8 mm width
Coolant	5% Water-Boron Oil
Cutting Speed [m/s]	20.94
Feed [mm/min]	250
Depth of Cut [mm]	0.02

Table 12- Cutting Conditions and Tool & Workpiece Properties

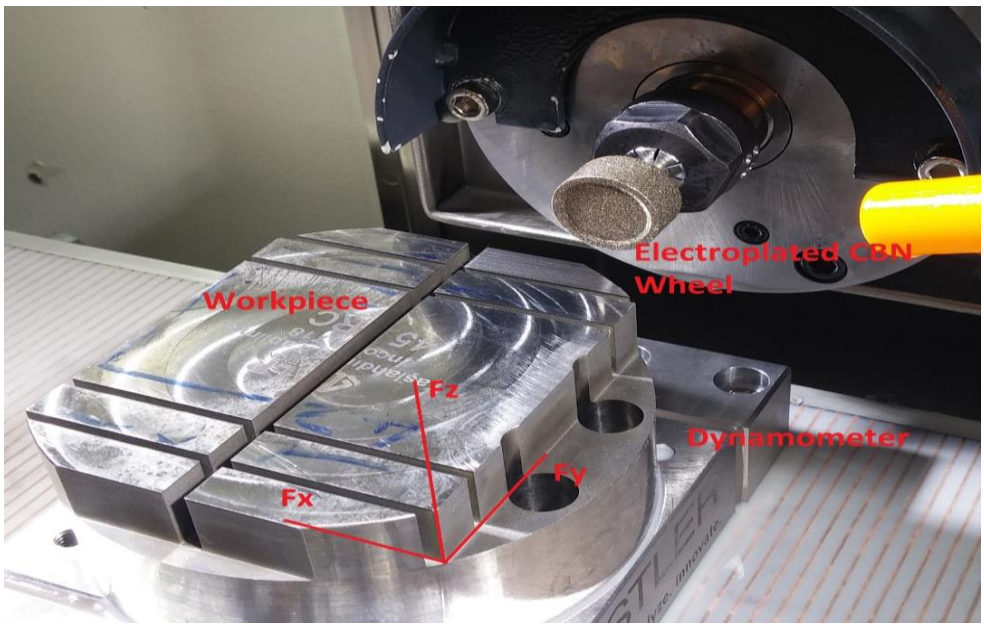

Figure 54-Test Setup for Tool Life Tests

4.4. Surface Roughness of the Workpiece and Grinding Wheel

The surface roughness of the workpiece and the wheel give an information about the tool wear condition. In order to make the measurements more accurate, wheel surface roughness has been measured 8 times at each step and the average of these measurements was taken. Measurement of surface roughness of electroplated CBN grinding wheel can be seen Figure 55.

During the grinding wheel measurements, some of the regions seemed to be more worn. One of the reasons for this is that sometimes vibrations occur during cutting action. The other reason may be eccentricity. However, eccentricity of the wheel was measured before the tests were conducted and it was found lower than 4-5µ. Thus, its effect on wear can be considered as negligible. Some darkened areas were observed on the grinding wheel, because some material melted and sticked on the wheel surface at the later stages of the process.

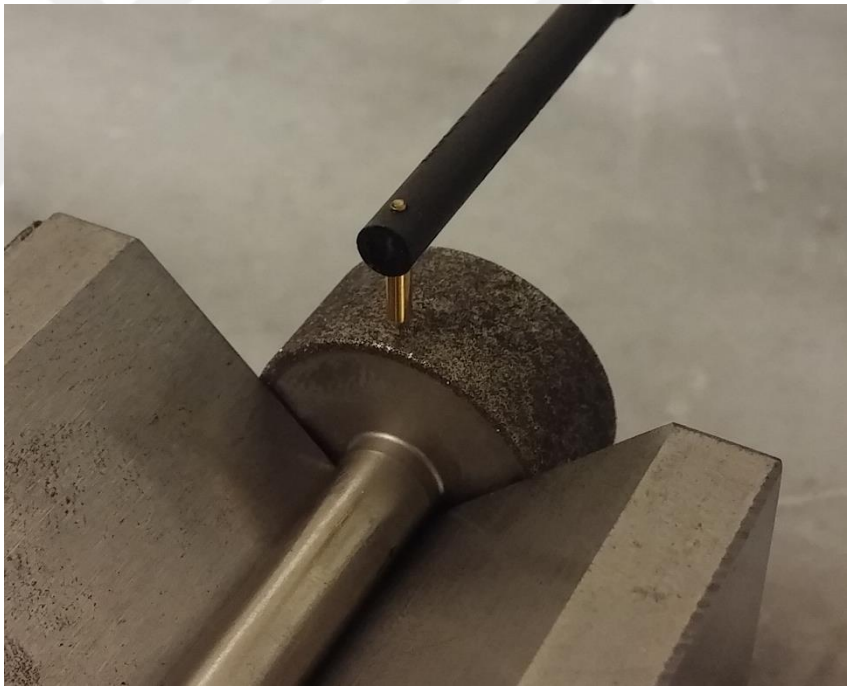

Figure 55- Surface Roughness of Electroplated CBN Grinding Wheel Measurement

Effect of wear on the grinding wheel is directly reflected to the surface of the workpiece. Thus, surface roughness of the workpiece was also measured to observe the effect of the wear and to investigate the quality of the surface throughout the tool life. The surface measurement can be seen in Figure 57.

In order to make the measurements more accurate surface of the workpiece has been measured six times. Twice are at the beginning of the cutting direction, twice are at the middle of the workpiece and the last two times are at the end of the cutting direction. The purpose of this kind of division into three is to observe the wear effect during a pass. However, there were no obvious changes observed in one pass. The measurement can be seen in Figure 56.

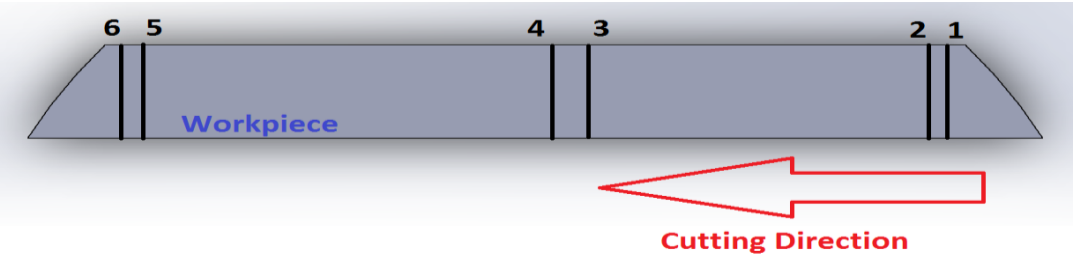

Figure 56-Measurement of Surface Roughness of the Workpiece

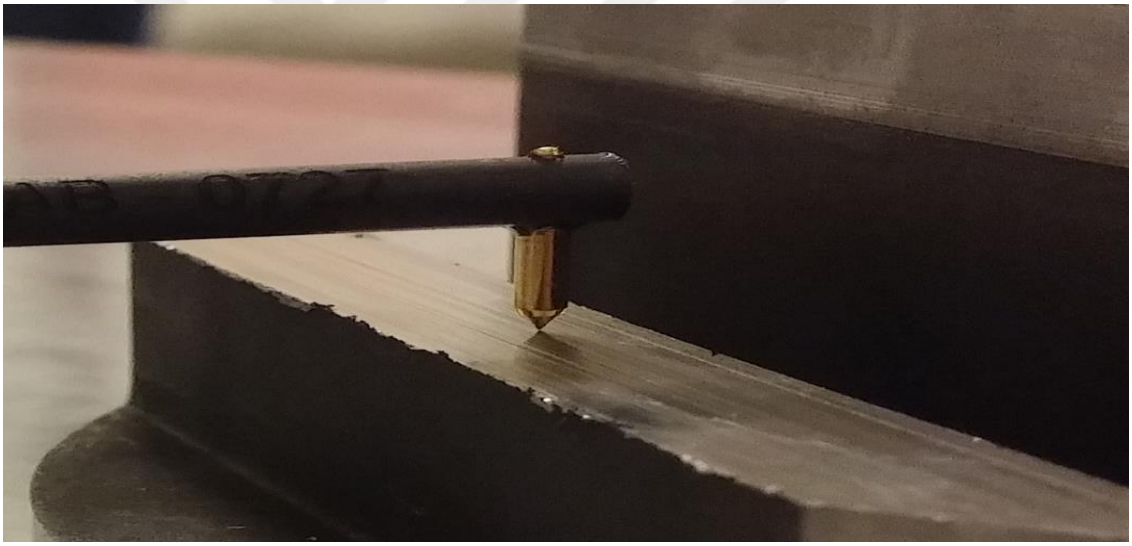

Figure 57-Measurement of Surface Roughness of the Workpiece

Surface roughness of the wheel and workpiece results are presented by using Ra and Rz parameters, in Figure 58 and Figure 59 respectively. There was a sharp decrease in the surface roughness values at the beginning of the cutting process and then it became stable around 10μ for wheel and 2μ for workpiece. The reason for sharp decrease at the beginning is high pullout rate.

Surface quality of the workpiece is really important in grinding processes and it is mostly related with the wear condition of the grinding tool. That is why every time surface roughness of the grinding tool has been measured. Moreover, a model has been

developed to predict the surface roughness of the wheel which is expressed in the following chapter.

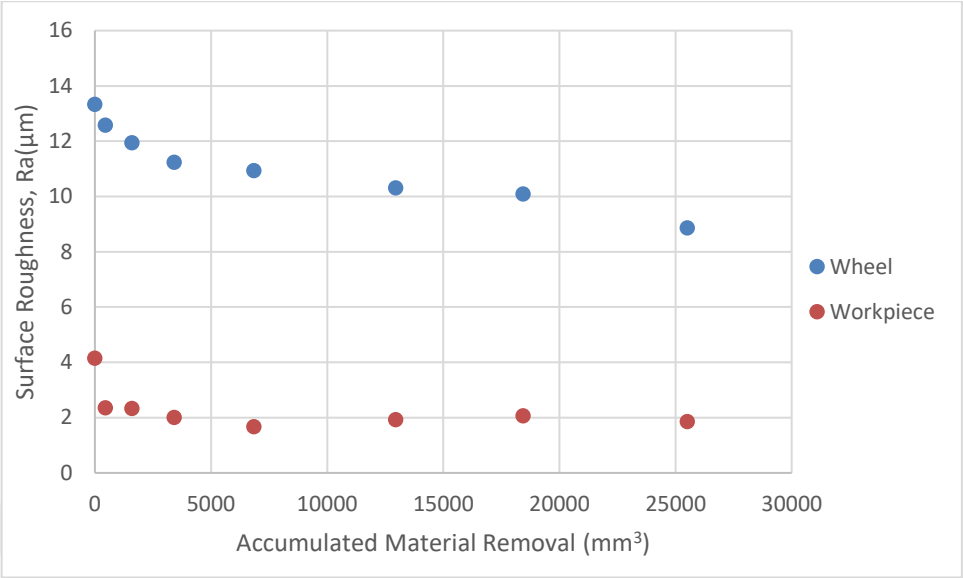

Figure 58- Surface Roughness of the Workpiece and Wheel, Ra

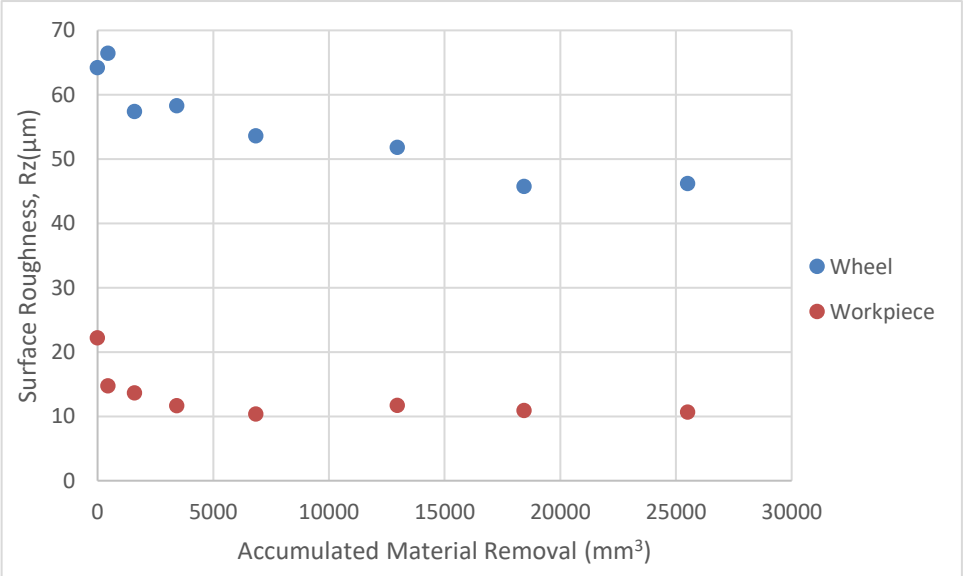

Figure 59- Surface Roughness of the Workpiece and Wheel, Rz

4.5. Effect of Wear on Cutting Forces Throughout the Tool Life

Grinding forces can be used as an indicator for the tool condition. At the beginning of tool life grits were new and they had sharp edges. That sharp edges made the cutting action easier, so the grinding forces were low at the beginning. However, these sharp edges became dull in time and so the grinding forces were increased because it was difficult to cut material with a dull edge.

Since the wear effects were observed over the wheel surface, it is needed to be measured under the microscope *periodically*. Thus, a determinant is necessary to adjust that period time during the process. Measuring force is an in-process method to understand tool condition without dismounting the tool. During tool life experiments, at the end of each step -when the tool has worn enough to be measured- force has been measured. Maximum and average force results in feed (X) and normal (Z) directions can be seen in Figure 60 and Figure 61.

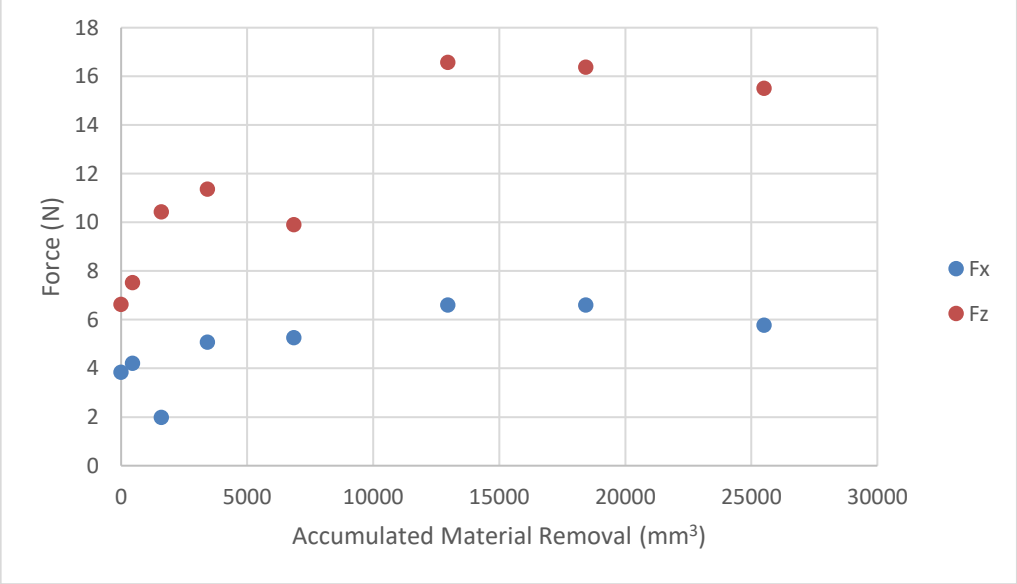

Figure 60- Average Force Results

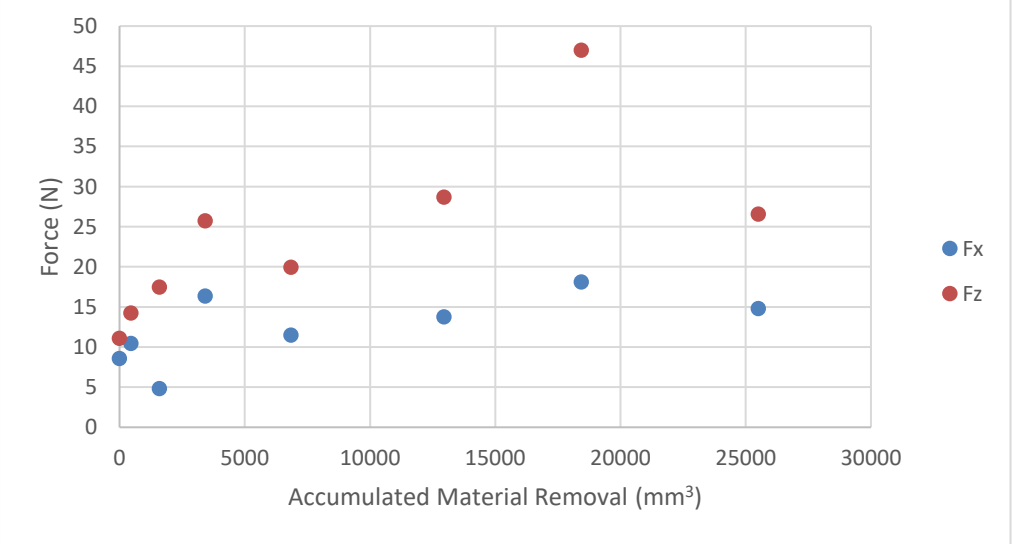

Figure 61- Maximum Force Results

At the beginning, average forces in Z axis was 6.6 N. However, after the tool has worn, it has become 17 N. It has been almost increased three times. On the other hand, the

forces in the feed direction was measured as 3.8 N at the beginning. However, at the end it has been increased to around 6.6 N. Although, it has been almost doubled, the increase was not as high as in normal direction.

4.6. Pullout Mechanism Throughout the Tool life

As it was explained earlier, all pullout measurements have been done via Nanofocus microscope. For these experiment series, 5 different location have been spotted on the wheel surface and grits have been counted at the end of each step. These 5 area can be seen in Figure 63, they are presented as A1, A2… The pullout behavior can be seen in Figure 62. These numbers in the graph present the percentage grit number. Sometimes pullouts were observed even at the brand-new tools. Thus, pullout was measured considering initial pulled out grits.

At the beginning, there was a sharp increase observed as expected and then increment continued linearly. It was expected to be stable after some point, however interestingly a jump has been occurred at 7th (last) step. The reason for initial jump is the low bonding force between the plate and grits. On the other hand, the reason for final jump is fatigue of the active grits. The final jump is also an indicator for the end of tool life.

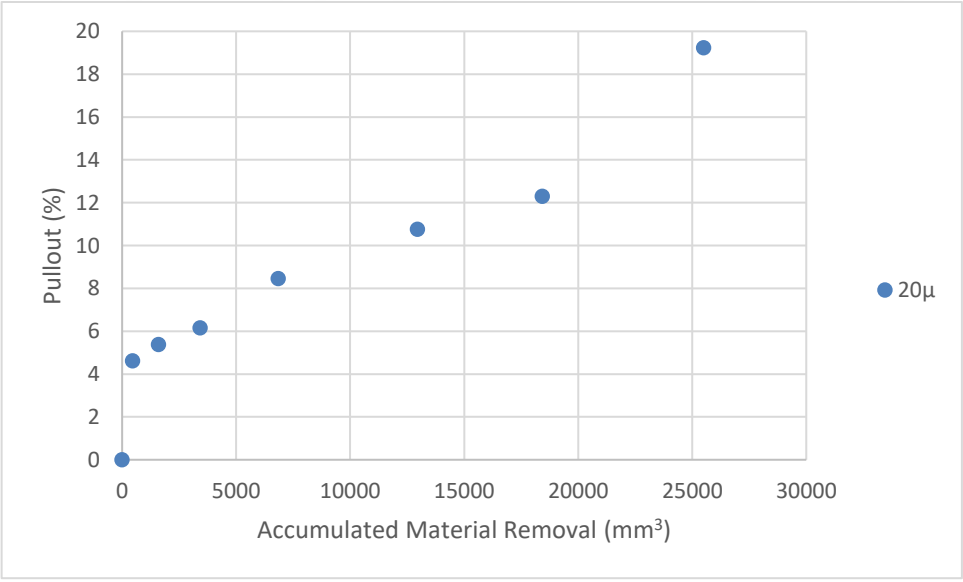

Figure 62-Pullout Behavior Throughout the Tool Life

4.7. Individual Investigation of Grits Throughout the Tool Life

In the literature, most of the time researchers measured the tool wear in a simple way. After the tool has worn, they took a shallow grinding pass over a ductile material and

measured the surface profile of the workpiece. However, applying this method could only provide the effect of the grits that left the trace on the surface. Yet not always all the grits leave trace on the surface. They may contribute as an active grit but sometimes they have a higher follower grit behind them which generates a new surface over the smaller grit's trace. Thus, more accurate method has been studied on this work, which is presented as *individual grit investigation*. In this method, high and notable grits have been selected randomly at the beginning. It was determined as 13 locations for this test set. In these areas, sometimes more than one grit was observed. Thus, that selected region can also provide the active grit behavior.

The opened version of the tool peripheral area is shown in Figure 63. It contains 5 areas and 13 grits which are shown as "A" and "G" on the figure respectively. These areas have been measured in a way that explained in chapter 2. 20x area measurements represent A, 50x individual measurements represent G. These selected areas have been observed at the end of each step. Grit and area selection stage have been done homogeneously over the surface to avoid the interaction between them and to obtain more accurate results.

The workpiece is 7mm in width on the other hand, tool is 8 mm in width. Thus, the below section on the Figure 63 was not measured because that area did not have any contact with the workpiece. So, it did not participate in the cutting action and no change was expected.

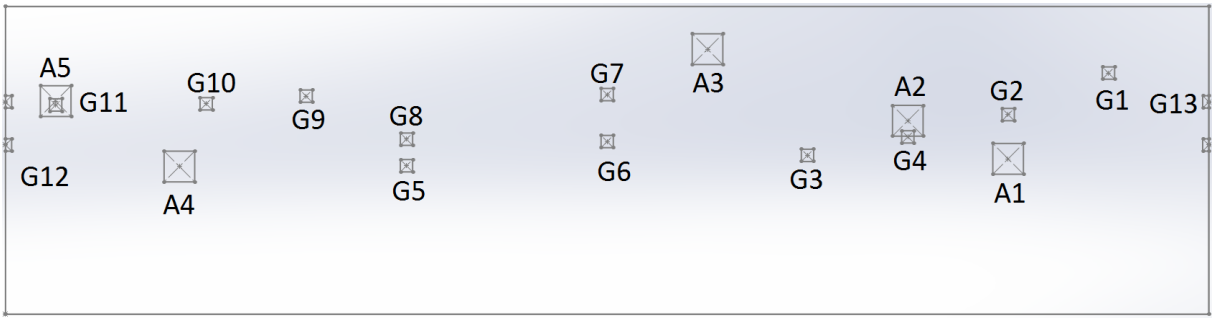

Figure 63- Grit Locations

The measurements were divided into two section. First one is the geometric shape change aspect. It contains the wear mechanisms such as micro-macro fracture, attritious wear and pullout. On the other hand, second section is about active grit density. In the literature [8], it has been found that active grit density has an increasing behavior in time.

4.7.1. Geometric Shape and Active Grit Investigation

In this section, selected grit regions have been investigated in detail which are shown as "G" in Figure 63. The changes over the grits are provided with grit pictures at each step (from step 0 to 7). The most important factor in the selection stage of the grits is their height. Although, all grits were chosen randomly, huge and clear ones have been taken as a sample because they were contributed to the cutting action. Since focused area was capable of capture more than one grit, the behavior of the smaller grits has also been investigated.

G1

The height of grit 1 has been found as 39.5 μ at the initial stage. Only a small fracture observed at the last step which can be seen in Figure 64. Thus, it can be said that almost no change has been observed during the tool life. It was not active due to its low height.

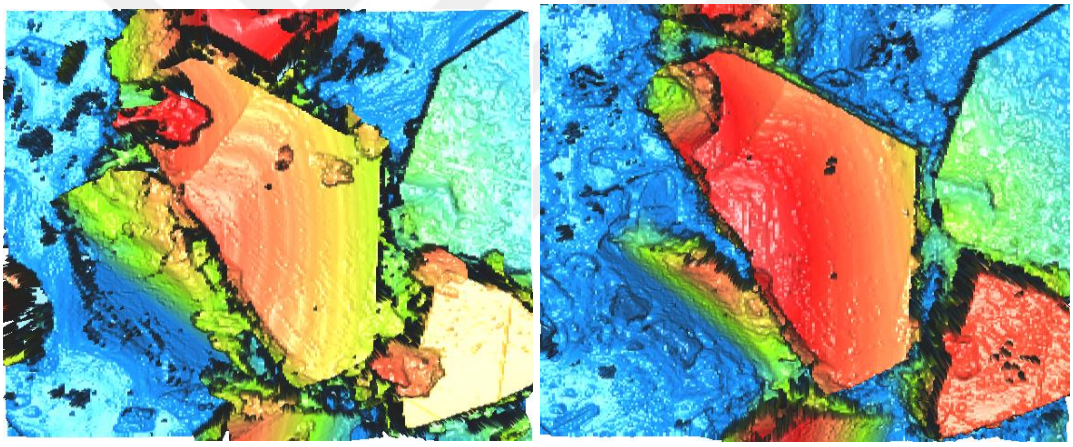

Figure 64- Grit1 Conditions @Step 0 and 7

G2

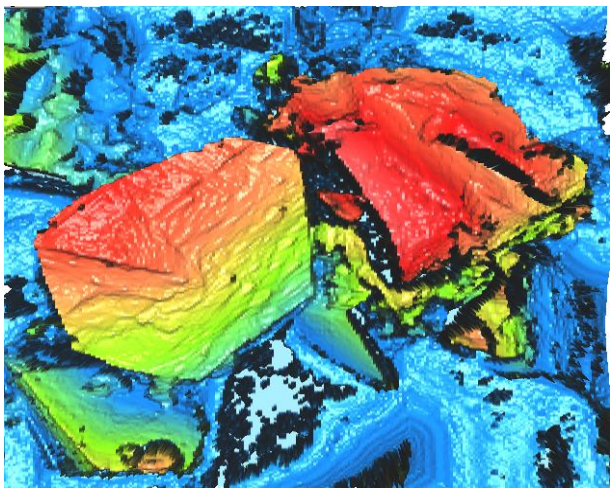

In Figure 65, two grits are shown. Their heights were measured as 38µ and 46µ at the initial phase of the wheel.

Figure 65-Grit2 Conditions @Step 0

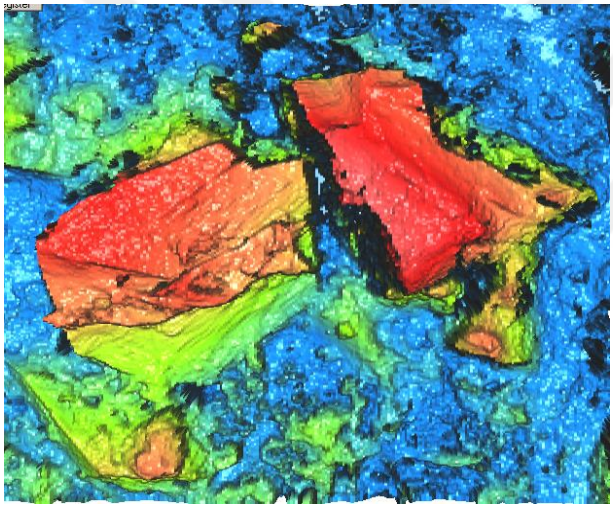

Until the 6th step, no changes have been observed at the G2 region. Due to their low heights, they were not become active until the 6th step. In Figure 66, some fracture occurred at the -top right- part of the left grit and at the top side of the right grit. Also, some sticked material has been detected on the grits.

Figure 66-Grit2 Conditions @Step 6

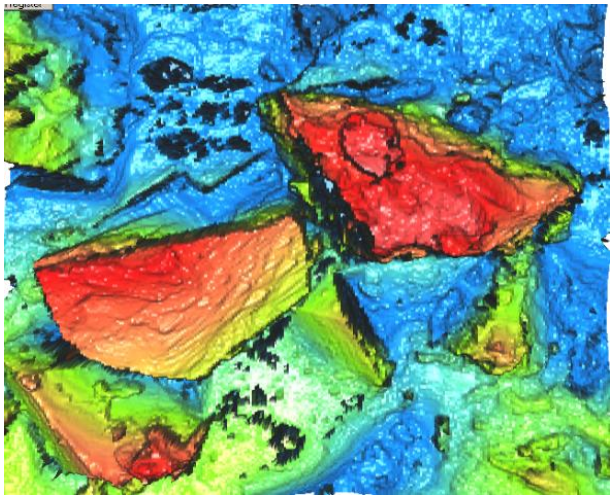

In the given figures, cutting flow is coming from up towards the bottom. The upper part of the grits has been destroyed due to that flow direction. Moreover, attritious wear were observed on the right grit. Wear mechanisms can be seen in Figure 67. Almost half of grits were broken.

Figure 67-Grit2 Conditions @Step 7

G3

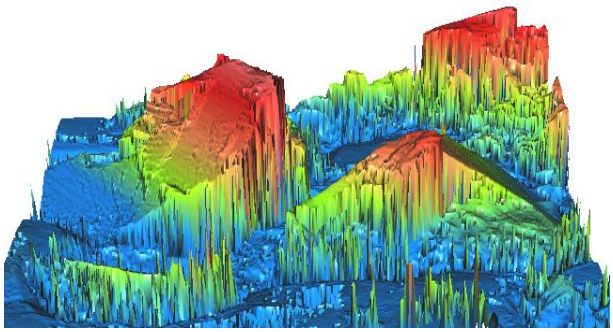

Initial condition of G3 area is shown in the . Two grits were focused. Left one had 58 µ height at the beginning and middle one had 40 µ height.

Figure 68-Grit3 Condition @step 0

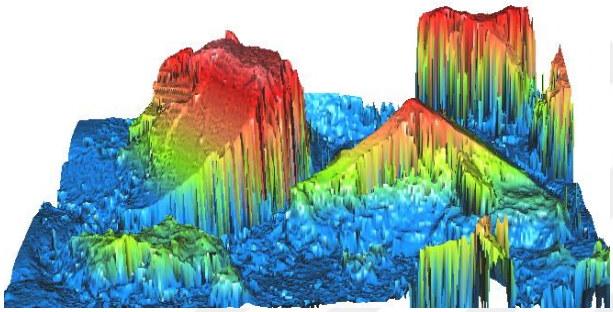

First change on area G3 was observed at 6th step. Right one did not change. Due to its low height, it is not active. In , attritious wear can be seen on the top part of the left grit. Its height has been measured as 49 µ.

Figure 69-Grit3 Condition @step 6

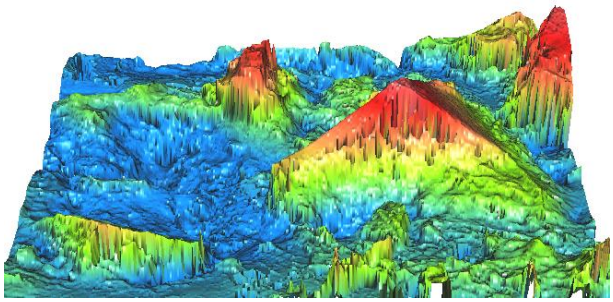

At the final step, left grit was totally broken which means pullout occurred at this step. Pullout at G3 region can be seen in Figure 70. Still no changes were observed at the middle grit.

Figure 70-Grit3 Condition @step 7

The first change has been observed on the grit at 6th step which was attritious wear. It was not participating into cutting action not due to its low height. Average grit height was measured as 62 µ at the beginning. So, its height was enough to participate in cutting. This shows that there was higher active grit on the cutting flow path. After 5th step that active grit has been gone or its height reduced, so that grit in G3 region became active.

In Figure 71, details of active grit concept have been shown more clearly. Color scheme has been used to express height distribution over the area. White layer means highest, dark blue layer means the lowest height in the region. In picture-a which corresponds to 0^{th} step, white layer at the highest point can be seen. In picture-b which corresponds to 5^{th} step, white color distribution is similar with picture-a because no big change has occurred. However, at picture-c which corresponds to 6^{th} step, grit has already been active and attritious wear on top part of the grit has been observed. The important point is the white color region has been increased, so all that white region is active now. Grits became duller and top part became flatter. Moreover, white color region has also been observed at the tip of the middle grit. Thus, it has also started to become active grit.

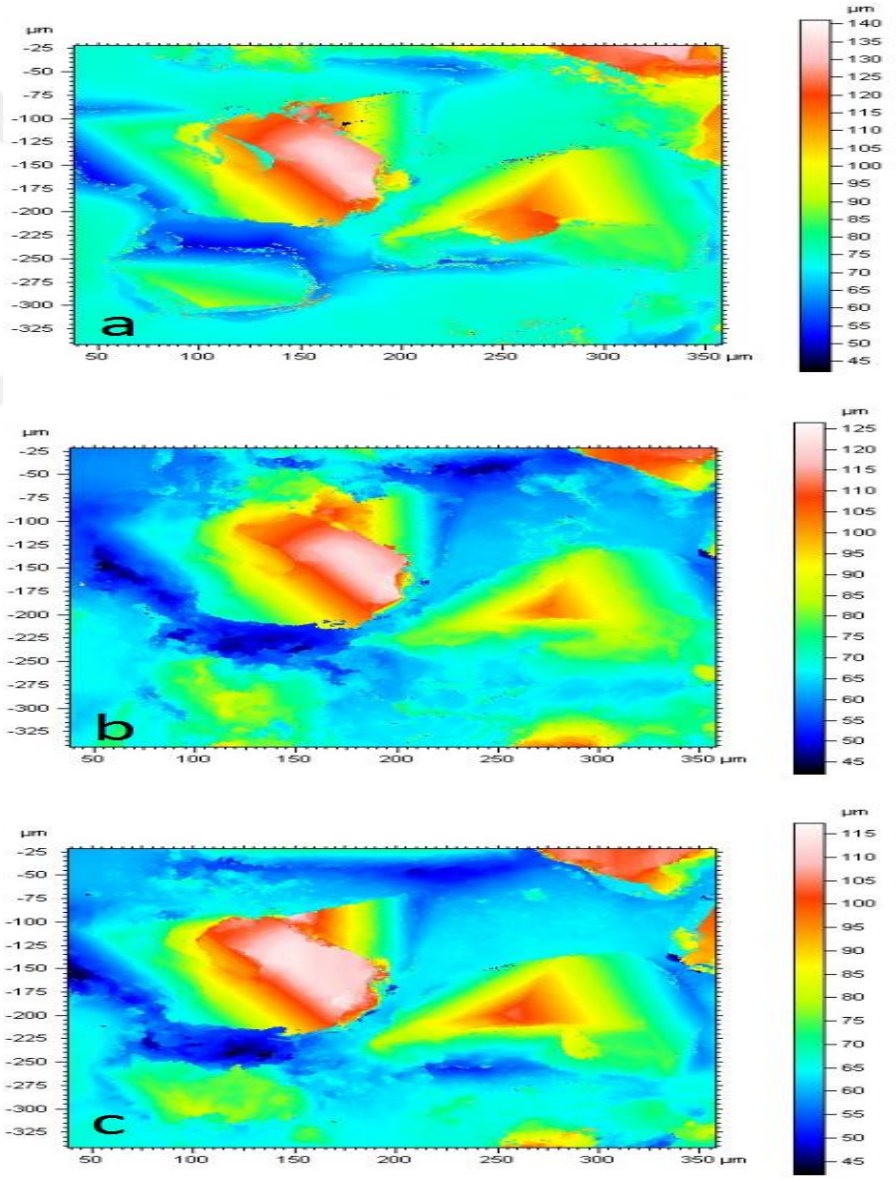

Figure 71- Active Grit Observation on G3; a) 0^{th} Step, b) 5^{th} Step, c) 6^{th} Step

G4

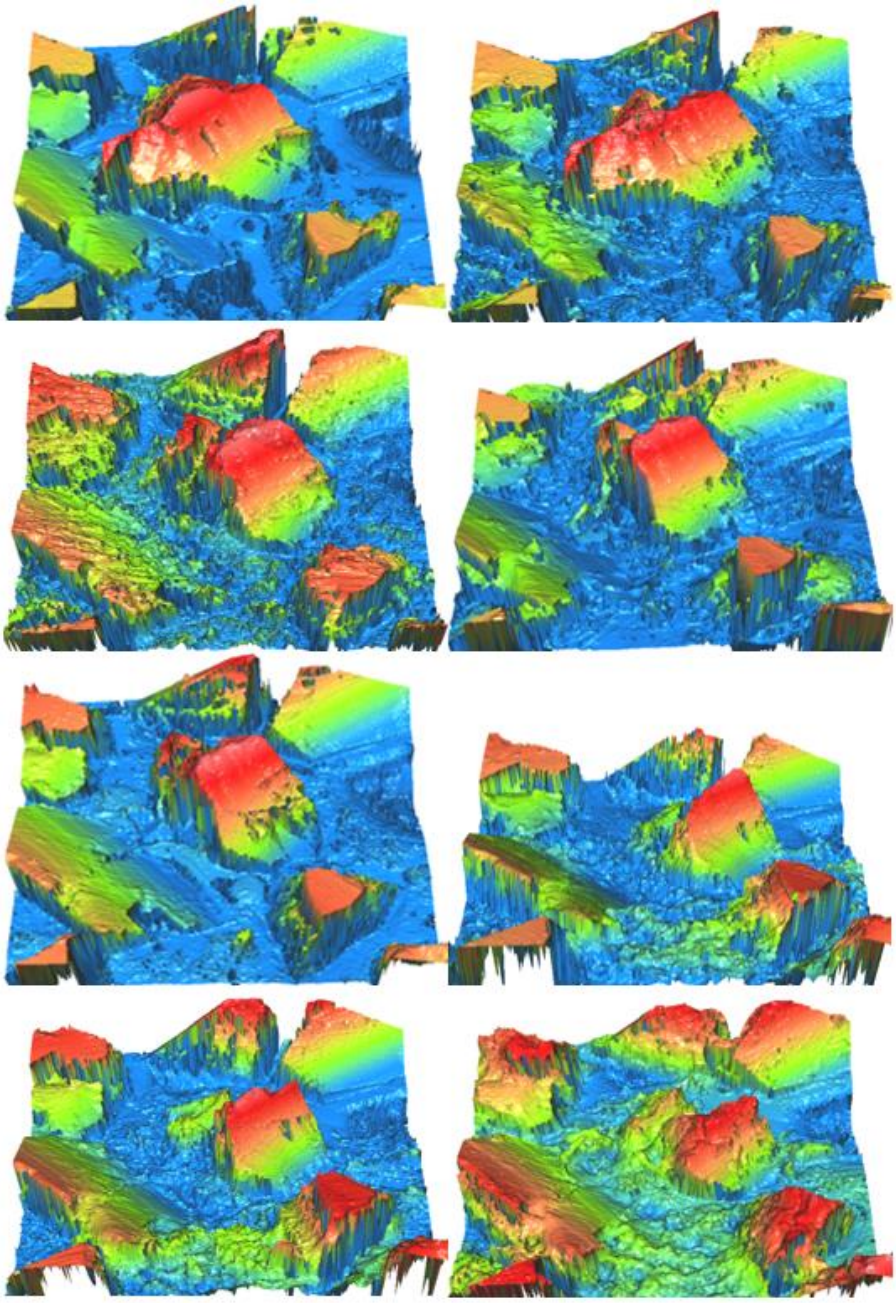

Figure 72-Conditions of G4 in all steps, Left to Right Steps: 0,1;2,3;4,5;6,7

In Figure 72, all phases of G4 region are shown. Although investigation in this region has been focused on the centered grit, some changes have been observed even for the smaller accompanying grits around it at the later steps. At the beginning, attritious wear has been observed at the centered grit. Then, left part of the grit fractured. Since it was getting smaller, activeness of it decreased and at step 3 and 4 there have no change observed. At final steps, it has been smaller due to fracture.

G5

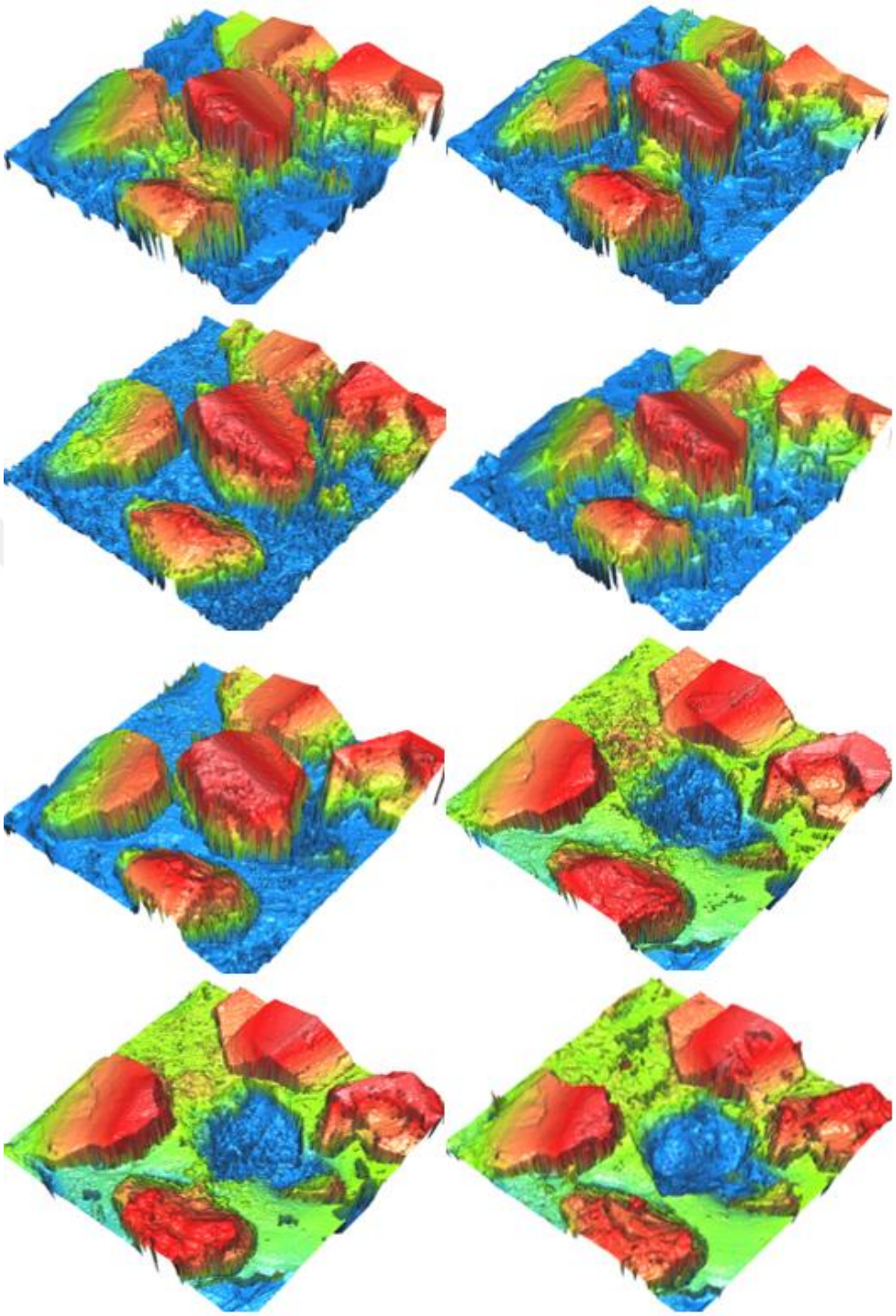

Figure 73- Conditions of G5 in all steps, Left to Right Steps: 0,1;2,3;4,5;6,7

In region G5, centered grit was mainly focused. In Figure 73, all steps of the region are shown. At the initial state, it had approximately 69.8µ height and it did not change during first phase because only small amount material has been removed. Later on at the 2nd step, attritious wear has been observed on top of the grit and its height decreased to

59.4μ. At the 5th step, it has been pulled out due to fatigue. It was active from the beginning but it held on until 5th step which proves its pullout reason was not low bonding force to the plate, it was *fatigue*.

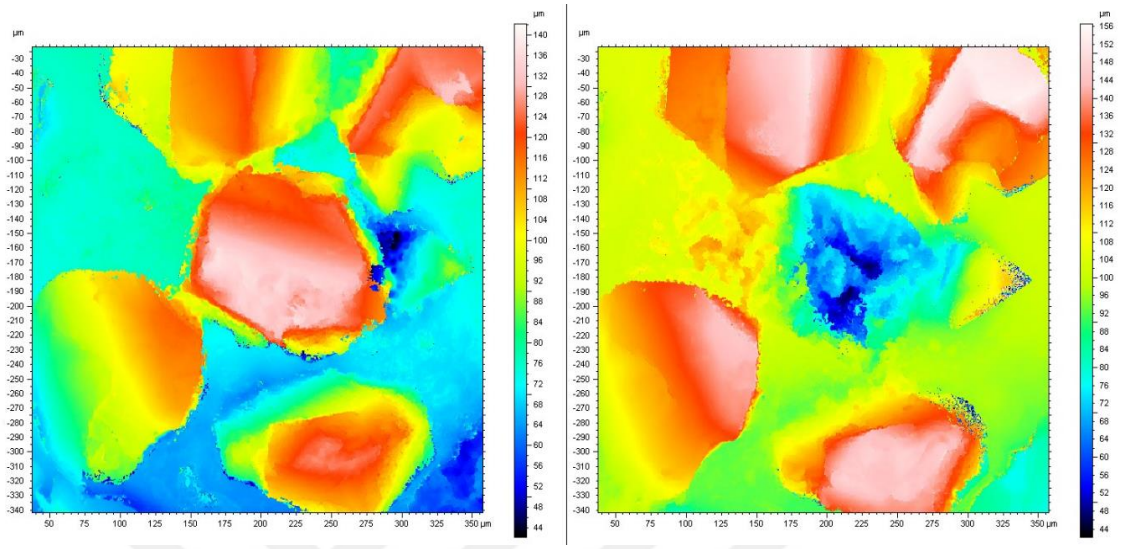

Figure 74-Activeness of G5 Region

Activeness of G5 region is shown in Figure 74. Before the centered grit has been pulled out, it was the highest grit on the area and it maintained the cutting action, because the surrounding grits were lower than the centered. However, after centered grit has gone, the others had the highest point in the area and then they became also active. White color is the highest region in the given area, so most of the cutting action has been done by the white regions. The distribution of the white regions are obvious in the right picture in Figure 74.

G6

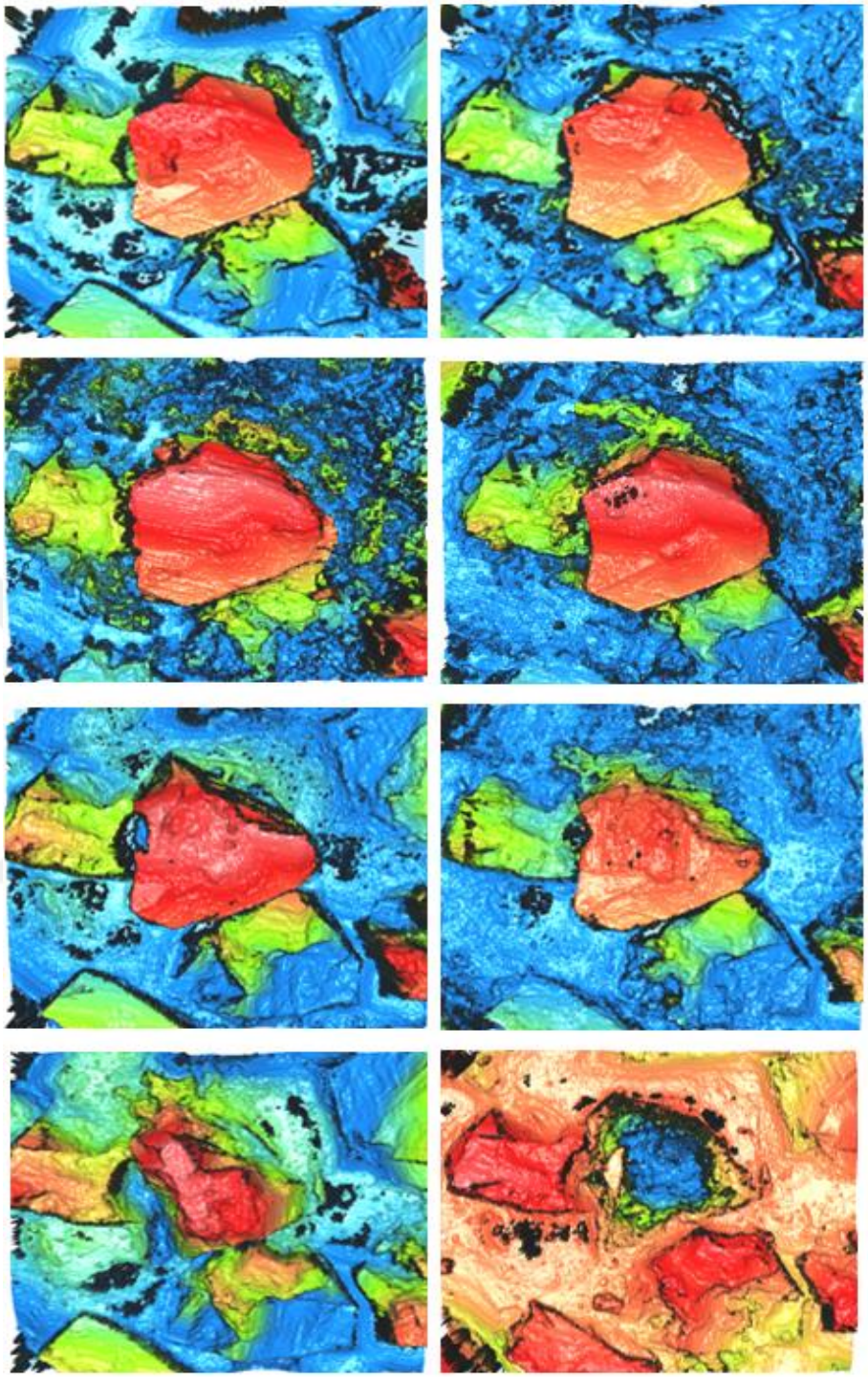

Figure 75- Conditions of G6 in all steps, Left to Right Steps: 0,1;2,3;4,5;6,7

Another region G6 is shown in Figure 75. There was a huge grit with average height of 52 μ. It was not so active at the initial steps. First change has been observed at 4th step with a fracture occurred at the flow direction (Up towards bottom). Later, it had a huge fracture at 6th step and then finally it pulled out. The activeness of this huge grit almost started at 4th step.

G7

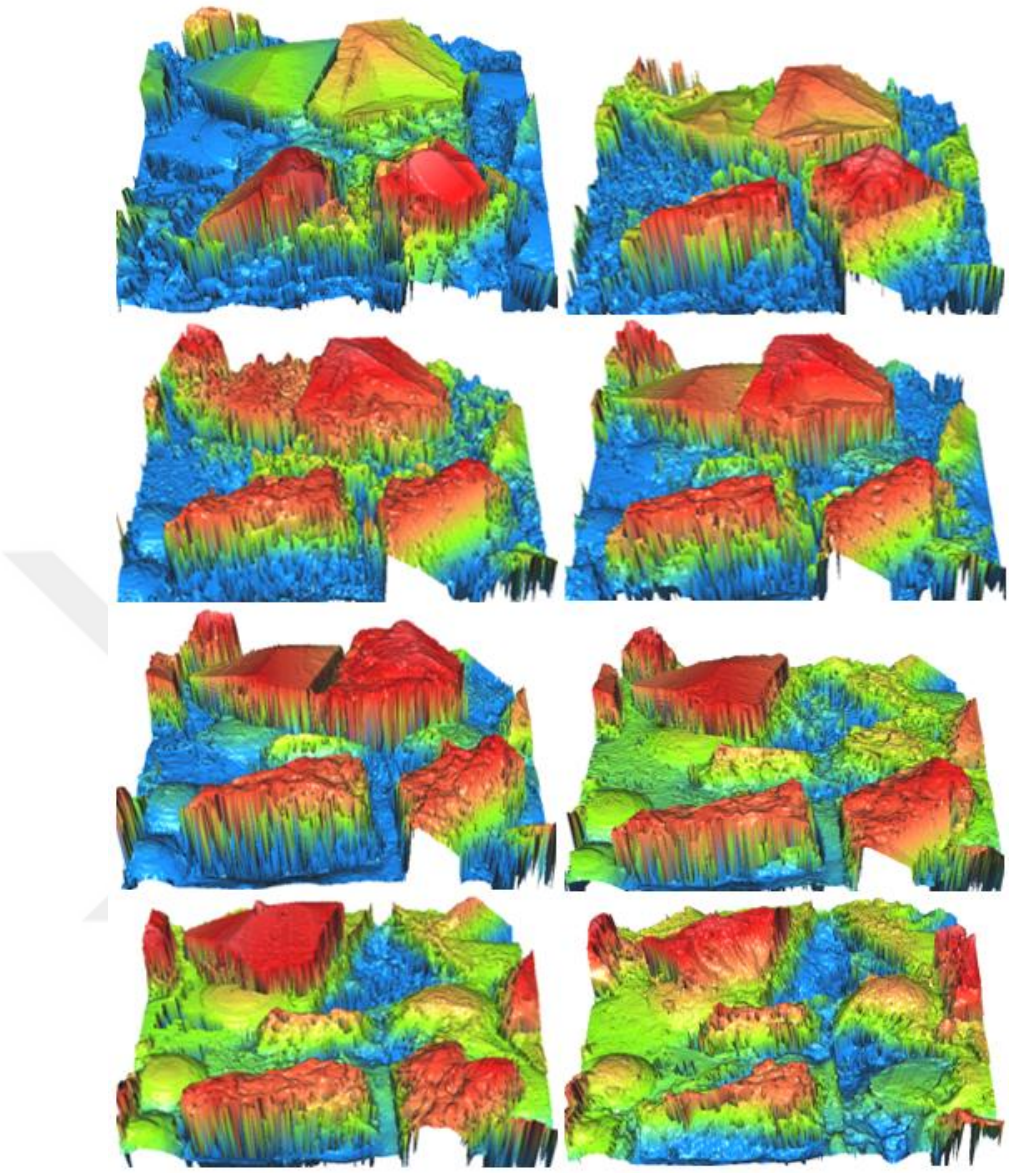

Figure 76- Conditions of G7 in all steps, Left to Right Steps: 0,1;2,3;4,5;6,7

Sometimes, it is difficult to distinguish the difference between the attritious wear and a flat surface of the grit. Whereas the difference can be seen clearly in step 4, right top grit has attritious and left top grit had flat non-touched surface. However, the biggest grit -active- has been pulled out at the 5th step. This proves that pullout may happen instantaneously or over time. That huge grit weakened in time and finally could not hold to the wheel surface. The 3 grits except the left top one were active during the process. Attritious wear has been observed for them initially. After the huge grit pulled out, the amount of material to be cut per grit was increased in the region. So, the remaining two

grit were still active and the left top grit started to cut. Finally, right bottom grit has also been pulled out at the last stage.

G9

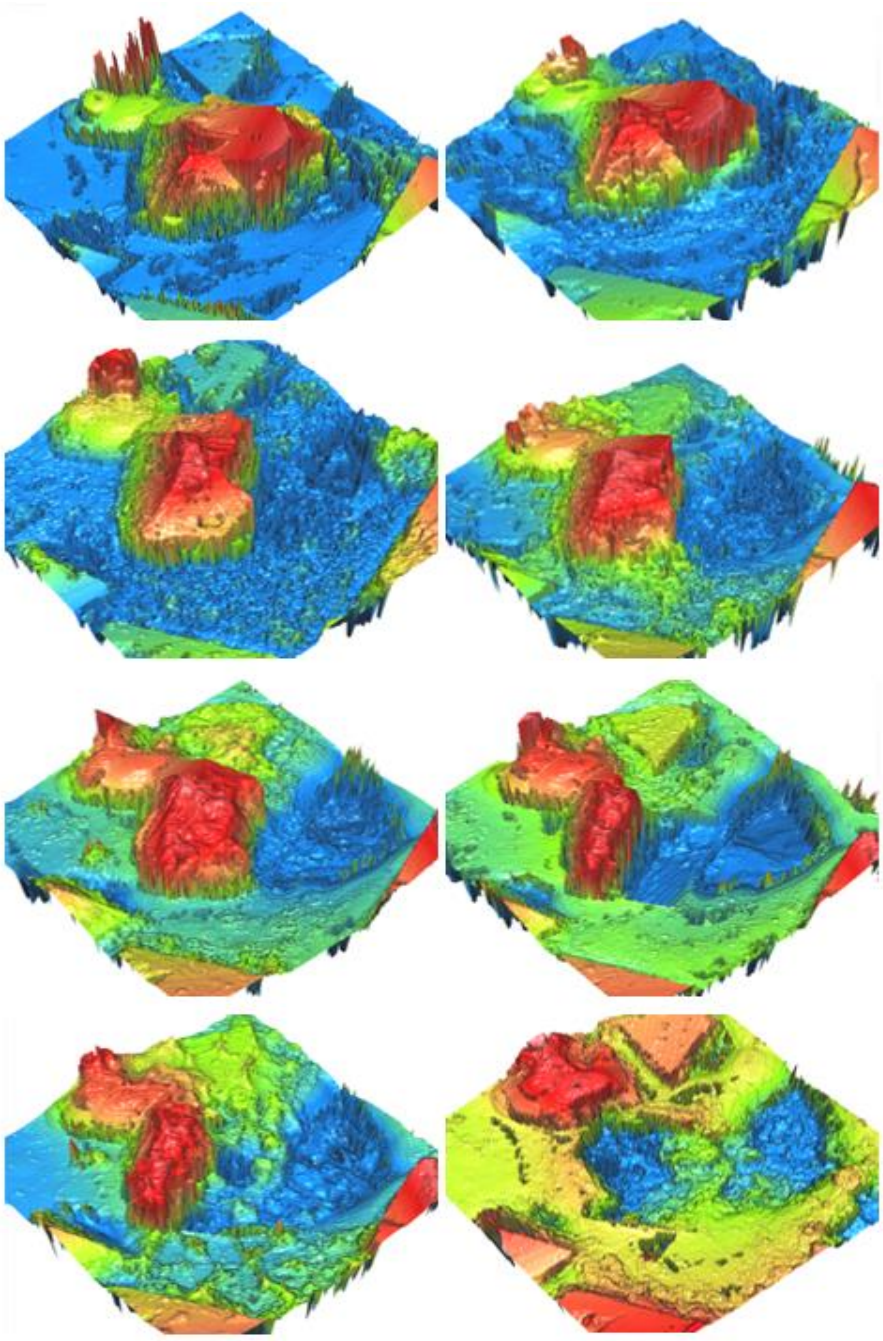

Figure 77- Conditions of G9 in all steps, Left to Right Steps: 0,1;2,3;4,5;6,7

Lifetime of a grit in region 9 is shown in the above Figure 77. Initial condition remained stable at the beginning. However, after first step huge fracture occurred and destroyed almost half of it. At the same time attritious wear were still observed. Through the end of its life, it was getting smaller at each step and finally it has been pulled out.

G10

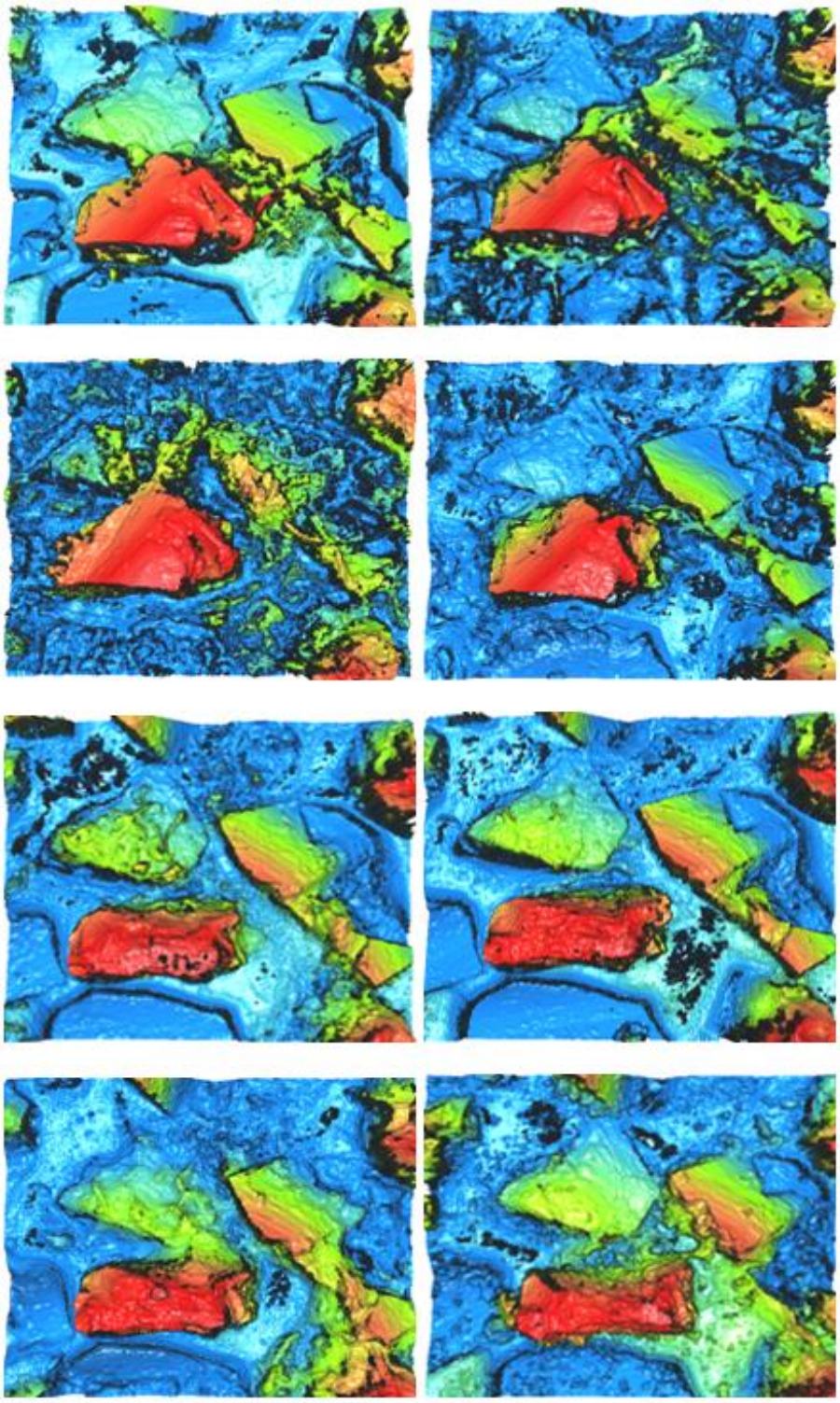

Figure 78-Conditions of G10 in all steps, Left to Right Steps: 0,1;2,3;4,5;6,7

Region G10 is another example for the effect of flow direction. Although, at some steps sticking material were observed around the grits, most of the time it was gone by the process. However, at the final step lots of sticking material can be seen at the right part of the grit.

4.7.2. Radial Wear

Radial wear can be considered as the height decrease of the grits. In the literature [17], radial wear was measured by taking a shallow pass over the workpiece and measuring the profile. However, in this study more detailed measurements have been done by investigating grits *individually*.

In the selected 13 grit area, 27 different grit have been observed and their heights have been investigated throughout the process. The average height results can be seen in Figure 79. Average height of the measured grit has been found as 62µ at the initial step. Tool supplier also provided that information as a grit dimension which is 120µ. Since half of the grit is buried under the plate in electroplated wheels, the measurements were validated and the number of selected grits was sufficient to obtain accurate data. In the literature [8], radial wear behavior was described as initially it is decreasingly growing and then reaches a steady-state at almost constant rate until the tool life ends. Supportively, the results were similar to the literature description. The reason for the initial decreasingly growth is high pullout rate.

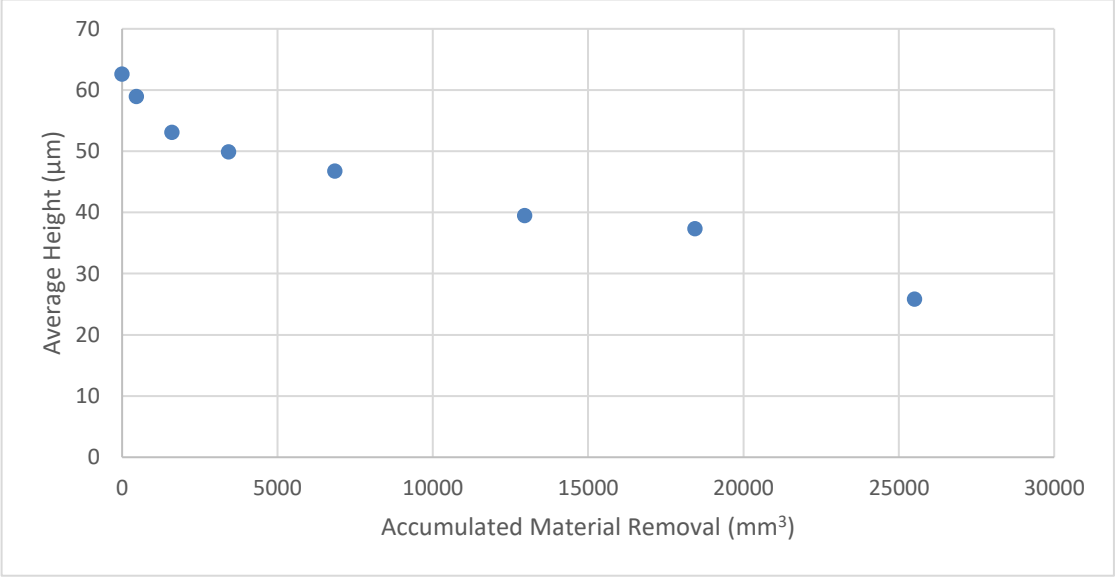

Figure 79- Average Height Changes of Grits During Tool Life Experiments

4.8. Effect of Depth of Cut on Wear

There are three main parameters that can be arranged in the grinding processes, which are cutting speed, feed rate and depth of cut. In this part of the chapter, effect of depth of cut has been investigated for wear and non-wear conditions on surface quality and force. Three different depth of cut variables were selected for non-wear test. Two

different depth of cut variable were chosen for wear condition to be compared. The variables were determined considering the average grit height which was 60µ. First doc was chosen as lower than 60, which was 20µ and the second was higher than 60µ, which was 100µ.

4.8.1. The Effect of Depth of Cut on Surface Quality

Before investigating the effect of depth of cut -wear included-, non-wear cutting tests have been conducted on Inconel 718 material with electroplated CBN grinding wheel. In these test, four different feed rates and three different depth of cuts have been selected. Tests have been conducted one after the other, so tool condition (no wear) kept similar in terms of wear. The aim of this experiment was to observe the effect of depth of cut over the surface roughness of the workpiece. The results can be seen in Figure 80.

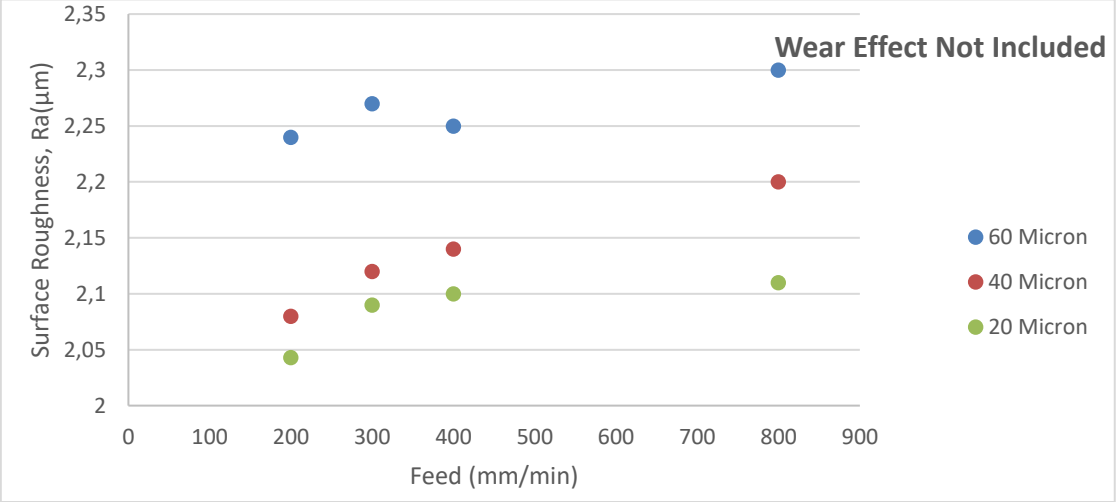

Figure 80-Surface Roughness of the Workpiece with Altered Depth of Cut and Feed Rate

First of all, feed rate effect over the surface roughness is obvious. Increase in the feed rate increased the surface roughness slightly. Compare to the feed rate, depth of cut was more dominant over surface roughness determination.

20µ, 40µ and 60µ depth of cut variations have been applied in the tests. The highest roughness results were obtained with the highest depth of cut as expected since increase in the depth of cut increases the penetration of the grit through the workpiece. Thus, more rough surface has been obtained.

On the other, later on some experiments have been conducted to observe the wear-depth of cut relation over surface roughness of the workpiece. Two different tools with same properties (identical tools) have been used in the experiments. Also, all the cutting parameters kept constant except depth of cut which were selected as 20µ and 100µ. One of tools has been used with 20 µ depth of cut all the time, on the other hand other tool has been used with 100 µ. The aim of this comparison was to observe the wear effect on the tools when different depth of cut used.

The tests results were expected to be similar to the previous non-wear tests however, the opposite has been observed. The results can be seen in Figure 81. The tool with high depth of cut resulted with low surface roughness in general. Surface has been measured 4 times for both tool at the similar accumulated material removal amounts. High surface roughness results were observed for 20 µ at each step. The tool with 100 µ depth of cut has worn faster than the 20 µ tool, so surface roughness results were lower. Also, the results which have been presented in Figure 82 are agreed. The surface roughness of the tool can be used as an indicator of tool wear. The tool with 100 µ depth of cut has seemed to be worn more than the other tool even it has higher roughness at the initial condition.

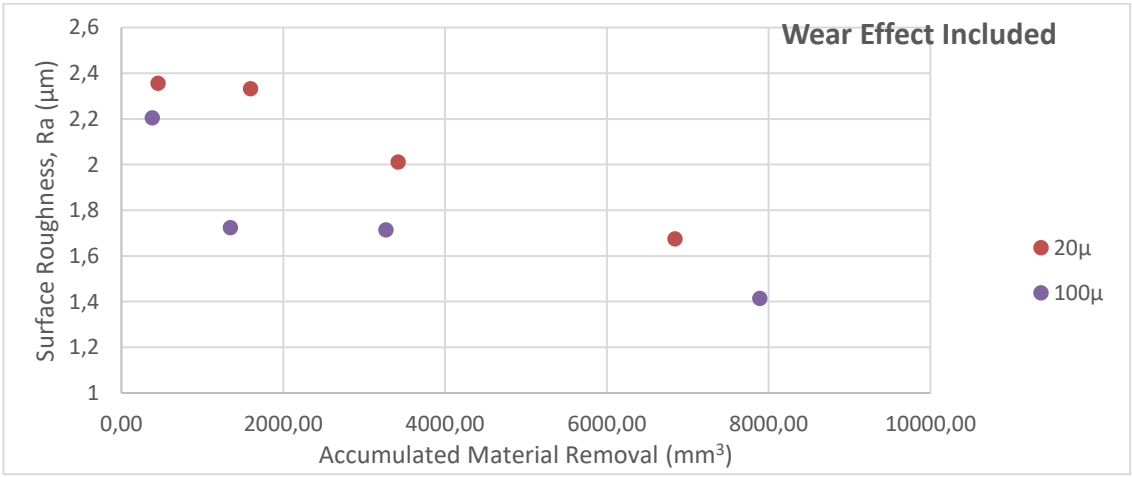

Figure 81- Surface Roughness of the Workpiece According to Wear-Depth of Cut

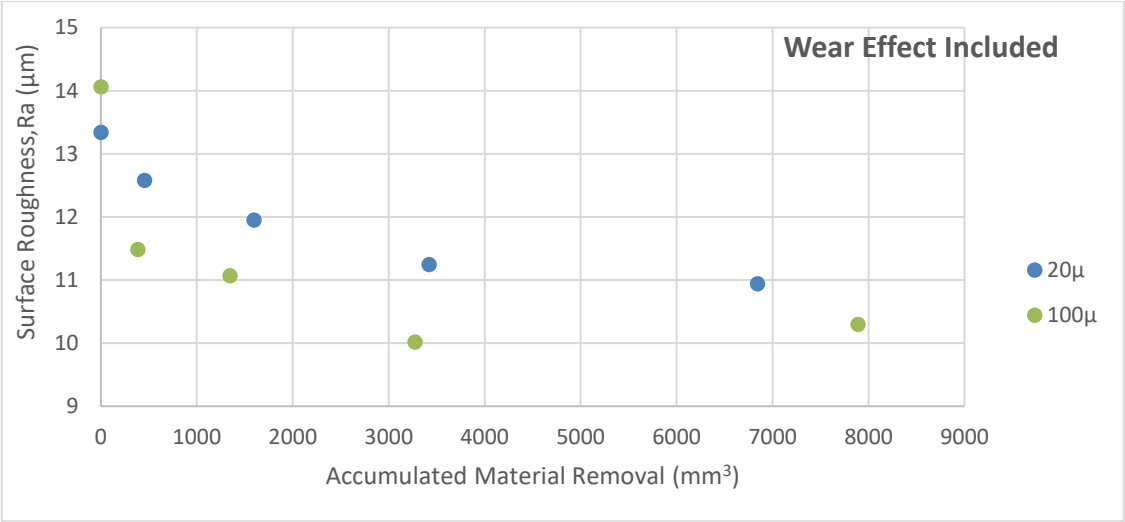

Figure 82-Surface Roughness of the Grinding Wheel According to Wear-Depth of Cut

To conclude, if high depth of cut is used in the grinding process for plated tools for a long time, the tool life will end faster. Whereas, better surface quality can be obtained in a shorter time and also process time will be short because the tool with higher depth of cut removes more material in same time interval. Thereby;

Non-wear Condition (Short Process)		**Wear Condition (Long Process)**	
High Depth of Cut	Low Depth of Cut	High depth of Cut	Low Depth of Cut
-High Surface Roughness	+Low Surface Roughness	-Faster Tool Wear	+Slower Tool Wear
-Low Surface Finish Quality	+High Surface Finish Quality	+Low Surface Roughness	-High Surface Roughness
		+Better Surface Finish Quality	-Low Surface Finish Quality
		+Short Process Time	-Long Process Time

Table 13- The Effect of Depth of Cut on Grinding Process

4.8.2. The Effect of Depth of Cut on Grinding Forces

As it was explained earlier, force measurements during the cutting process can be used as an indicator of tool wear because nothing has been changed (parameters were same) except the tool cutting condition during process. When the first condition of the tool was investigated under microscope, it was observed that grits had sharp cutting edges. However, after some time most of the grits were observed to be gone or to be dulled which made the cutting action harder so cutting forces were increased.

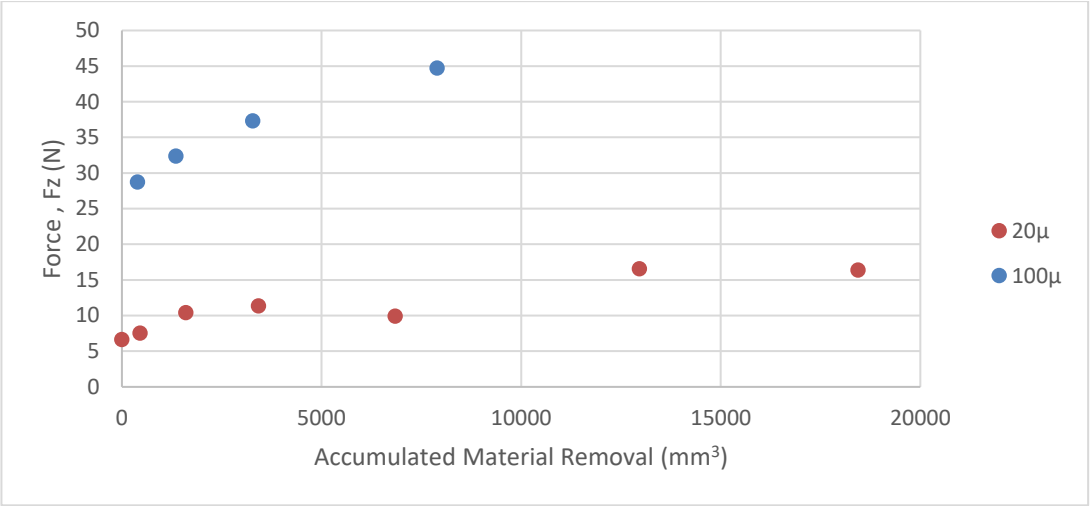

Figure 83-Effect of Depth of Cut and Wear over Forces

Both tool exhibit an increase in the force results due to the tool wear as expected and the results are shown in Figure 83. When the results are compared, it is obvious that the tool with high depth of cut resulted with higher force due to more material removal per pass. Whereas, there is clue in the Figure 83 about wear behavior of the tools. The acceleration in the force results is higher for high depth of cut which indicates that the tool with high depth of cut worn faster.

4.8.3. The Effect of Depth of Cut on Pullout Percentage

In this part, two different depth of cuts have been compared in terms of pullout percentages and the results are shown in Figure 84. It is obvious that pullout percentage is high for high depth of cut at every step due to high wear. Initially high doc almost doubled the low doc but in the later steps pullout percentage becomes stable for high doc. Whereas, pullout percentage was linearly increasing for low doc. 13% pullout percentage has been reached around after 8000 mm^3 material removed with 100µ depth of cut. On the other hand, this percentage has been reached after 18400 mm^3 material removed with 20µ depth of cut. In other words, pullout percentage was increasing faster for high depth of cut.

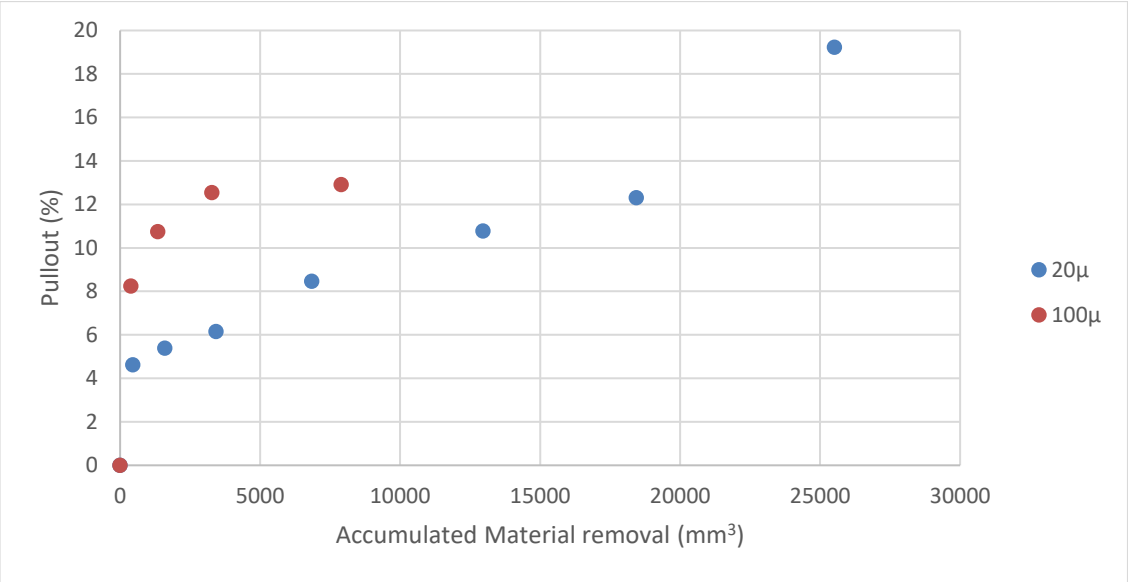

Figure 84-Effect of Depth of Cut on Pullout

4.9. Tool Life Criteria

There have been some studies about tool life in the literature. For example, in one of them [8] tests were conducted with 1.8-3-6 µ depth of cuts for hardened AISI 52100 steel (62 HRC). It was stated that grinding wheel life comes to end when the grit dimensions becomes 20-30%. Also, he found that most of the pullout occurs at the initial transient phase of radial wear. However, we have found something different in the experiments that we have conducted. When the tool life ended, it was seen that grit heights were decreased to 40%. Although average grit height was high at the final stage, pullout percentage was so high. Almost 20% of the grits seemed to pulled out at the final step. Moreover, force results can also be used in the determination of wheel life. Cutting forces have been increased 3 times at the end of the wheel life which indicates an increase in the number of pulled-out and dulled grits. To conclude, workpiece-wheel pair, wheel properties and even the selection of the cutting parameters such as depth of cut can change the tool life of the grinding processes.

4.10. Summary

In this chapter, tool life investigation of an electroplated CBN grinding wheel were explained. Main aim was to understand the wear mechanisms during the tool life and their consequences on process results. In the wear identifications, the methods that have been expressed in Chapter 3 were used.

All the parameters were kept constant and tool has been used until the end of its life. During this experimental process, tool and process results were measured in 8 steps in order to understand the effect of wear on force, tool surface roughness, workpiece surface roughness, pullout amount, grits' geometrical changes, active grit amount and radial wear.

It was seen that cutting forces have increased almost 3 times at the end of tool life. Tool surface roughness decreased and stabilized at approximately 10 μ. In a similar way workpiece roughness decreased around 2μ and stabilized. On the other hand, pullout behavior was expected to stabilize after some point however, it was *linearly increasing*. Even at the last steps, pulled out grits were observed. Most of the time these grits were the ones being active all time. Among the active grits higher ones were more tend to be pulled-out during the cutting process. And then the inactive grits became active and they have attritious wear mostly. The increase in active grits were explained with pictures by showing height distributions using colors.

Due to flow direction, most of the damage occurs at flow direction side of the grit. Most of the time fracture was observed in the *flow direction*. Also, tip of the grits were affected by cutting action and attritious wear and fracture were observed at the tips. After huge fracture occurred, grit activeness may change. Depending the decreased height amount, also wear type may change on that grit.

Tool life experiments were stopped when

- Radial wear reached 40% of the initial grit dimension.
- Pullout percentage reached 20%.
- Cutting forces increased 3 times.

The results that have been found in tool life experiments such as radial wear and pullout percentages were used in the next chapter in tool surface roughness model and good results were obtained.

Finally, wear included and non-wear tests were compared in terms of depth of cut effect on process results. It was found that the tool with high doc worn faster than the low doc. As a result, in high depth of cut case surface roughness of the workpiece reached better quality in a shorter time.

5. THE MODEL OF SURFACE ROUGHNESS OF THE GRINDING WHEEL

5.1. Introduction

There are many different surface roughness parameters, but the arithmetic average of the absolute values -*Ra*- is the most commonly used one to determine surface quality. In this chapter, the modeling of the surface roughness -*Ra*- of the electroplated CBN grinding wheel is presented for the first time. Since the model is based on experimental results, its application to the other single layer grinding tools, such as brazed wheels is possible. This model can be used not only for CBN abrasive, but also for other types of abrasives such as diamond, aluminum oxide etc.

One of the most important outputs of the grinding processes is the surface quality of the workpiece. The quality of the ground surface is usually expressed with the surface roughness [27]. The most dominant factor that affects the surface roughness of the workpiece has been found as wear of grinding wheel from the experiments that have been conducted. Grinding wheel surface roughness model provides information about instantaneous condition of the wheel during its tool life.

Modeling of the surface roughness of the workpiece and modeling of the grinding wheel topography are common in the literature [27, 28, 23, 29]. However, the surface roughness of the grinding tool is not commonly discussed. Previous studies mostly focused on the wheel topography and the roughness of the workpiece surface. In order to predict the surface roughness of the workpiece, the models of wheel topography and chip thickness are used in general [28]. First, the surface topography of the grinding wheel and all the grits on the wheel surface had been modeled by describing the geometrical properties of the grits, including randomness. Then, the trajectories of the grits had been modeled accordingly. In addition, the penetration amount of the grits to the surface had been modeled. Finally, the surface roughness of the workpiece had been predicted [23].

The investigation of tool wear in grinding processes is highly significant, because the wear affects all the outcome and is time-varying. Thus, the modeling of grinding wheel’s initial topography is not sufficient for further stages of the process. Because

after some time grit shapes change due to wear, as a result their penetration amounts change as well. In order to obtain the in-process surface roughness predictions more accurately, the model was developed by including wear base approach, which provides the real-time effect over the grinding wheel. The advantage of this model is its ability to predict the wheel condition during the process, due to the wear.

5.2. Calculation of Roughness

The surface quality can be expressed with some parameters such as roughness and waviness. Roughness can be defined as a measure of the finely spaced surface irregularities. On the other hand, waviness can be defined as part of the texture on which roughness is superimposed [30]. It can be caused by vibrations, chatter or work deflections. The difference between surface roughness and waviness can be seen in Figure 85.

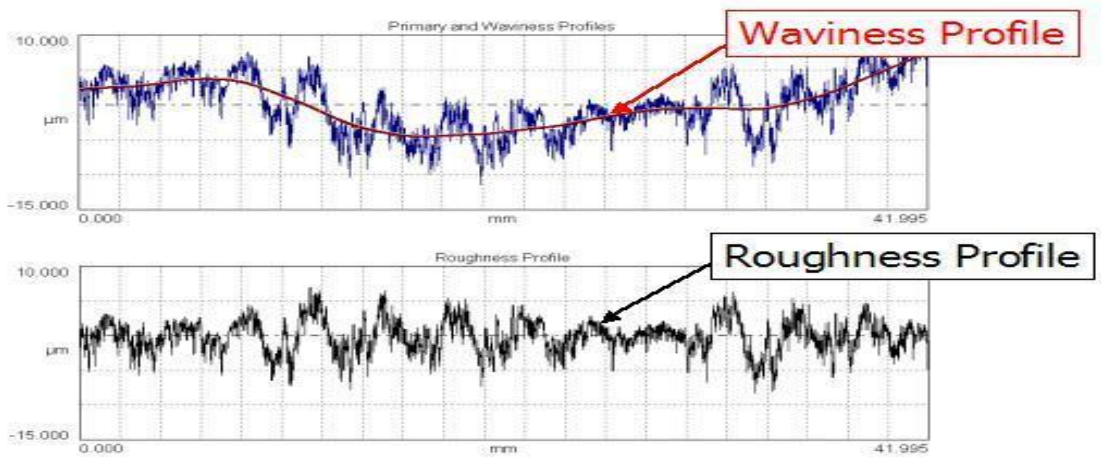

Figure 85-Roughness and Waviness

After the grinding wheel passes over the surface, active grits leave traces on the feed direction. These scratches (traces) are parallel to each other and lie in the feed direction (x-axis), the scratches can be seen in Figure 3. Thus, roughness in the x-axis is much smoother than the y-axis (perpendicular to the feed direction) and probe moves in y-axis to measure roughness of the surface. These scratches were formed by active abrasive grits on the grinding wheel, which are shown in Figure 86.

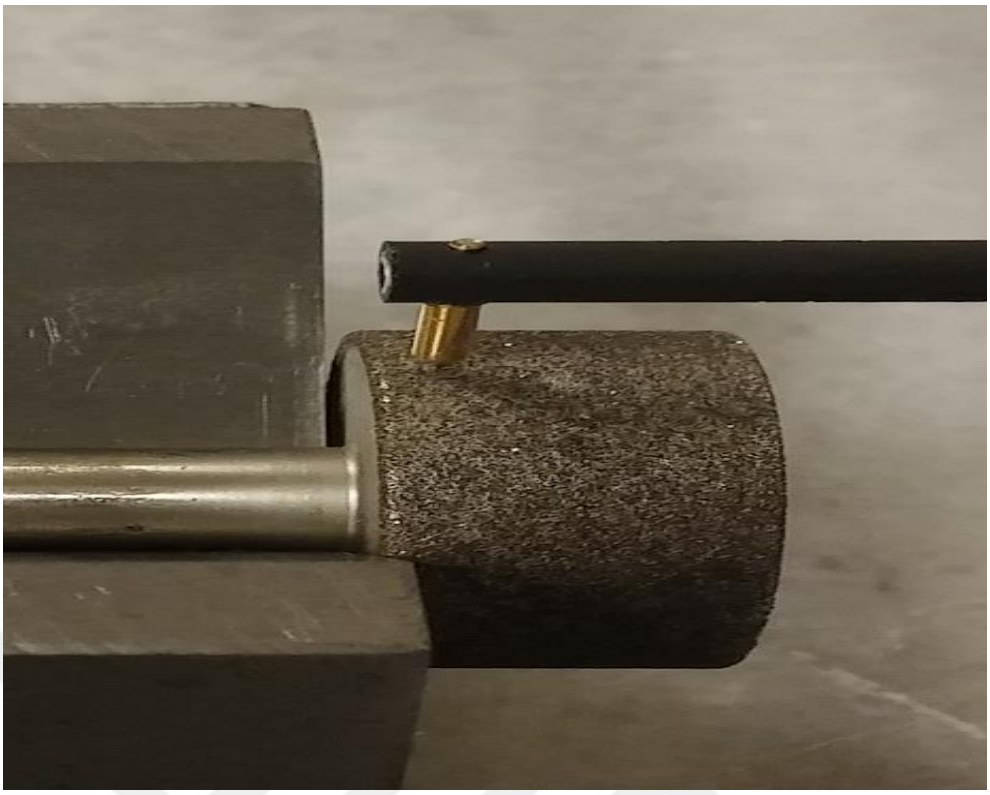

Figure 86- Grinding Wheel Surface Measurement

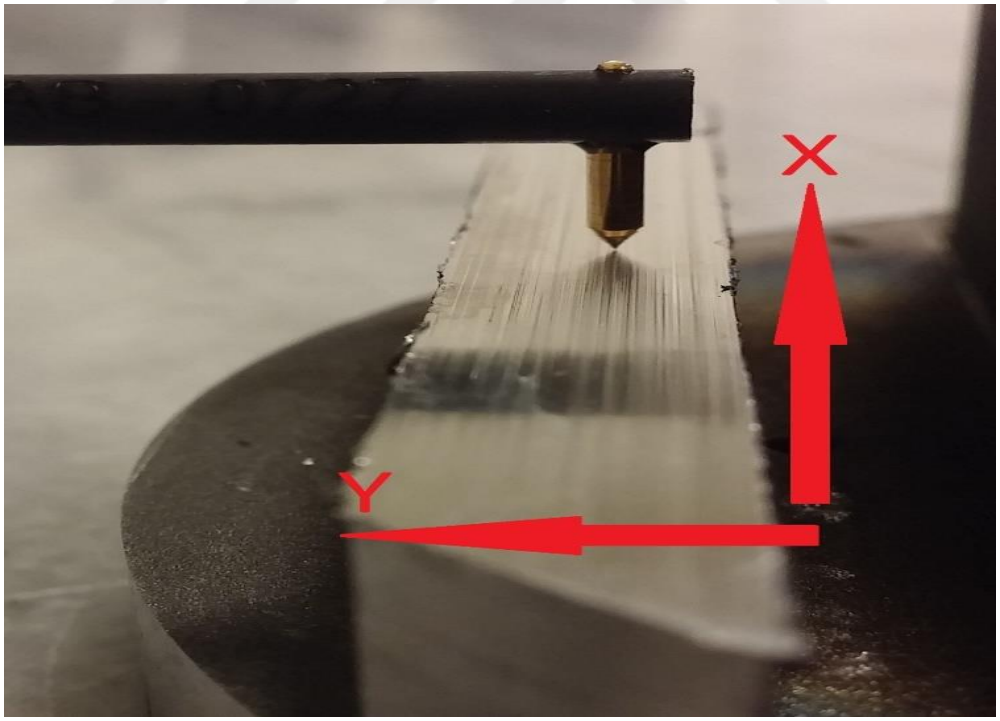

Figure 87-Scratches on the Workpiece Surface

In this chapter, calculation of arithmetic average of absolute values -*Ra*- has been modeled for the single-layer grinding wheel. In the literature, it is formulated as

$$Ra = \frac{1}{n}\sum_{i=1}^{n}|y_i|$$

-*Ra*- calculations have been modeled for grinding wheel surface roughness. The calculation of -*Ra*- can be seen in Figure 88. There are the peaks and valleys on the surface. Their average height is referred to as the mean height (horizontal line at the middle). After finding the mean height, the valleys are inverted. The average distance of the inverted valleys and peaks to the mean height is called mean roughness -*Ra*-. The surface length which is shown in Figure 88 can be considered as axial direction in Figure 86.

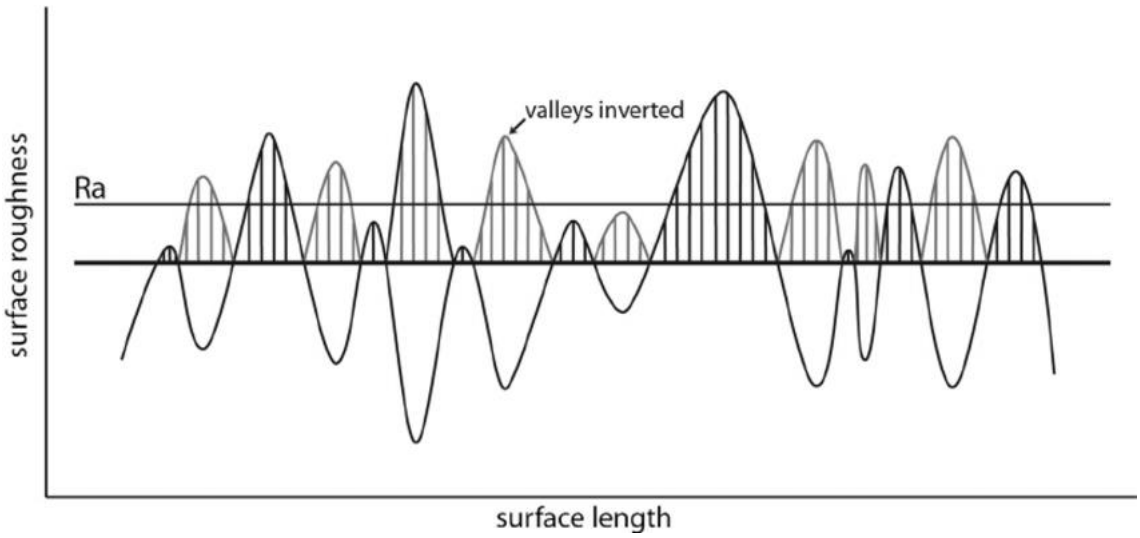

Figure 88-Ra Calculation

5.3. The Model for -*Ra*- Calculation for Grinding Wheel

In the literature, mostly the modeling of surface roughness of the workpiece has been discussed. The modeling of surface roughness of the grinding wheel is presented in this study for the first time. Before explaining the model in detail, I would like to briefly describe the logic behind the model. The model uses three different experimental results & observations as an input, which are *average grit height*, *average grit number* and *pullout percentage*. Then, the model makes the calculations using geometrical properties of grits and obtains the -*Ra*- of the grinding wheel.

Defining the geometric shapes of the grits is the starting point of the presented model. Three different geometries are given in the Figure 89. These are spherical shape, truncated cone and cone. The geometrical parameters of the grit shapes such as diameter

and height were taken from the literature. The dimensions were chosen such that the volumes of all three shapes would be identical [31].

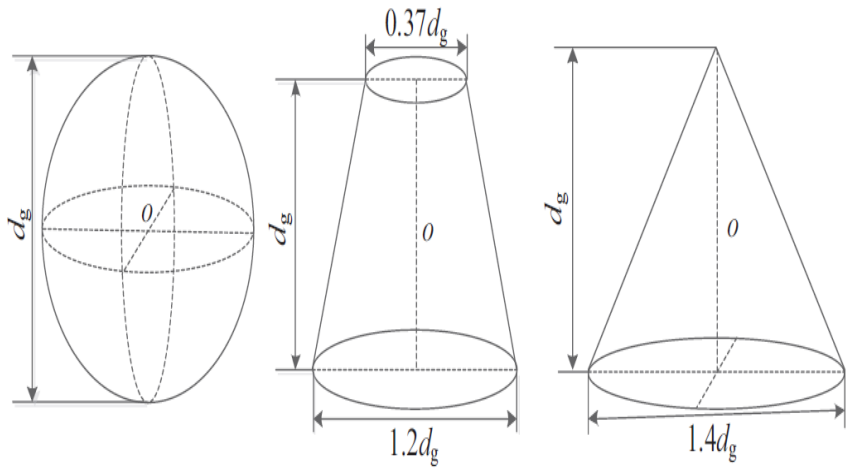

Figure 89-Geometric Models of the Grits

There are some assumptions in the presented model:

- After a geometric shape is selected, all the grits are assumed to be the same (identical). For example, if the spherical model is selected, all the other grits are assumed to be spherical on the tool as well.
- In the production of the electroplated CBN grinding tools, half of the grits are buried under the plate, that is why the same concept was used in the model.
- After the pullout occurs, it leaves a flat surface behind.
- Since the grits have a 3D shape, the probe tip may miss the valley tip. It can be assumed that averagely *70%* of the grits' heights were scanned while the probe is passing over the grit.

The important thing in the model is the density of the grits in the area, not the distribution. The number of grits in a specified area was measured 10 times. For example, the average number of grits in 0.64 mm^2 area has been found to be 28 in the selected tool. Then, one grit area on the surface has been calculated with the referenced dimensions.

Grit width, which is presented as d_g, was calculated based on the following formula [31]:

$$d_g = \frac{15.2}{m}$$

m is the particle size and in this case, it is 120.

For example, the area covered by one grit is

$$A = \pi * \frac{(0{,}7 * d_g)^2}{4}$$

for a conical shape, because half of the grit is assumed to be buried under the plate. After that, the area covered by average number of grits has been found. The selected area was divided into two separate sections. The first one is the grits that are aligned side by side, while the second is the remaining flat area. The division of the area can be seen more clearly in Figure 90. In the given figure, the left square represents the top view of an area (areal measurements were expressed in chapter 3) and the circles represent the grits. The sketches on the right represent the front view of the grits and the remaining flat surface.

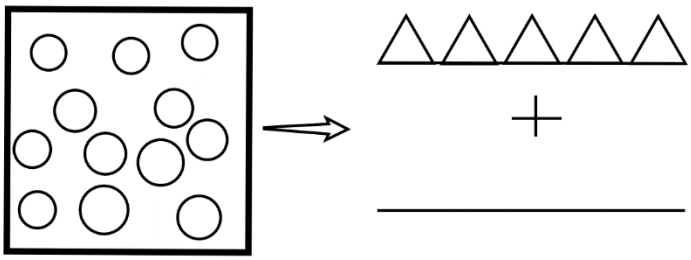

Figure 90- Modeling of the Area on the Wheel Surface

The centroid of the geometric model is represented as “h”, and is different for all shapes. However, one important point should be made. In these geometric shapes the bottom line was not considered in centroid calculations. Only the points that the probe was touching were considered. The “height” in the given formula represents the real average height of the grits, which was measured by Nanofocus microscope. Since all the grits are assumed to be the same, the average height was used in the formulation for all. The centroids of the geometrical models are given as follows:

Sphere:

$$h = \frac{2 * (height)}{\pi} * 0.7$$

Truncated Cone:

$$h = height * 0.736 * 0.7$$

Cone:

$$h = \frac{height}{2} * 0.7$$

While calculating centroids, the probe of the profilometer was assumed to pass averagely 70% of the grit height. For example, for a cone shape grit, the probe starts measuring from the left bottom of the girt to the top and then to the right bottom, which can be seen in Figure 91. However, it is not possible to always pass through the tip of the grit. Thus, a coefficient of 70% was added as an assumption. This movement of the probe can be considered as a 2D action because it is moving over a line. Thus, geometric models were considered as 2Din the centroid calculations. For example, 2D view of a spherical shape was taken as *semicircle arc*.

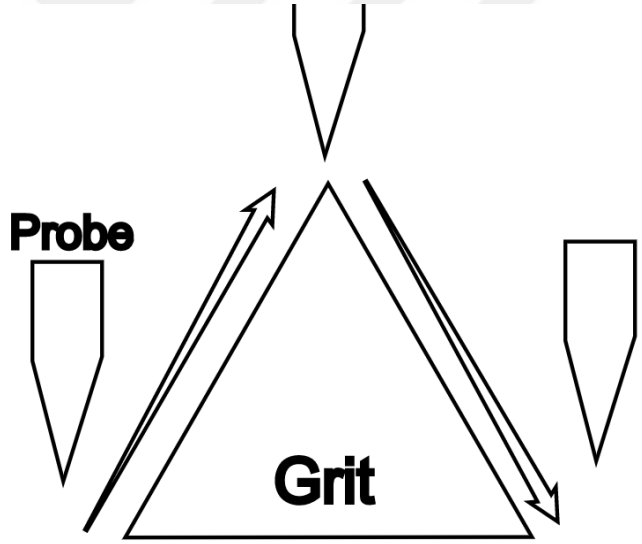

Figure 91-Probe Movement over the Grit

After finding a centroid of one grit, the *mean height* of all the area was calculated and is represented as "h_m". The formulation for h_m is given below.

$$h_m = h * \frac{Total\ Grit\ Area}{Total\ Area} * (1 - Pullout\%)$$

The wear effect was included to the model using this formulation. Centroid (h) and pullout percentage (Pullout%) are changing with time. At each step "h_m" was calculated. "Pullout%" represents the percentage of the pulled-out grits. While the grinding process was advancing, the tool became more worn. Thus, the pullout

percentage was increased at each step. On the other hand, the average height of the grits was decreased in time due to wear.

Final formulation consists of two parts, as explained in Figure 90. Parts can be considered as before and after the "+" sign. The first part of the formulation represents -*Ra*- value of the grit area and the second represents the -*Ra*- of the flat area. Roughness of the "grit area" and "flat area" have been calculated separately and then added to obtain the overall -*Ra*- value.

$$Ra = abs(h - h_m) * \frac{Total\ Grit\ Area}{Total\ Area} * (1 - Pullout\%) + h_m$$
$$* \left(1 - \frac{Total\ Grit\ Area}{Total\ Area} * (1 - Pullout\%)\right)$$

By using "h", "h_m" and "%Pullout" variables, it is possible to predict the surface roughness of the grinding wheel considering wear.

5.4. Results

The inputs for the model are pullout percentage, average height, average grit number and geometric shapes. These have been obtained from the experimental findings, except geometric shapes. On the other hand, geometric shapes are the analytical part of the model. The surface roughness of the grinding wheel has been obtained as an output of the model and the verification of it has been done by experiments. Model results have been presented for two different test sets. The first set is the wear mechanisms tests, which was presented in Chapter 3. The second set is the tool life tests, which was presented in Chapter 4.

5.4.1. Model Results for Wear Mechanisms Tests (Chapter 3)

In this part, the model has been applied for the first test set. This test contained five steps and only investigated the initial part of the tool life. The model results and experimental results are shown in Figure 92. Although, all the findings have a similar decreasing behavior, the most accurate results were obtained with the truncated cone shape with a maximum of 7% error. Also, spherical shape had close results with a maximum of 8% error. Although spherical and truncated cone shapes worked accurately in the model, the cone shape results were not correct and had around 40% error.

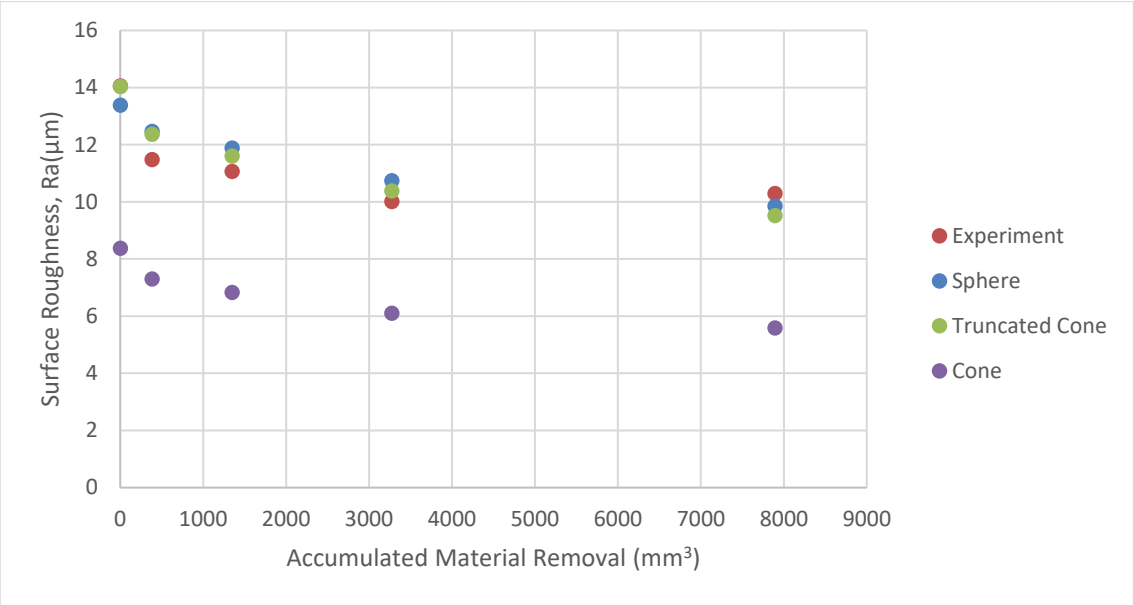

Figure 92-Surface Roughness Model Results for Wear Mechanisms Tests

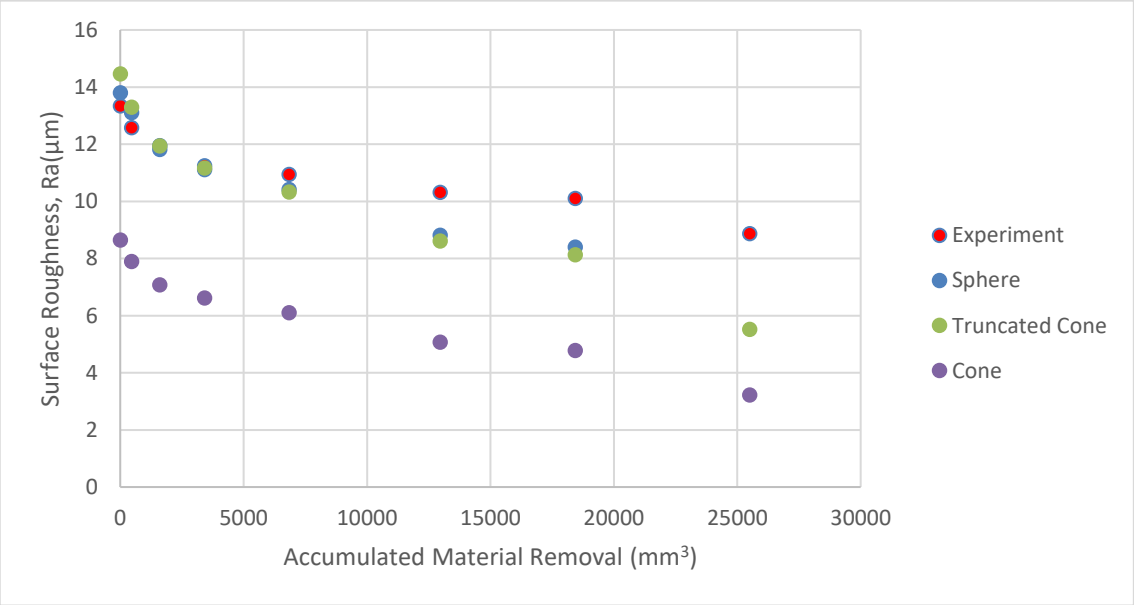

Figure 93-Surface Roughness Model Results for Tool Life Tests

5.4.2. Model Results for Tool Life Tests (Chapter 4)

The results are shown in Figure 93 for tool life test. At the beginning, truncated cone had the closest results however, after 4th step the sphere became closer to the experimental results. Towards the end, error was increasing for all shapes due to the pullout. When a grit is pulled out from the surface, it generally leaves a hole behind. The size of the hole almost equals to the half of one grit. However, pulled-out grits were assumed to leave flat surface behind in the model. Thus, it is logical to obtain higher

experimental surface roughness results through the end because pullout was increasing. For example, a grit had some height before being pulled out like a peak. However, after it was pulled out, it became a valley.

5.5.Summary

In this chapter, the surface roughness model of the single layer electroplated CBN grinding wheel has been presented. The main purpose of the model is calculating the -*Ra*- roughness parameter. Some of the experimental findings were used in the model, such as pullout percentage, average grit height and average grit number in an area. The model works stepwise. At each step, the model uses experimental results and findings from the wear tests, which have been used for the prediction of the surface roughness of the wheel. Three different geometric shapes were used in the model separately and -*Ra*- parameter of the grinding wheel surface has been found for each shape. Results show that the spherical and truncated cone shapes are working well in the model, but results are not so accurate for cone shape. Accuracy of the model was decreasing at the end of the wheel life for all shapes due to high pullout rate.

The initial condition of the tool included a wide variation of grits' height, so the roughness was high at the beginning. In time, height variation decreased because of dulling and other type of wear mechanisms and, as a result roughness of wheel surface decreased. The surface roughness of the grinding wheel is directly related with the wear. Thereby, surface roughness of the wheel can be used as an indicator of telling the tool condition. After the general behavior of the tool wear has been obtained for a specified cutting condition, instantaneous wear condition of the tool can be found during the process.

The surface of grinding wheel projects its surface topography to the workpiece during cutting. Thus, the surface roughness of the workpiece and grinding wheel are correlated to each other. Since the workpiece quality is mostly determined by the wheel condition, the surface condition of the grinding wheel can be used to predict the workpiece surface in further studies.

6. DISCUSSION AND CONCLUSION

Investigation of tool wear in grinding processes has been studied within the scope of this thesis. A new measurement procedure has been applied to the wear research which is *individual* grit investigation. This aspect provides a clear observation on the wear mechanisms. These mechanisms can be classified as attritious wear, fracture and pullout. Throughout the electroplated CBN grinding wheel life, all phases of grits were shown. A new measurement device was developed to observe all the wheel surface under the microscope which provides accurate results. Two different experimental tests have been conducted which are investigation of wear mechanisms and investigation of tool life. A new model which predicts Ra value of the surface roughness of the electroplated grinding wheel was developed. Experimental and model results were compared and the model has been validated.

Conclusions of the thesis are as following:

- Four different feed rate have been compared in terms of spark-out by monitoring force changes. It was experimentally proved that increase in feed rate, increases the required number of spark-out passes.
- The ploughing forces of the brand-new tool and worn tool were compared. It was found that after the wheel has worn, ploughing forces were increased compared to the brand-new wheel.
- Wear mechanisms have been investigated under microscope. Four main wear mechanisms were observed which are attritious wear, fracture (micro & macro) and pullout. Most of the fracture was observed where the chips occurred. In other words, fracture occurred at the flow direction predominantly. Attritious wear dulled the sharp edges of the grits, so cutting forces were increased.
- Pullout mechanisms seemed more dominant at the initial stages of the tool life due to low bonding force between the grits and the plate. Therefore, initially sharp decrease was observed at the surface roughness of the workpiece and wheel results due to high pullout rate.
- Pullout mechanism is more effective in the processes with high depth of cut parameter compare to the low. They almost reached to the same pullout percentage

when the tool with low depth of cut removes more than two times material of the high depth of cut.

- During the tool life experiments, effect of wear on the process results which are grinding forces, surface roughness of the wheel and workpiece was investigated. Grinding forces in the normal direction were increased throughout the tool life and at the end approximately it was three times higher than the initial condition.
- Throughout the wheel life pullout was linearly increasing. At the end, pullout percentage increased up to 20%. On the other hand, radial wear decreased to 40% of the initial grit height. All these consequences depend on the selected process parameters and wheel-workpiece pair type.
- Grinding burn was not observed for the selected cutting parameters during the experiments.
- Most of the SAM processes are conducted with 100% oil based coolant. However, 5% oil-water mixture was used in the experiments, which believed that it is the reason for high pullout rate.

Contributions of the thesis are listed below:

- A model that predicts the Ra parameter of the surface roughness of the wheel was presented for the first time. Radial wear and pullout percentage results which were obtained from the experiments were used in the model. Three different type of geometric shapes which are sphere, truncated cone and cone were used in the model separately. Model calculates Ra parameter instantaneously according to the measured wear results. Spherical and truncated cone shapes had a good agreement with the model; however, error at cone results was high. The model accuracy was not good at the end of the tool life due to pullout assumption. It can be improved by considering after grit pulled-out, it leaves a hole not a flat surface.
- An individual investigation method was developed by designing a wheel stabilizer to analyze wear mechanisms on grits. It provided the geometrical shape changes of a grit during its lifetime.
- Surface quality investigation has been done by using two different depth of cut value. First non-wear condition was applied and it was found that the tests with high depth of cut resulted with high roughness values. Then, wear included tests were conducted and it was observed that the tests with high depth of cut resulted with low

roughness value. The reason is that the tool with high depth of cut parameter worn faster, it can be understood by looking the surface roughness of the wheel. When less rough surface projected to the ground surface, less rough surface was obtained at the ground surface.

7. FUTURE SUGGESTIONS FOR FURTHER RESEARCH

Investigation of wear in grinding processes are presented by conducting many experiments and modeling the surface roughness of the grinding wheel. The model was validated by experimental studies; however, there are still some points that can be improved. Following recommendations may advance the presented study:

- An extensive research has been done with the selected grinding parameters and its results are presented step by step. Thus, a structure was developed for the selected tool. Only by changing one parameter, the effect of that parameter on wear can be investigated.
- This study is mostly based on Inconel 718 and electroplated CBN wheel pair. The other workpiece-wheel pairs can also be investigated for comparison.
- Pullout mechanism was only investigated in terms of depth of cut. The effect of other grinding parameters can also be examined such as cutting speed and feed rate in order to analyze the reason for pullout mechanism whether it is mechanical or thermal.
- 5% oil-water mixture was used as a coolant in this study. The effect of other type of coolants on the wear behavior may be investigated such as cryogenic cooling system.
- Wear on conventional wheels can also be examined considering dressing effect and filling mechanism; although, it is really difficult to observe.
- The effect of wear on grinding forces and surface quality has been investigated. In addition to these, temperature variation may be investigated during the tool life considering wear effect.
- Increment in the active grit density due to wear was presented by showing the stepwise pictures of grits. However, it would be better if an accurate measurement method is added.

Model for the surface roughness of the grinding can be improved by doing these:

- Mixing the geometries and using them all in the model and reaching optimum. For example, distribution of the grit geometric shapes can be 30% spherical, 40% truncated cone and 30% cone.
- Spherical, truncated cone and cone shapes were used in the model. Other types of geometrical shapes may be added.
- The logic behind the model can be applied to the other type of wheels such as brazed wheels.

8. REFERENCES

[1] C. Guo, Z. Shi, H. Attia and M. D, "Power and Wheel Wear for Grinding Nicke Alloy with Plated CBN Wheels," *Annals of the CIRP*, pp. 343-346, 2007.

[2] A. A. Vieira, M. A. Baptista, L. M. P. Parente and N. R. M. Jorge, "On the temperature field during superficial grinding: an experimental study," *International Advance Manufacturing Technology*, vol. 40, pp. 1084-1092, 2009.

[3] B. W. Rowe, Principles of Modern Grinding Technology, Waltham: Elsevier, 2014.

[4] Y. Altıntaş, Manufacturing Automation, Cambridge: The Press Syndicate of the University of Cambridge, 2000.

[5] S. Malking, "Selection of Operating Parameters in Surface Grinding of Steels," *ASME*, vol. 1, no. 98, pp. 56-62, 1976.

[6] E. Uysal, "Analytical and Experimental Investigation of Orthogonal Turn-Milling Processes," Sabancı University, Istanbul, 2015.

[7] P.L. Tso, "Study on the grinding of Inconel 718," *Journal of Material Processing Technology*, pp. 421-426, 1995.

[8] Z. Shi and S. Malkin, "Wear of Electroplated CBN Grinding Wheels," *Journal of Manufacturing Science and Engineering* , vol. 128, no. 1, pp. 110-118, 2005.

[9] S. Malkin and N. H. Cook, "The Wear of the Grinding Wheels Part I: Attritious Wear," *ASME J. Eng. Ind.*, pp. 1120-1128, 1971.

[10] S. Malkin and N. H. Cook, "The Wear of Grinding Wheels Part II: Fracture Wear," *ASME J. Eng. Ind*, pp. 1129-1133, 1971.

[11] E. J. Duwell and W. J. McDonald, "Some Factors That Affects the Resistance of

ABrasive Grits to Wear," *Wear 4*, pp. 372-383, 1961.

[12] Y. Chen, H. J. Xu and Y. C. Fu, "The experimental study on wear performance of brazed diamond grits," *Key Engineering Materials*, Vols. 359-360, pp. 28-32, 2008.

[13] G. Q. Zhang, H. Huang and X. P. Xu, "Study on the wear mechanism of brazed diamond grains," *Key Engineering Materials*, Vols. 532-533, pp. 58-62, 2008.

[14] S. Li, J. H. Xu, B. Xiao, M. H. Yan, Y. C. Fu and H. J. Xu, "Performance of brazed diamond wheel in grinding cemented carbide," *Material Science Forum*, Vols. 532-533, pp. 381-384, 2006.

[15] A. Ghosh and A. K. Chattopadhyay, "Performance enhancement of single-layer miniature cBN wheels using CFUBMS-deposited TiN coating," *International journal of machine tools and manufacture*, vol. 47, pp. 1799-1806, 2007.

[16] Z. Shi and S. Malkin, "An Investigation of Grinding with Electroplated CBN Wheels," *Annals of the CIRP*, pp. 267-270, 2006.

[17] R. P. Upadhyaya and S. Malkin, "Thermal Aspect of Grinding with Electroplated CBN Wheel," *ASME J. Manuf. Sci. Eng.*, pp. 107-114, 2004.

[18] A. Ghosh and C. A. K, "On grit-failure of an indigenously developed single lyer brazed CBN wheel," *Industrial Diamond Review*, vol. 67, no. 1, pp. 59-64, 2007.

[19] R. P. Upadhyaya and J. H. Fiecoat, "Factors Affecting Grinding Performance with Electroplated CBN WHeels," *Annals of the CIRP*, vol. 56, no. 1, pp. 339-342, 2007.

[20] C. P. Bhateja, "A proposal for some functional characteristics parameters of abrsive grinding wheels," *Annals of the CIRP*, vol. 27, pp. 237-241, 1978.

[21] A. Azizi, S. M. Rezaei and A. Rahimi, "Study on the rotary cup dressing of CBN grinding wheel and the grinding performance," *International Advance Manufacturing Technology*, vol. 47, pp. 1053-1063, 2010.

[22] S. Malkin, Grinding Technology: Theory and Applications Machining with Abrasives, West Sussex: Ellis Horwood Limited, 1989.

[23] D. Aslan and B. Erhan, "Surface roughness and thermo-mechanical force modeling for grinding operations with regular and circumferentially grooved wheels," *Journal of Materials Processing Technology*, vol. 223, pp. 75-90, 2015.

[24] X. Chen, W. B. Rowe and R. Cai, "Precision grinding using CBN wheels," *International Journal of Machine Tools and Manufacture*, vol. 42, no. 5, pp. 585-593, 2002.

[25] C. Zhang and S. Y. C, "Wear of Diamond Dresser in Laser Assisted Truing and Dressing of Vitrified CBN Wheels," *International Journal of Machine Tools and Manufacture*, vol. 43, pp. 41-49, 2003.

[26] F. Klocke and K. W, "Appropriate conditioning strategies increase the performance of vitrified-bond CBN grinding wheels," *Annals of the CIRP*, no. 44, pp. 305-310, 1995.

[27] R. L. Hecker and S. Y. Liang, "Predictive modeling of surface roughness in grinding," *International Journal of Machine Tools and Manufacture*, vol. 43, no. 8, pp. 755-761, 2003.

[28] E. Brinksmeier, G. E. Aurich J.C:, C. Heinzel, H.-W. Hoffmeister, F. Klocke, J. Peters, R. Rentsch, D. Stephenson, E. Uhlmann, K. Weinert and W. M., "Advances in Modeling and Simulation of Grinding Processes," *CIRP Annals*, vol. 55, no. 2, pp. 667-696, 2006.

[29] X. Zhou and F. Xi, "Modeling and predicting surface roughness of the grinding process," *International Journal of Machine Tools and Manufacture*, vol. 42, no. 8, pp. 969-977, 2002.

[30] E. P. Degarmo, J. T. Black and R. A. Kohser, Materials and Processes in Manufacturing, Lewiston: Wiley, 2003.

[31] Y. Liu, A. Warkentin, R. Bauer and Y. Gong, "Investigation of different grain shapes and dressing to predict surface roughness in grinding using kinematic

simulations," *Precision Engineering*, vol. 37, no. 3, pp. 758-764, 2013.

[32] S. C. Salmon, Modern Grinding Process Technology, New York: McGraw-Hill, 1992.

[33] S. Malkin and C. Guo, GRINDING TECHNOLOGY, New York: Industrial Press, 2008.

[34] W.-F. Ding, J.-H. Xu, Z.-Z. Chen, H.-H. Su and Y.-C. Fu, "Wear behavior and mechanism of single-layer brazed CBN abrasive wheels during creep-feed grinding cast nickel-based superalloy," *Adv Manuf Technol,* vol. 51, no. 5, pp. 541-550, 2010.

[35] T. Tawakoli, E. Westkamper and B. Azarhoushang, "Effects of vibration-assisted grinding on wear behavior of vitrified bond Al2O3 wheel," *Advanced Materials Research*, Vols. 76-78, pp. 21-26, 2009.